博士論文

2D Planar Biosensors Utilizing Impedance Spectroscopy on a Thin Film Transistor Plate
(薄膜トランジスタ基板を用いたインピーダンス特性計測に基づく２次元平面型バイオセンサ)

31 May 2019

Supervisor: Professor Hiroshi Toshiyoshi

Department of Electrical Engineering and Information Systems
Graduate School of Engineering
37-167292

Cathcart Grant Alexander
カツカルト　グラント　アレクサンドル

Dedicated to my parents, Martha and David Cathcart for always supporting me, and teaching me to question and investigate everything about the world as well as my brother Blair Cathcart for always being there for his annoying little brother.

Abstract

Real-time In-vitro characterization of cells and cell cultures is an instrumental aspect of modern biological science. While conventional fluoroscopy is an extraordinarily versatile technique, it suffer many critical drawbacks. The optical measurement apparatuses are bulky, expensive, and difficult to scale. Additionally, the necessary image analysis is computationally expensive to automate and can be difficult to reproduce. Furthermore, fluorescent dyes are inherently damaging to living cells forcing either the use of complex sampling apparatuses or time limited experimentation.

Electrical measurements are more limited in the scope of properties they can measure, but they have the significant advantage of being non-mutative obviating the need for sampling or experiment termination. Additionally they can be trivially integrated with conventional Micro Electro-Mechanical Systems (MEMS) and microfluidic devices. While electrical measurements can measure most mechanisms involving ion transfer, complementary measurements are needed for many experiments. Thus the creation of a transparent electrode substrate is necessary for the utilization of simultaneous optical and electrical measurement. Unfortunately current transparent devices are either limited in scale (MEA), opaque (CMOS/ISFET) or require sampling in order to function (sandwich electrodes). We present the use of impedance spectroscopy on Indium Gallium Zinc Oxide (IGZO) channel Transparent Thin Film Transistors (tTFTs) as an arbitrarily scalable 2D planar electrical analysis platform for biological systems.

By analysing the impedance between electrodes on this device, we have demonstrated the detection of the spatial location of cells upon the device. Furthermore we have been able to differentiate between the gross state of cells by detecting the differences between living and dead cells. We have extended this principle to create several types of chemical sensors utilizing olfactory cells to detect volatile organics, and antibodies to detect antigens. We have also demonstrated the arbitrary 2D differentiation of media and cells using this same device.

These sensing methodologies can be used to create large scale cell culture analytical systems with real time state based data obviating the need for cumbersome, expensive, mutative, and non-scalable optical equipment for most of the experiment life cycle. Importantly, the transparent nature of the device enables end of life optical analysis of non-electrical phenomena without requiring complex microfluidics or sampling mechanisms.

Additionally, the chemical sensors demonstrated in this work can be applied to create arbitrarily scalable assays. By spatially isolating different sensing intermediaries, whether biological or bio-chemical, we can determine which of a variety of analytes is present based on the detection of where a change in signal is detected spatially on the device.

This work will function as portion of a greater micro total analytical system (μTAS) using the previously demonstrated applications of this device such as the movement of droplets (EWOD), physical differentiation of particles (DEP), and the detection of activation potentials of neurons and other electroactive cells. It is our hope that these pieces will combine into a system that will fundamentally change real time biological analytical systems in the years to come.

Table of Contents

List of Tables

List of Figures

Chapter 1:Introduction

This chapter starts by introducing recent research trends in the analysis of cells and cell cultures. Then we will enumerate the ideal properties of an analytic method followed by how conventional methodologies are insufficient. We will then explain the basic principles of our device, an Indium Gallium Zinc Oxide (IGZO) transparent Thin Film Transistor (tTFT) gated high density electrode array. This chapter will then conclude with the significance, originality of this work as well as the challenges involved.

1.1 Purpose of This Work

Cells are the building blocks of life and come in a wide variety of shapes, sizes and functions. A deeper understanding of how they function is of the utmost importance when it comes to understanding the nature of life itself. Understanding how and why they can experience dysfunction and how those dysfunctions may be ameliorated is the cornerstone of modern medical science. It is vital that any observation of cells minimally interferes with the cells themselves so as to ensure a more thorough understanding of their nature.

The purpose of this dissertation is to discuss the current state of the art when it comes to cellular observation as well as to demonstrate a novel application of technology that is capable of solving several of the fundamental flaws with those technologies. The device has been successfully designed, fabricated, characterized and applied to the detection of cell state across a large surface area utilizing electrical impedance measurements in a manner that is less mutative, and does not interfere with conventional testing methodologies. One of the two major applications of this work is replacing cumbersome mutative optical measurements on cellular cultures for coarse state based measurements while not interfering with end of life optical analysis. The other primary application of this work is the creation of sensing assays, whether biological or biochemical, that can detect a wide variety of materials at arbitrary sensitivities by spatially isolating electrogenic cells or antibodies that respond to a given analyte in spatially isolated regions.

1.2 Background

Cells were initially discovered and named by Robert Hooke in 1665 when he looked at a wine cork under a microscope and noticed it was filled with small chambers that looked like a monk's cell.[1] This paved the way for the discovery of the differences between plant and animal cells, most notably the cell wall, in 1838 by Theodor Schwann and Matthias Schleiden who later codified the first Cellular Theory.[2]

The conventional means by which most cellular properties are observed is through fluorescence, the stimulated emission of light. Fluorescence was discovered in 1833 when David Brewster discovered that when a cell is illuminated by white light sent through a clear alcohol, it emits a red light, due to what we now know is the fluorescence of chlorophyll.[3] The first characterization of fluorescent dyes was done in 1905 by E. Nichols in their study of sidot blende materials.[4]

The study of the electrical property of materials goes back millennia. The first recorded instance of the study of electrical phenomenon was the research of Thales of Miletus in 600 BC when he discovered that amber when rubbed with cloth interacted with sheets of paper, the first observation of static electricity.[5] The first study of the direct electrical properties of materials was performed by Stephen Grey in 1730 when he characterised the conductive and insulative properties of materials, and in one case those of a child(these were quite different times) suspended from the ceiling.[6] The first numerical studies on the conductive and insulative properties of materials were codified by George Ohm in 1826 when he discovered the relationship between voltage and current as it passes through materials and thereby

developed the quintessential electronic law, Ohm's law (V=IR).[7] The first impedance measurements of cells were performed in 1938 by Dr. Curtis on the impedance of squid axons.[8]

1.3 Research Motivation

The impedance analysis of biological materials has long been utilized as a simple, quick, and non-mutative method to determine the electrical properties of cells. This has been used to detect the properties of cells for decades.[8][9] However, due to the nature of cell culture and cell growth, it can be difficult to guarantee that the position of a given cell will be in a measurable location making small surface area measurements inherently unreliable.

One of the simplest means to get around this is through the use an array of electrodes to measure the impedance. The oldest and most commonly used type of electrode array for bio-impedance is a set of electrodes directly connected to external pads known as a Multi-Electrode Array (MEA).[10]–[13] Unfortunately, while these are easily made transparent by depositing them on a glass substrate, these devices rapidly become unwieldy at larger electrode numbers due to the linear relationship between the number of electrodes, the number of electrode pads and corresponding pathing. Pathing constraints, particularly making sure the paths do not experience cross-talk and have the same length, are a limiting factor for all large scale arrays, but technology such as MEAs that have a 1:1 ratio between electrodes

and control lines rapidly become an impossibility even at smaller arrays of under 1000 electrodes.

Another commonly used device type is a Complementary Metal Oxide Semiconductor(CMOS) transistor gated electrode arrays, which are 2D electrode arrays gated with CMOS transistors.[14]–[16] They have the advantage of being arbitrarily scalable if gate and source lines are common among rows/columns. Unfortunately CMOS substrates are inherently opaque due to their reliance on silicon meaning they inherently interfere with conventional fluoroscopic measurements that necessitate a transparent substrate.

Another technology of interest is the Ion Sensitive Field Effect Transistor (ISFET). An ISFET is structurally very similar to a conventional MOSFET in that it consists of a semiconducting channel fabricated by ion implantation that controls the flow of current from source to drain. However, unlike a conventional MOSFET the gate oxide is open to the medium being studied and the flow of current is modulated by the ion concentration at that interface.

In order to attain both scalability and transparency, we have decided to utilize a transparent transistor gated electrode array, which we fabricated using an Indium Gallium Zinc Oxide (IGZO) Thin Film Transistor(TFT) process to gate our electrode array which was deposited upon a glass substrate.[17]

1.4 Research Proposal

Studying biological systems is complicated by their inherently chaotic and sensitive nature. As previously mentioned the non trivially predictable growth patterns of cell cultures makes the end position of the cells non-deterministic. Thus it is vital that the array of electrodes used to measure them is large enough to stochastically ensure valid sensing of cells. Additionally, most devices designed for monitoring cells (conventional electrical measurements, fluoroscopy, etc.) are highly specialized for a specific purpose. While it is not possible to create a device that is better in all aspects than those specialized approaches, a device capable of multiplicity would open up a variety of applications, optical, chemical, electrical. This could be further expanded if such a device could integrate the physical manipulation of the cells and medium within the culture.

In order to facilitate all of these goals, we have decided to utilize a platform that uses transparent (ITO) electrodes gated by Indium Gallium Zinc Oxide(IGZO) transparent Thin Film Transistors (tTFTs) deposited on a transparent (glass) substrate. This has the advantage of being transparent like an MEA while being fully 2D addressable like a CMOS gated array. Additionally, the fabrication of such devices is well established as they have been used for decades in the fabrication of Liquid Crystal Display (LCD) backplanes in monitors and cell phones.[18] This type of device has already been shown to be effective for electrogenic potential sensing[19], electroporation[20], DiElectroPhoresis(DEP)[21], and ElectroWetting On Dielectric(EWOD)[22] making the integration of impedance measurements with those applications trivial on one monolithic device. The simplest method of

accomplishing such integration is by enclosing the cell culture in a PDMS chamber adhered on top of the device as shown in Figure 1 and integrating conventional microfluidic processes.

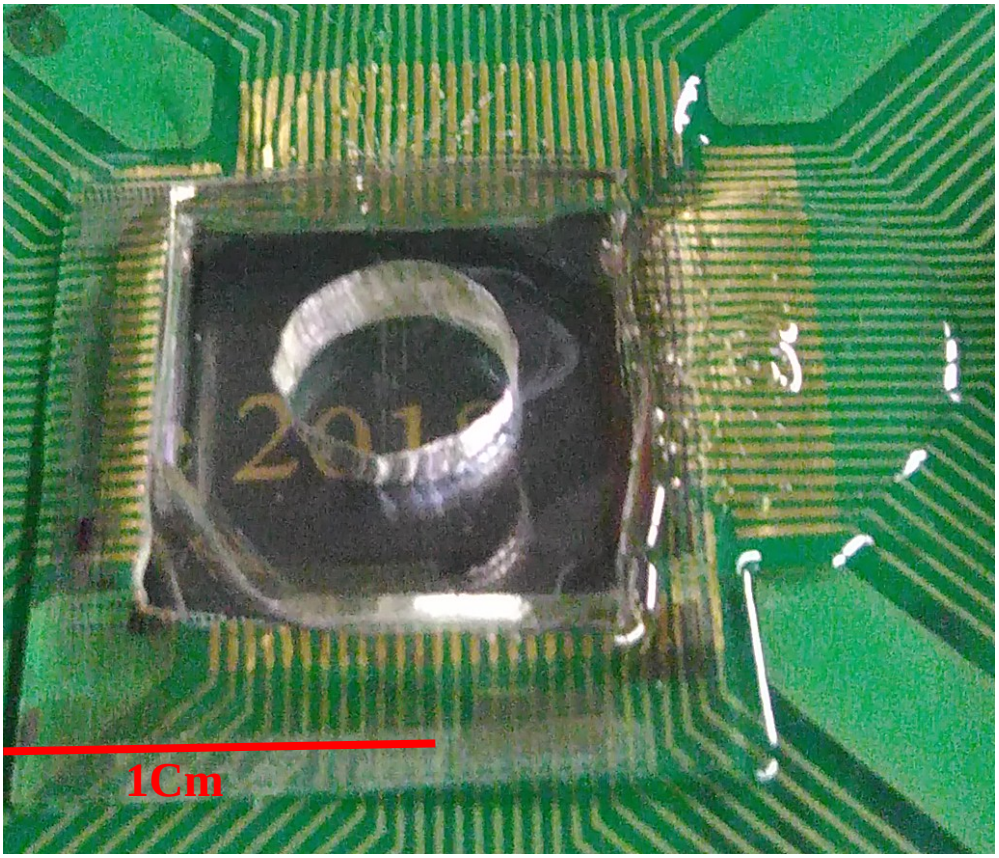

Figure 1: PDMS Chamber attached to our device

When deciding on an optimal measurement system for biological cells and structures one must carefully balance a variety of different fundamental properties and while trade-offs are inherent to any design calculus, one needs to carefully weight the importance of each one

1.4.1 Bio-compatibility

The most fundamental property any bio-analysis device must posses is biocompatibility. In the case of cells this is cytotoxicity, how likely the device is to damage or kill cells cultured on the device. For some types of cells, most cancers and plant cells for example, this is less of an issue as they are inherently durable. Unfortunately, many cells of interest, particularly neurons and organ cells are extremely sensitive requiring careful testing of devices both to ensure that the device in and of itself is not harmful to the cells, but also that contaminants can be easily cleaned from the device such that they will not interfere with cellular function and growth.

1.4.2 Transparency

As previously mentioned, the ability to perform electrical and optical measurements on the same device would be extremely beneficial to biological research. The reason that transparency is necessary for optical analysis is that it is typically done an inverted microscope where the light path from the microscope goes through the bottom of the device under test as shown in Figure 2.

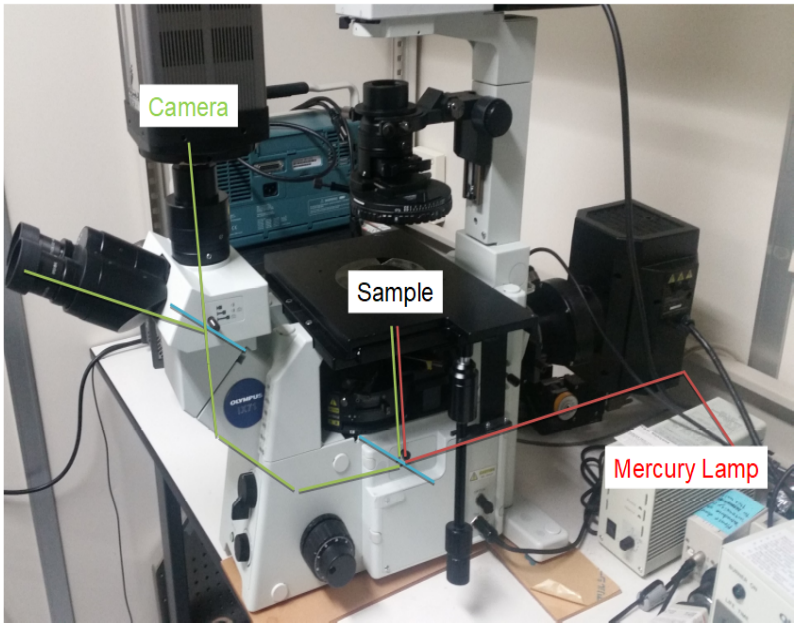

Figure 2: Inverted Microscope with Light Paths

It's important to keep in mind that the device does not need to be perfectly transparent, merely enough that one can see fluorescence through an inverted microscope in the operational region. For some applications it may even be sufficient to have a transparent window in a region separate from the electrode array on the same substrate. It is also important to keep in mind the autofluorescence of the device, the fluorescence that the device exhibits even in the absence of any fluorescent dyes. If this is larger than that exhibited by the dye it applies an artificial limit to the sensitivity achievable on the device.

1.4.3 Scalability

The more multiplicitous a device is, the easier it is to stochastically analyse materials with it. This is because localized aberrations, contaminants, dead

electrodes, etc. can be ignored with minimal effect on the overall sensing resolution. Additionally it makes microfluidic integration significantly easier by obviating the need for precise placement. It can also be critical for experiments requiring multiplicity. If one needs to analyse dozens of different factors simultaneously, it is much easier to do so in different regions on the same device rather than fabricating and controlling dozens of devices.

1.4.4 Addressability

The dimensionality of the addressability of electrodes is critical in controlling the device, especially as the number of electrodes increase. Often-times the controlling hardware or interface is a limiting factor, and thus if you can only control N input lines, the effective limit of the number of controllable electrodes is limited by that. For example 1D addressing would only be able to activate N electrodes through N control lines, while pure 2D addressing could control $(N/2)^2$ electrodes through N control lines. This is shown in Figure 3.

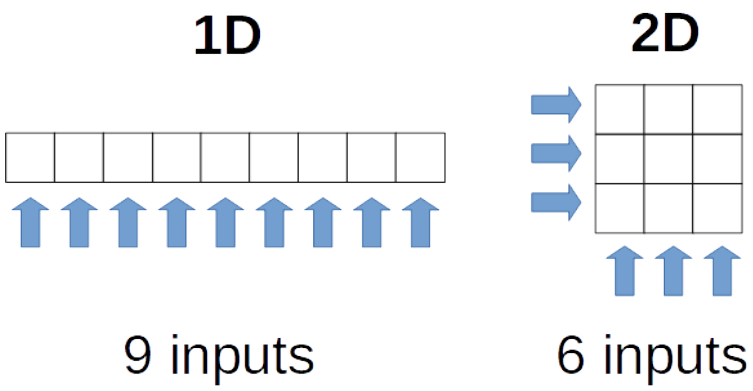

Figure 3: 1D vs 2D addressing

1.4.5 Fill Factor

When measuring networks, sparse cultures, and other spatially limited biological systems it is important to guarantee that event of interest is electrically detectable. The Fill Factor (FF) is the percent of the surface of the device is that covered by addressable electrodes. This is a property that can be spatially modified because the electrodes on the device do not need to be universally coherent. When monitoring biological systems, particularly sparse ones, care must be taken that the event of interest occurs in a measurable area, thus the higher the fill factor, the higher the likelihood of such a successful match. For example, in the case of a single neuron firing, assuming its position is random and its size is small with respect to the substrate, if the FF is 0.5, there would be a 50% chance of detecting that signal, while if the FF is 0.9 there would be a 90% chance of detecting it.

1.4.6 Spatial/Temporal Resolution

Complementary to the FF is the spatial resolution, the space between electrodes within a given area. The necessary spatial resolution is primarily determined by both the size of the object or structure being analysed as well as the necessary specificity. For example, if two actions of interest are occurring simultaneously, and they occur on the same electrode they cannot be meaningfully differentiated. If one is only interested in a binary determination this is of less importance, but for specific measurements such as the measurement of smaller structures and single cell measurements, it is vital. However, some properties need only be considered in aggregate and as such require lower spatial resolution.

Similarly, the temporal resolution required is determined primarily by the speed of the phenomenon being studied. This is mostly determined by the gating and control mechanism. Many biological phenomenon, for example the response of electrogenic cells, are time-limited, for example the pulsing of a neuron occurs on the scale of a few ms, and unless a system has temporal resolution on a similar scale such events become impossible to measure reliably. However, state based actions such as cell death or the bonding of actions occur on much slower timescales, minutes to hours.

1.4.7 Sensing/Stimulation

Some devices for electrical measurement are incapable of stimulation. Most methods of electrically induced motion require stimulation, and as such being able to stimulate is functionally equivalent to having a built in mechanical control system. Electrical stimulation is necessary for impedance measurement, but it is also commonly used in stimulating many electrogenic cells such as neurons. Additionally, the ability to apply electrical signals to an electrode can be a mechanism for inducing motion through methodologies such as ElectroWetting On Dielectric (EWOD)[22] to move bulk fluids, and DiElectroPhoresis (DEP)[21] to move cells and smaller particles.

1.5 Research Challenges

While all of the above properties are critical to the final device, it's important to separate them into gross and fine categories. Gross properties are those that are

fundamental to the device technology itself, for example addressability is primarily determined by the device technology so it would be a gross property while biocompatibility, which is arguably the most fundamentally critical property, is modifiable with most technologies by changing electrode materials or depositing surface films. Thus when choosing the initial technology the gross properties we will consider are addressability, scalability, transparency, and whether it can sense and stimulate simultaneously.

When it came to performing impedance analysis and experimentation on cells and biochemical structures, the primary structures dealt with control and stability. It is important to control the synchronicity between the fluoroscopic, stimulating, and sensing apparatus through a monolithic control program that will communicate with all the equipment and collate their data. Furthermore the process stability to ensure an absence of cytotoxicity or degradation of compounds.

1.6 Significance & Originality

State analysis, and specifically electrical and impedance analysis of biological cell cultures is a mature, and well proven field. Most of them however, focus in exclusivity on either that or optical analysis of cell state. There has been some work on sandwich impedance measurements using electrodes to measure the impedance, but unfortunately these rely on either MEA or CMOS technology making them opaque and unsuitable for in-vitro application, instead monitoring sampled flows passed through the array.[23]–[28] These have done many of the same measurements we hope to do in our device, but they are limited in scale compared

to our device. There has been some work on using tTFT electrode arrays similar to our device, but they utilize an amorphous silicon channel rather than an IGZO channel resulting in inferior electrical properties and limiting the scale of the process. [28]

This is the first research on using 2D planar tTFT electrode arrays to collate fluorescent and impedance spectroscopy information of cell cultures in-vitro simultaneously. This enables an increased efficiency in the operation of a variety of experiment archetypes such as those explained later on in this work, by reducing assumptions on cell location by enabling direct observation. Additionally it makes initialization of novel experiments trivial as you can perform simultaneous optical and electrical measurements during that stage, and save the mutation induced by the fluorescent dyes for more critical stages later on in development. Furthermore, it greatly increases the multiplicity of a simultaneous experiment by allowing the spatial isolation of various sensing materials on the same substrate, and by determining the location of a change in the electrical properties the presence of an analyte in a given area can be determined.

1.7 Current Methodologies

1.7.1 Fluorescence

The current gold standard in biological analysis of cells is fluorescent microscopy. It was developed in 1967 by Dr Ploem, who demonstrated the use of beam splitting with dichroic mirrors to induce fluorescence and monitored it via an inverted microscope.[29] The basic tool of fluorescent microscopy is caged dyes

also known as caged fluorophores. A fluorophore is a material that emits light at one wavelength, when excited by light at a different wavelength. It is known as a “caged” fluorophore because it does not fluoresce under normal conditions, but only when it bonds with a certain molecule that it is targetted to which makes it “uncaged” and thus fluorescent.[30] Unfortunately these tend to be cytotoxic, damaging to cells, though recent advances have been made in reducing the damage done by these cells to allow monitoring on the scale of days rather than hours.[31], [32]

1.7.2 Voltage Sensing

One area of interest when electrically analysing cells is that of the voltage sensing of cells, which is fundamentally broken into two sub-groups, direct and indirect. Direct voltage sensing involves directly reading the voltage of an electrogenic cell such as a neuron with minimal mutation of the signal. This has been done on a wide variety of devices, particularly for neurons and cardiac cells. [10], [19], [33]–[35]

Indirect voltage sensing is the detection of signals modulated by the ionic activity of an electrogenic cell. This is primarily done with Ion Sensitive Field Effect Transistors (ISFETs) which modulate the current between the source and the drain of the transistor through the ion accumulation above the gate oxide.[36]

1.7.3 Impedance Spectroscopy

Impedance Spectroscopy is using the impedance between two electrodes to differentiate between different object and materials. By analysing the impedance across an entire spectrum of driving AC frequencies, quite sensitive

characterizations can be performed on a wide variety of objects. While there are many properties this cannot measure, any cell function involving ion transfer or a change in membrane capacity can be accurately measured. This has been applied to applications ranging from cell counting, cell state differentiation, detection of electrogenic activity, and even differentiation between different varieties of cancer. [8], [20], [37]–[39].

1.7.4 Comparison

Table 1: Methodology Comparison

	Fluorescence	Voltage	Impedance
Measurable Properties	All	Membrane potential	Ionic transfer, Conductivity,
Substrate	Transparent	Electrodes	Electrodes
Equipment	Microscope	Circuitry	Circuitry
Cytotoxicity	High	Low	Low

1.8 Current Devices

1.8.1 Metal Oxide Semiconductor Field Effect Transistors (MOSFET)

The oldest and most established method of constructing electrode arrays is through integration with conventional MOSFET fabrication technology. Their miniaturization, and thus potential density is unparalleled as the transistors can be built on even the nano-meter scale, small enough for essentially any desired observable biological agent. Due to their miniaturized size, not only can they measure conventional biological agents they can even be used for the detection of some of the larger bio-molecules.[14]–[16], [40], [41] Unfortunately due to the reliance of conventional MOSFETs on silicon substrates they are inherently opaque,

making optical analysis difficult. They do however offer an extremely large surface area and have feature size fabrication on the nm scale.

1.8.2 Multi Electrode Array(MEA)

An MEA is a series of electrodes deposited on a substrate directly connected to control pads on the exterior ring of the device. An example of an MEA designed by the company MED64 is shown in Figure 4.[42]

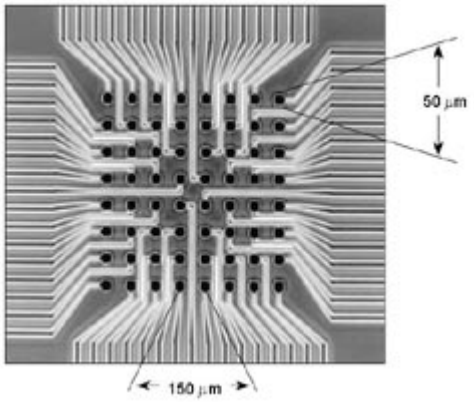

Figure 4: Commercially available MED64 MEA[42]

The first MEA was developed in 1972 by Thomas et. al who deposited metal structures on a glass substrate in order to analyse the electrogenic activity of cells in-vitro.[43] They utilized Pt/Au gold electrodes in their design, but unfortunately platinum has a tendency to degrade making it suboptimal for long term observation or reuse.[44] Since then there has been a great deal of experimentation with electrode materials/design, as well as electrical isolation of the pathing lines.[45]–[47] While they tend to have by far the best electrical properties compared to other electrode arrays, they are steeply limited in their scalability and addressability due to the direct connection between control pads and the electrodes.

1.8.3 Ion Sensitive Field Effect Transistor (ISFET)

ISFETs, also known as Open-gate Field Effect Transistors (OFETs) are devices commonly used to detect ion transfer in biological systems. They are essentially MOSFETs with the gate electrode removed and having the insulating layer connecting with the culture as shown in Figure 5.

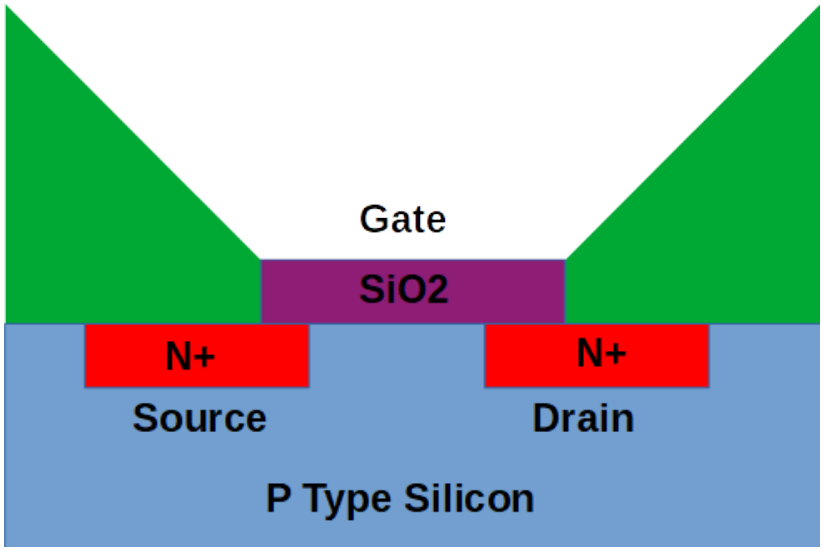

Figure 5: ISFET Structure

These are commonly used for the detection of electrogenic cells such as neurons and olfactory cells.[36], [48] Unfortunately, these devices are limited to pure sensing applications due to the interactive terminal being the gate, and additionally they tend to be made with conventional MOS processes making them opaque and thus unsuitable for optical observation. Additionally, due to the photovoltaic effect, the electrical properties of the device could be changed unless care is taken during experiment design.

1.8.4 Thin Film Transistor (TFT)

TFTs, are transistors composed of thin layers of deposited materials upon an arbitrary substrate as shown in Figure 6.

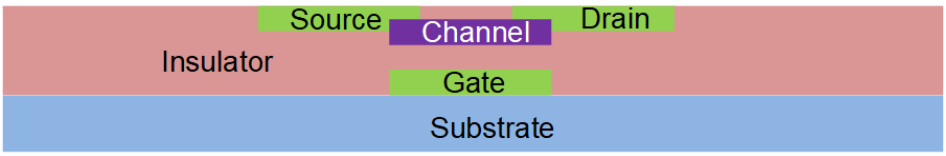

Figure 6: TFT structure

They were originally developed for the backplane of Liquid Crystal Displays where they control the activation of pixels.[18] They are functionally quite similar to MOSFETs, however due to their fabrication method differing they are capable of being nearly transparent if the semiconductor, metal, and substrate materials are appropriately chosen.

1.8.5 Comparison

Table 2: Comparison of state of the art device types

	CMOS	MEA	ISFET	OTFT	tTFT
Reference	[49]	[50]	[36]	[51]	This Work
Stimulation	Y	Y	N	Y	Y
Transparency	N	Y	N	Y	Y
# Electrodes	59760	64	100	1	22500
Active Area	10.9mm^2	0.180mm^2	1.25mm^2	1.05mm^2	240mm^2
Pitch	60µm	100µm	500µm	N/A	50µm,100µm
Gap	13.5µm	30µm	400µm	N/A	2.5µm-15µm

Density	4%	12%	20%	N/A	95%
Die Size	12mm x 8.9mm	76.2mm x 25.5mm	10mm x 10mm	N/A	25mm x 27mm
Addressability	√N	N	√N	N	√N

1.9 Impedance Spectroscopy Device Structures

When it comes to device for impedance spectroscopy there are two primary electrode configurations. The more common type of device is the microchannel impedance spectroscopy structure. This consists of a microfluidic channel with an electrode on the alternate sides. The reason this structure is prevalent is that, due to being integrated in a microfluidic channel, measurement of a given analyte can be guaranteed even with a small amount of electrode coverage. These types of devices have been used for decades to perform cell counting and characterization. [27], [31], [38], [52] The downside of these devices is that due to the microfluidic integration they necessitate cell sampling apparatuses to function and are unsuitable for direct application to living cultures. The general structure of a microchannel impedance spectroscopy setup is shown in Figure 7.

The other electrode configuration commonly used for impedance spectroscopy is the planar setup. In this configuration the electrodes are organized on the same horizontal plane. This has been used to identify and characterize a large number of biological systems, though is commonly used for cells, particularly sensitive cells that are difficult to sample such as neurons.[53]–[56] The main downside to this configuration is that its sensitivity is significantly worse than that of the channel configuration. This is a result of the difference in the pathing of the

electric field lines, in the case of the microchannel structure the planar opposing sections are the main surface area of the electrode, while in the planar structure the planar opposing sections are the edge of the electrode, having significantly lower surface area. This in turn makes the use of conventional transistor gating difficult as it is multiplicatively interactive. The two structures are visualized below in Figure 7.

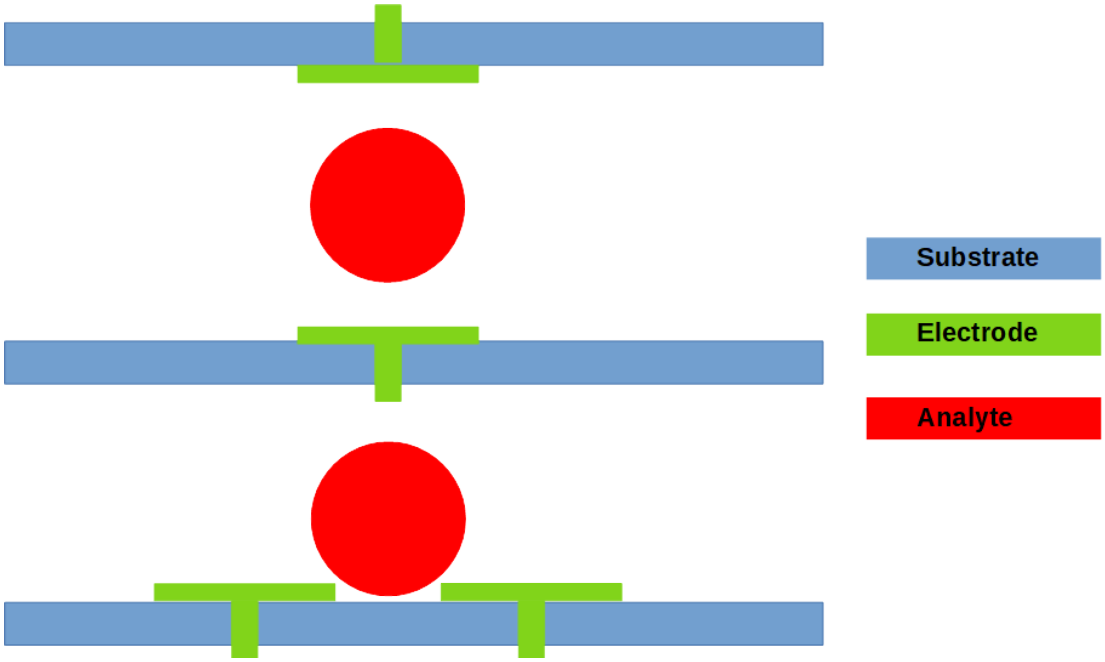

Figure 7: Comparison of channel impedance spectroscopy device(Top) and planar impedance spectroscopy device(Bottom).

1.10 Thesis Structure

This thesis will continue with a discussion of the theory behind the experimental methodology and analysis in Chapter 2. Afterwards we will discus the design, preparation, and characterization of the device in Chapter 3. We shall then proceed with an explanation of the experimental setup and equipment used in Chapter 4. We will then explain the specific experiments and their results in Chapter 5. Discussion of the results and future work will continue in Chapter 6. The

Appendices will contain the code for the control program as well as specific information on some of the techniques used. A pictographic representation of the structure is shown in Fig. 8.

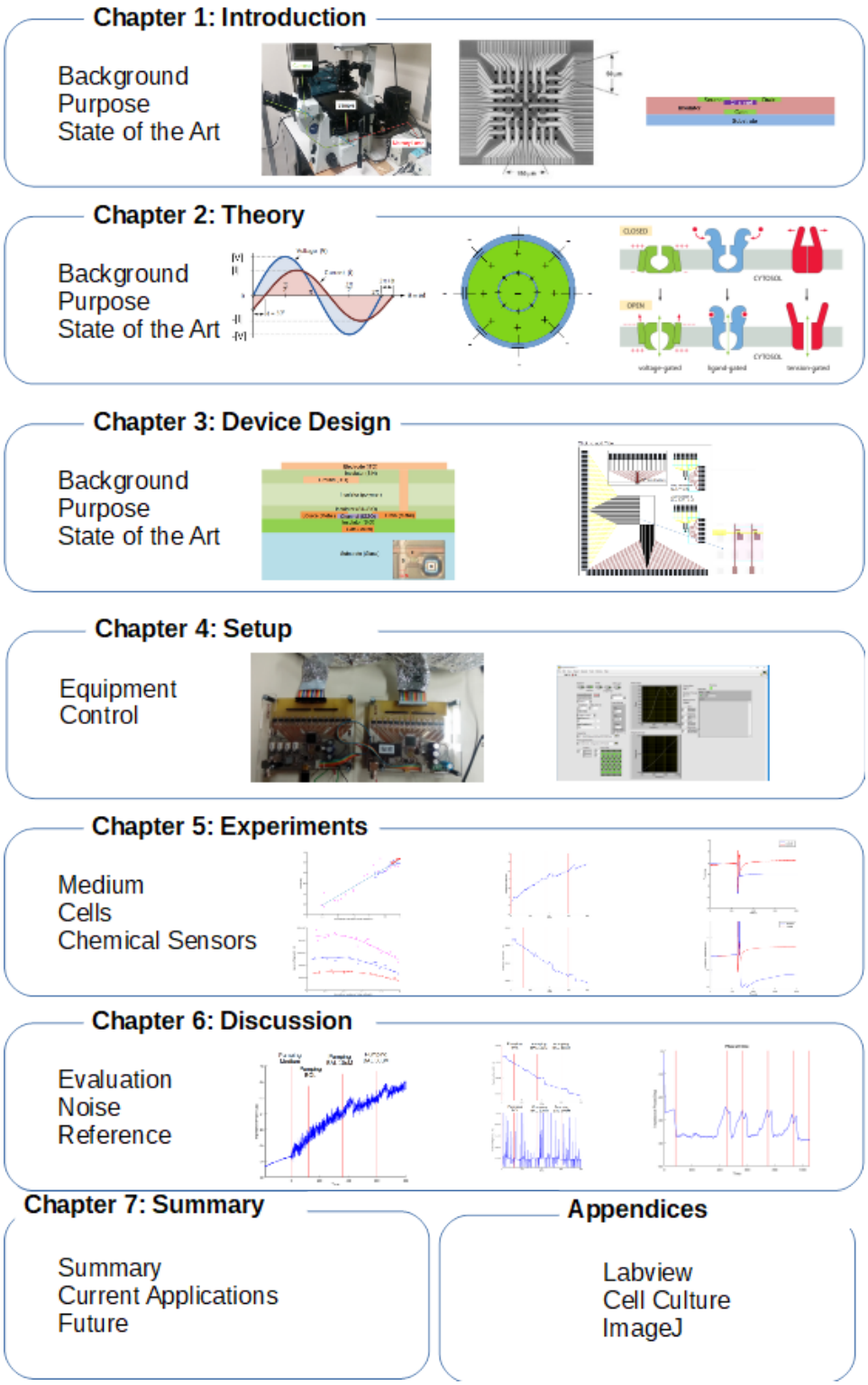

Figure 8: Chapter Schematic

1.11 Chapter Summary

In this chapter we introduced our work on In this chapter we laid the background for our research on 2D planar biosensors utilizing impedance spectroscopy on a thin film transistor plate. We described the background of this work, as well as why it needs to be improved. We explored several different device methodologies, and demonstrated why we believe a tTFT system is optimal. We have also explained how this work differs from others in the field.

Chapter 2:Theory

This chapter elucidates the theory and principles behind the electrical and optical analysis of cell cultures and biological agents. We will start with the physical structure of a cell, and how it can be treated as an electrical system. Then we will discuss various means of analysing cellular cultures, and continue with a discussion of the inherent noise in biological systems. We will then proceed with different potential TFT designs and the theory behind some of the previously demonstrated applications of our device that will be integrated with our work.

2.1 Impedance

2.1.1 Impedance Basics

Electrical impedance is the AC analogue of resistance. It can be thought of as the complex domain abstraction of the purely real valued resistance. The equation is on the surface quite similar to the conventional Ohm's law.

$$R = V / I$$

$$Z = V / I$$

Where V is voltage, I is current, and Z is the impedance.

Because the AC impedance, current, and voltage are sinusoidal this form is impractical. Thankfully it can be broken down into real, measurable components. The common way it is envisioned involves the complex exponential described by Eulers formula.

$$e^{j(\omega t-\phi)} = \cos(\omega t-\phi) + j\sin(\omega t-\phi)$$

Where ω is the frequency, and φ is the phase shift of the sinusoid.

By representing all factors, which we know are sinusoids and thus representable by complex exponents, we get the exponential version of Ohm's law (V=IR), which can be used to calculate the impedance

$$|z|e^{j(\omega t-\phi_z)} = \frac{|V|e^{j(\omega t-\phi_v)}}{|I|e^{j(\omega t-\phi_i)}}$$

$$|Z|e^{j(\omega t+\phi_z)} = \frac{|V|}{|I|}e^{j(\omega t-(\phi_v-\phi_i))}$$

Where φ_x is the phase shift of the component in the subscript.

This demonstrates that the impedance can be calculated if we measure two values, the relative magnitude of the voltage and the current, as well as the phase lag between the voltage and the current, both of which are real, and physically measurable.

$$|Z| = \frac{|V|}{|I|}$$
$$\phi_Z = \phi_V - \phi_I$$
$$Z = |Z| e^{j(\omega t - \phi_z)}$$

A graphical representation of this is in Figure 9.

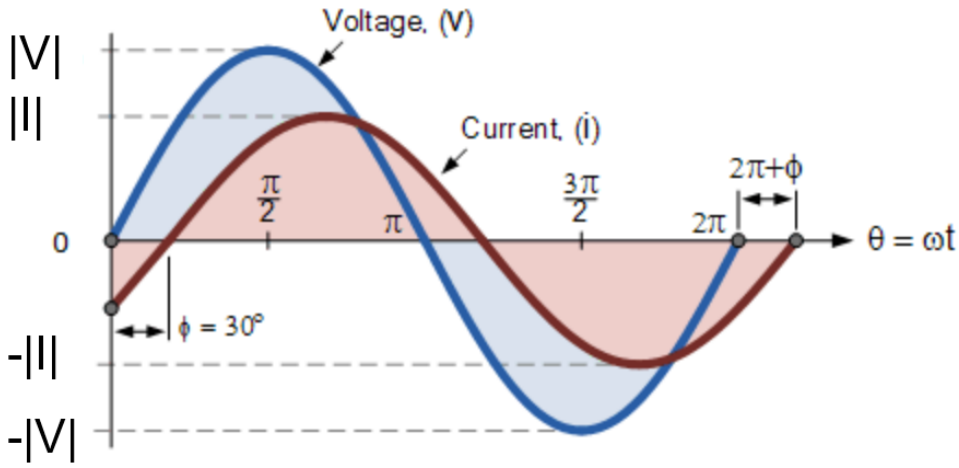

Figure 9: Diagrammatic representation of impedance

2.1.2 Electrochemical Impedance

When looking at the impedance measured between two electrodes in an electrolytic solution, there are several factors that must be accounted. While the electrical properties of the medium and the analyte obviously have an effect on the measured impedance, there are multiple other components that influence the measurement.

One factor that must be accounted for is the double layer capacitance of the electrodes. An electrical double layer is formed as ions from the electrolytic solution approaching the electrode, but located several angstroms away. That small gap acts as an insulating layer. This can vary with the voltage being applied, the electrolyte being used, and any impurities or roughness of the electrode but is typically assumed to be 20-60 uF per cm^2 of surface area.[57]

When a given electrodes voltage is pushed away from its null state value, it naturally opposes that reaction. The process is known as polarization, and the opposition is physically caused by a redox reaction, in our case the oxidation and reduction of ITO to and from ITO black. This in turn causes the polarization resistance as it opposes the induced change. This is the dominant property at high frequencies. This is governed by a property known as the charge transfer coefficient, which roughly relates how easily a material undergoes a reduction or oxidation reaction. O'Mullane et. al found that the anode and cathode charge transfer coefficient was 0.55 and .45 respectively assuming symmetric stability.[58] The net voltage caused by this reaction is given by the equation below where V_{corr} and I_{corr} are the corrosion voltage and current respectively, β_a and β_c are the anode and cathode charge transfer coefficients respectively, and r_p is the polarization resistance.

$$V_{corr} = \frac{\beta_a \beta_c}{2.303(\beta_a + \beta_c)}$$
$$I_{corr} = V_{corr} / r_p$$

Another electrochemically induced confounding factor is that of the charge transfer resistance, which is the resistance to the measured signal caused by a unidirectional reaction. This effect is dominant at low frequencies where only an exclusive anodic or cathodic reaction is occurring. Its operation is given by the Butler-Volmer equation given below with the assumption of an absence of over-potential.

$$R_{ct} = \frac{RT}{nFi_0}$$

When combining these factors together it is important to know what frequency range we are operating in as typically either the polarization resistance or the electrical transfer resistant will be negligible. In the case of our experiments where we are operating at around 1kHz, a relatively low frequency, we can ignore the polarization resistance. From this, we can construct a conventional Randles Cell with the only significant difference being that instead of using the solution resistance, we will be measuring an analyte, a cell or bio-molecule, which will be abstracted later on. This is shown in Figure 10.

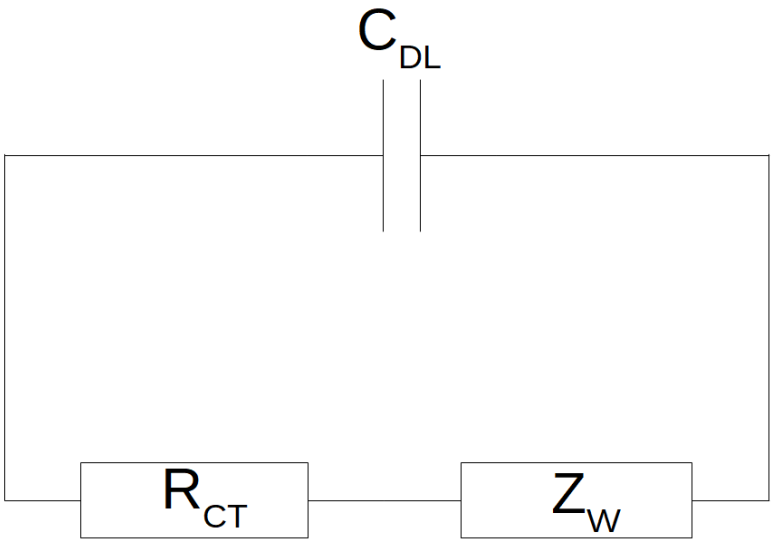

Figure 10: Randles Circuit combining electrochemical elements

2.2 Biological Compounds

2.2.1 Cellular Structure

Cells can be broken down into two major categories, eukaryotes, and prokaryotes which are defined by the presence or absence of a nucleus respectively. [59] The nucleus isolates the genetic material of the cell and is generally impermeable to large molecules. All cells have a lipid bi-layer known as the cell membrane which isolates the cell from its environment. The cell wall, commonly found in prokaryotes, and rarely in eukaryotes is a harder fibrous structure on the outside of the cell membrane that further protect the cell from its environment. The fluid inside the cell is known as the cytoplasm and functions as the cells storage for desirable biomolecules and ions. Cells need ions to function properly, and the transmission of ion across the cell membrane is regulated by ion channels which maintain dyshomeostasis between the cytoplasm and the cells environment. Within

the cytoplasm are a large number of organelles that form a variety of functions within the cell that are outside the scope of this work. A diagram of a eukaryotic cell is shown in Figure 11.

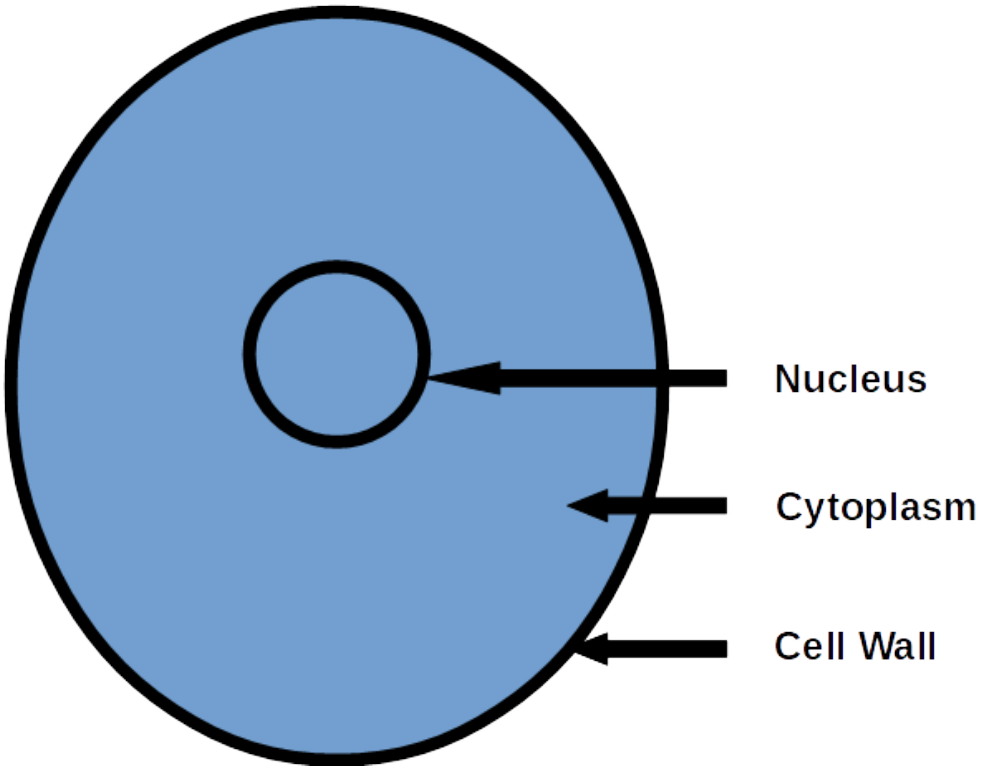

Figure 11: Cellular Structure

When dealing with prokaryotes, particularly in the case of dependent cells such as organ cells, it is also important to consider their growth environment. They are incapable of growing in a raw environment and require what is known as an extracellular matrix in order to remain viable. An extracellular matrix is a three dimensional network of primarily structural macromolecules such as collagen as well as glycoproteins for adhesion and enzymes for controlling growth and communication pathways.[60], [61] When a cell that relies on an extracellular matrix

grows it exudes new areas of the extracellular matrix extending beyond the cell, called feet, that the cells descendants can grow into.

2.2.2 Cellular Electrodynamics

As previously mentioned, the electrical property we are most concerned with when it comes to analysing cells is the impedance of the cells. This is primarily determined by two physical factors, the resistance change of the cytoplasm and its immediate environment, and the double layer capacitance across the cell membrane. Both of these properties are primarily controlled by the degree of ion transfer across the cell membrane, which as mentioned before is mediated by ion channels. Ion channels are protein structures that enable either the passive or active flow of ions into or out of the cell depending on their configuration We are primarily concerned with gated channels as they enable dyshomeostasis. A gated channel is one in which the channel is only “active” when a condition is met, most commonly when a certain voltage differential across the membrane is reached or a signalling chemical contact the channel as shown in Figure 12.[62]

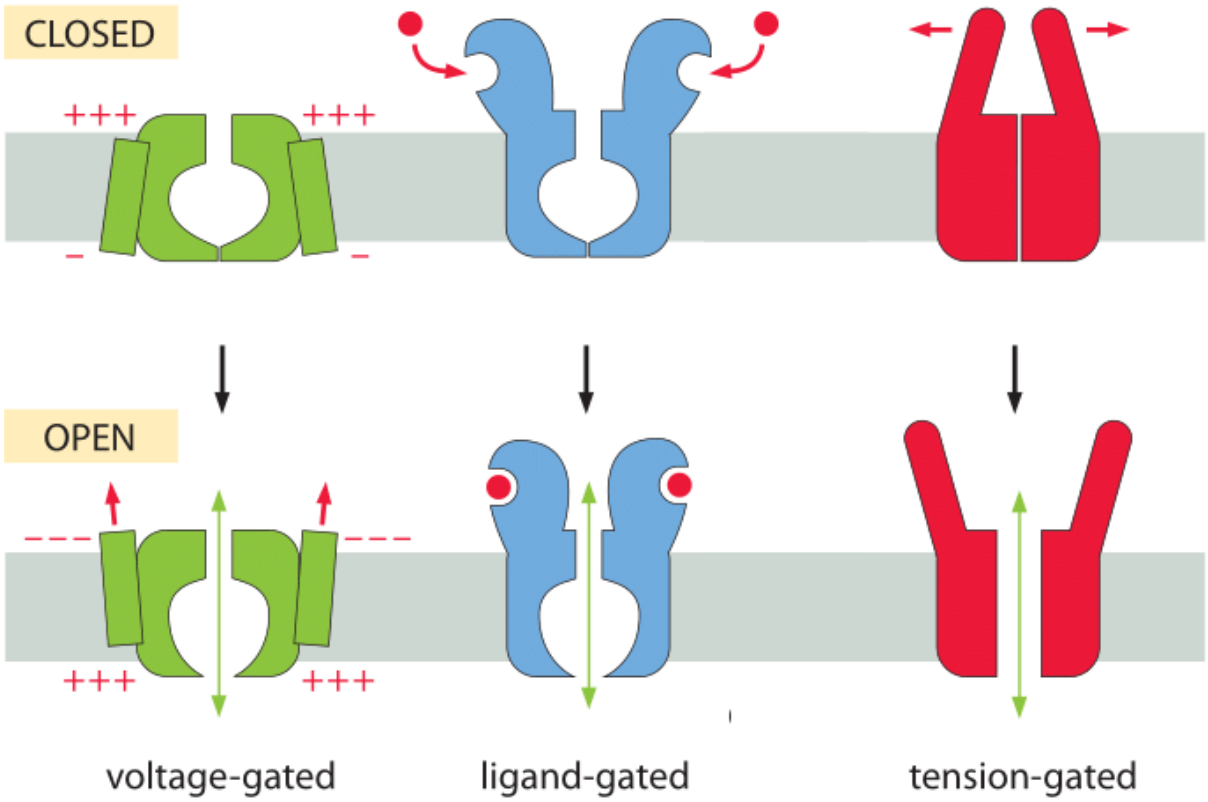

Figure 12: Common types of ion channels[62]

Ion channels are often extremely selective, only transferring a particular type of ion such as K^{+}, Na^{+}, Ca^{+2}. By controlling the genes that a particular cell expresses, the quantity and type of gated ion channels can be controlled.

2.2.3 Electrical Model

When it comes to building an electrical model, as mentioned we are primarily interested in the resistance changes due to ion concentration as well as the double layer capacitance across the cell membrane. In the case of prokaryotic cells, this is relatively simple to represent using conventional circuit terminology, with || representing the two components are parallel with one another.

$$Z_{Cell} = Z_{solution} \| \left(2\, Z_{Membrane} + Z_{Cytoplasm} \right)$$

However, in the case of eukaryotic cells, one must also make sure to account for the effects of the nucleus, which will have its own double layer resulting in.

$$Z_{Cell} = Z_{solution} \| \left(2\, Z_{membrane} + \left(Z_{Cytoplasm} \| \left(2\, Z_{NucleusMembrane} + Z_{NucleusCytoplasm} \right) \right) \right)$$

By using the common assumption that inductance is negligible and components are either resistive or capacitative, this can be represented as a circuit schematic in Figure 13.

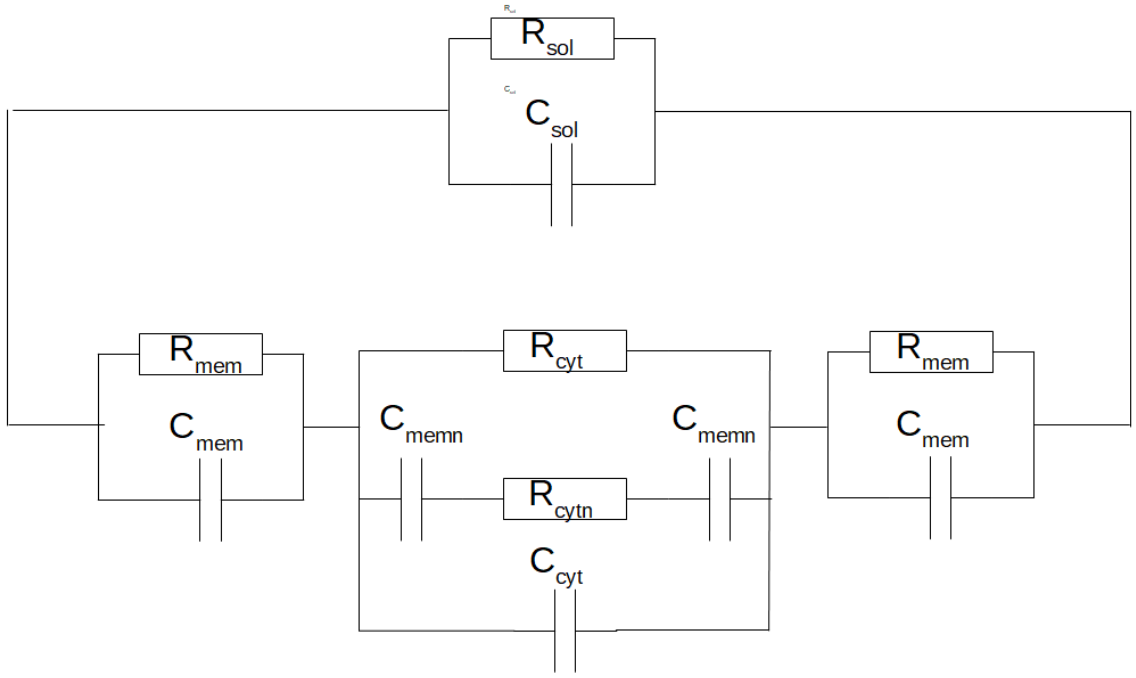

Figure 13: Electrical schematic of a biological cell

Unfortunately, when dealing with a live culture, it is unlikely that only one cell will be measured, so one must use an approximating linear scaling factor, $k_{culture}$ to account for multiplicity as well as imperfectly positioned cells. Assuming that the field lines doubly intersect the membrane this would be a constant factor

$$Z_{Culture} = k_{Culture} * Z_{Medium} \| \left(2 Z_{EDL} + \left(Z_{Cytoplasm} \| \left(2 Z_{NucleusEDL} + Z_{NucleusCytoplasm}\right)\right)\right)$$

It is important to remember that in the event of a cell that requires an extracellular matrix, that impedance will be in parallel with the medium with a magnitude depending on its thickness relative to the electrode height. In theory this value should be stochastically, if not deterministically consistent for a given cell culture. When dealing with an array of electrodes, it important to take into account that the signal will not take only the shortest path, but will in fact spread infinitely throughout the electrode array weighted by the path length, with k_{length} being equal to the integer path length times the culture constant defined above.

$$Z_{Total} = \sum_{\|} k_{Length} * Z_{Medium} \| \left(2 Z_{EDL} + \left(Z_{Cytoplasm} \| \left(2 Z_{NucleusEDL} + Z_{NucleusCytoplasm}\right)\right)\right)$$

Putting this all together with the transistor and electrochemical effects, we get the schematic shown in Figure 14.

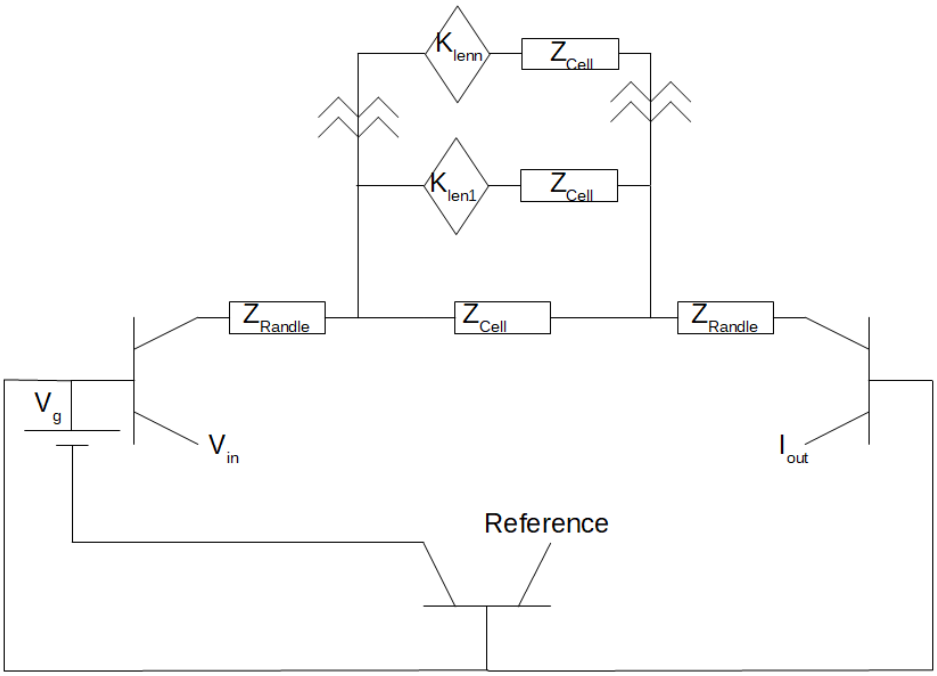

Figure 14: Schematic of entire system

2.2.4 Antibodies

Antibodies are a fundamental part of our immune system. They evolved to bind to potentially harmful cells such as bacterium. They do this by attaching to specific molecules that they use to identify specific antigens, or even classes of antigens depending on the type of bonding site. A pictographic representation of this is shown in Figure 15.[63]

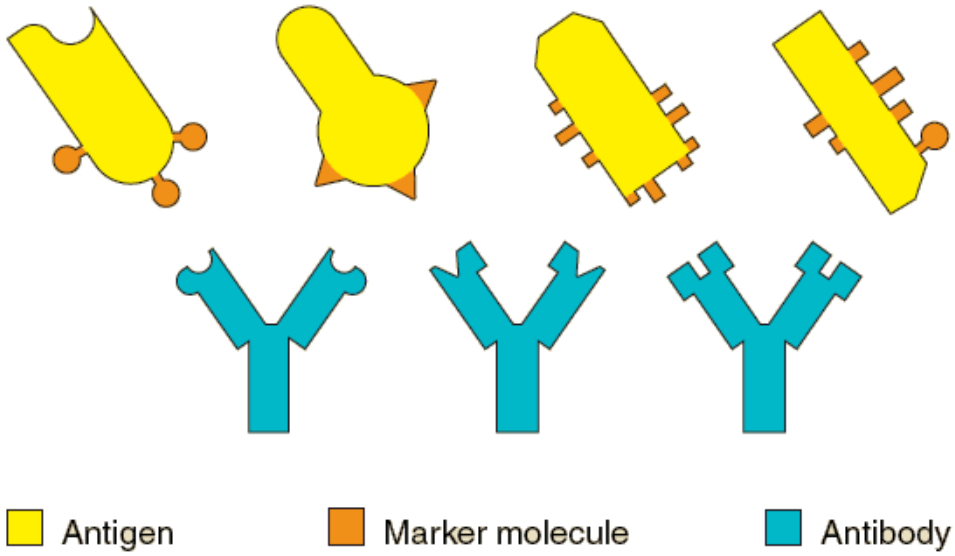

Figure 15: Antibody/Antigen interaction[61]

They do this in order to either mark the target cell for termination by white blood cells, or in some cases if enough antibodies bond to an antigen they are capable of destroying it by collectively causing enough pressure to tear its cell membrane apart, killing harmful bacteria.

2.2.5 Antibody Electrodynamics

The electrical detection of antibodies, and particularly the bonding of antibodies and antigens is primarily done by detecting the changes in surface properties. It has been known for decades that the conductivity and dielectric

constant of an antibody is significantly different from that of an antibody/antigen complex. This in turn will represent a change in resistance and capacitance that will be represented in the impedance. Additionally, due to electrochemical effects, the randles circuit, and more specifically the charge transfer resistance will drop as the antigens are bonded to the antibody due to the prolonged antibody/antigen chains disrupting the inherent ionic double layer formed at the surface of the electrodes as an AC voltage is applied.

2.2.6 Antibody Electrical Model

As we have previously mentioned, the bonding of the antigen with the antibody will be represented in a change in local conductance and dielectric constant, which in turn will manifest as a change in capacitance and resistance. [64] The standard equation for planar capacitance, and resistance are given by

$$C = \frac{\epsilon_0 \epsilon_r A}{D}$$

Where C is the capacitance ε is the permittivity, A is the area of the plate, and D is the distance between them.

$$R = \frac{D}{\sigma A}$$

Where R is the resistance, and σ is conductivity.

This gives the equation for a single antibody/antigen complex as

$$Z = R_{medium} \| \left(R_{Antibody} \| C_{Antibody} \right)$$

However, much like cells, and in fact to a much greater degree, stochastic multiplicity must be taken into account resulting in

$$Z_{Electrode} = k * R_{Medium} || \left(R_{Antibody} || C_{Antibody} \right)$$

Where K is a linear scaling factor accounting for the number, positioning, and bonding ratio of the antibodies deposited on the device.

Taking into account the distributed electric field pathing The final equation becomes

$$\sum_{||} k_{len} * R_{solution} || \left(R_{Antibody} || C_{Antibody} \right)$$

where k_{len} is the path length * k for each respective path. This block will simply replace the cellular structure described in the prior section, but otherwise the full device structure is identical.

2.3 Indirect Bio-Sensing

While impedance spectroscopy is a powerful tool, it is typically limited in the size and classes of objects that it can measure. To get around this we can use intermediate objects which are large enough to detect objects that we cannot detect directly. The two components we will be concerned with are electrogenic cells and antibodies.

2.3.1 Electrogenic Cell Sensing

By using the electrical properties of electrogenic cells that we can detect the electrical properties, we can indirectly detect the molecules, typically volatile organics, that signal them to pulse their ion channels. There are many types of cells

that are good for this, but one of the most common are olfactory cells. Insect olfactory cells in particular are extremely effective, and multiple biochemical sensors have been developed that utilize their ionic transfer mechanism.[36], [65]–[67] The effect that will be measured by such a system is a direct result of the ionic pumping of the system causing a localized change in voltage as well as a modification of the capacitance across the cell and the double layer formation in the randles circuit at the surface of the electrode.

2.3.2 Antibody Sensing

Through the use of intermediary antibodies we are capable of measuring any antigens, or arbitrary objects labelled with antigen marker proteins. Depending on the specificity of the antibodies in question and how they are modified, this gives us a variety of assay for creating arbitrary specificity. These kind of antibody systems have been shown to have strong impedance responses in a variety of studies, and the immobilization process has become quite consistent and reliable.[68]–[72] These have demonstrated that the impedance of the bonded antibody/antigen increases by an approximately O(1) factor as compared to that of the antibody on its own. As such, we would expect similar results when those experiments are performed on our device, albeit with lowered efficiency due to the use of ITO and the losses across the transistor.

2.4 Noise

In this section we will give a description of the various types of noise and randomness we encounter in our experiments, and the mechanisms for mitigating them.

2.4.1 Biological Noise

All biological systems are inherently chaotic. One of the fundamental sources of this is the inherently stochastic nature of cell seeding, adhesion, and mitosis. Under conventional conditions, cells will typically grow in all directions. However, certain proteins, chemicals, and physical structures can influence the directionality of cell growth.[73]–[75] Even in the controlled cases however, the growth is only predictable stochastically, variations in cell size and position are essentially impossible to predict with specificity.

While an ideal electrogenic cell would respond only to a provided stimulus, in practice this is not always the case. In real cultures auto-activation, the activation of ion channels without a triggering signal, is a common phenomenon. These are a common source of electronic noise when measuring electrogenic cells due to the possibility of overlapping or interfering signals that can cloud measured data, and even prevent the recording of a desired signal from an intended stimulus. This is compounded by the fact that certain types of electrogenic cells, particularly neurons, form networks wherein the activation of one cell triggers the activation of others nearby greatly magnifying this issue.

One of the other source of randomness in biological systems is that cells are not uniform. Viable and functional cells can have a great deal of variance in size, membrane properties, growth speed, and even ion channel number and distribution. While rarer, significantly more drastic cellular dysfunctions can occur, the most notable of which is cancer, which can result in drastic changes of physical properties.

In a cellular culture the cells are not typically freely mobile and isolated. Typically they will strongly adhere to the substrate through the use of what is known as an extracellular matrix which also facilitates and enhances cell-growth and function.[61] While the composition of the matrix tends to be uniform, it's thickness can be highly variable, and in particular its surface morphology can present variable roughness that can interfere with measurement processes. Additionally its dielectric properties can also vary greatly warping signals as they traverse it.

2.4.2 Environmental Noise

When taking electrical measurements of anything, it is important to control and mitigate the effect of unintended electrical signals from within and outside the device from interfering with the measurement. One of the most common sources of noise is interference caused by stimulus signals, particularly when there are long parallel wires near the stimulating wire. One of the primary means of eliminating this kind of noise is by using twisted wire pairs rather than straight wires. As shown in Figure 16 this results in localized induced noise currents, but no net current resulting in minimal measured interference.

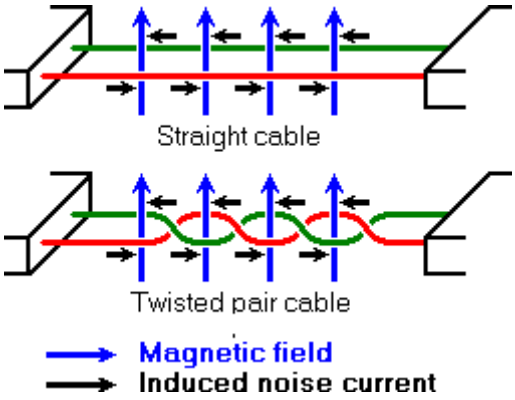

Figure 16: Twisted pair Vs. Straight comparison

Additionally, particularly in a laboratory environment, any other active electronics or wiring in the walls can result in electromagnetic noise that can influence measurement. AC wiring noise can typically be filtered out due it being between 50-60Hz depending on the country. For a more robust and universal solution to external noise, a Faraday cage is often used. A Faraday cage is a metal box or mesh structure that encloses the device under test. It operates by causing all induced remnant charges to be in the surface of the cage itself canceling out any externally induced electric fields within the cage.

2.4.3 Signal Processing

If information is known about the nature of environmental noise expected, or conversely about the measured signal it is often possible to extract the signal from the noise computationally. The simplest means of accomplishing this is through band pass filtering around the frequency range of the signal ignoring signals of a higher and lower frequency than expected, which logically can only be due to noise. If only one frequency is of interest a significantly more powerful method is available,

taking advantage of the orthogonality of sinusoids. Orthogonality is a property of sinusoids given by the following relation of two sinusoids of frequencies ω_1, and ω_2.

$$\begin{array}{c} iff\ \omega_1 = \omega_2 \\ \int_{t_0}^{t_0+T} \sin(\omega_1 t)\sin(\omega_2 t) = \frac{T}{2} \\ else \\ 0 \end{array}$$

The importance of this property for noise reduction is that it is an analytical method by which all frequencies except for that of interest can be removed for the purpose of measurement. This is accomplished by integrating the sensed signal with an input signal removing from the sensed signal all frequency components not present in the input signal.

If the noise can be assumed to be zero mean, then another mechanism by which noise can be mediated is using a sliding window aka moving average. A sliding window measurement is performed by taking a subset of N measurements, calculating their average, then incrementing the subset index by one as shown below for a discrete signal X with window size N.

$$Windowed[i] = \frac{\sum_{j=i}^{i+N-1} X[i]}{N}$$

While only applicable in circumstances where the noise can be assumed to be zero mean, or of a known bias, it is an effective mediation technique if the system is over-sampled.

2.5 TFT Designs

TFTs are a type of Field Effect Transistor(FET) that are largely defined by their fabrication technique; being constructed from thin layers of materials. The first TFTs were developed in 1962 by Dr. Weimar, who constructed them with a Cadmium Sulfide semiconducting layer.[76] Since then, the major improvements in the device design have come with advances in lithography as well as experimentation with different semiconducting materials ranging from those with better electrical properties such as Cadmium Selenide, to those with different optical properties such as Indium Gallium Zinc Oxide.[77], [78] In this section we will explore the various structures and basic types of TFTs.

2.5.1 Basic structure

The physical structure of a TFT is defined by two factors, gate position and the planarity of the conducting channel formed in the semiconductor. Depending on whether the gate is positioned above(Conventional) or below(Inverted) the semiconducting channel. A co-planar TFT is one in which the conducting channel formed by the MOS junction is directly between the source and drain, while a staggered TFT is one in which the conducting channel is above or below the electrodes depending on gate configuration. A demonstration of the different types of TFTs is shown in Figure 22.

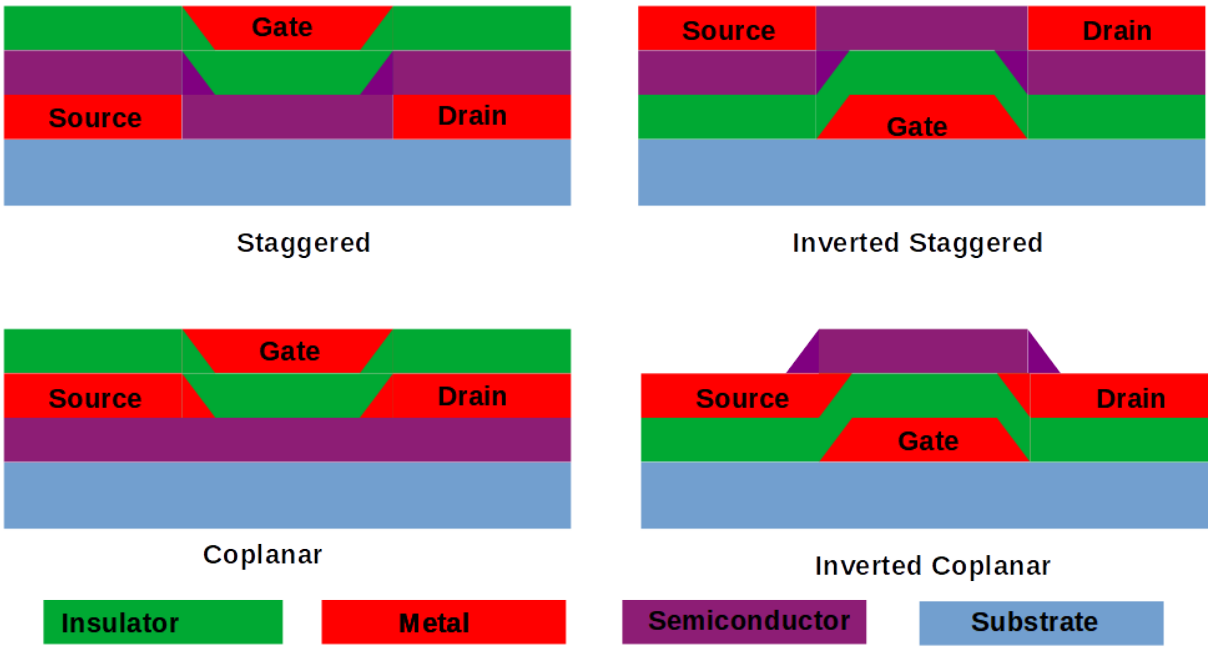

Figure 17: Different TFT structural designs

2.5.2 Hydrogenated Amorphous Silicon TFT

The most common modern type of TFTs are Hydrogenated Amorphous Silicon(a-Si:H) TFTs. As the name implies, their semiconducting layer is made from hydrogenated amorphous silicon, which has the advantage of being easy to manufacture on a large scale as well as being transparent.[79] They were first developed by Dr. Spear in 1979, and the semiconducting channel properties were moderated by Phosphorous (P) and Boron (B) impurities. Because of their ease of fabrication at large (m^2) scale, they are commonly used in the manufacture of Liquid Crystal Displays (LCDs). Since their development they have been continuously proved, and have a very high field effect mobility; 4.7 cm^2/Vs for inverted type TFTs. [80]

2.5.2 Poly-Silicon TFT

Poly-crystalline silicon is a form of silicon in which there are multiple pure crystalline regions within the structure. Its applications are quite similar to that of hydrogenated amorphous silicon TFTs, but TFTs with mobilities as high as 46 cm^2/Vs.[81] Further advances have been made by adapting the gate structure, which resulted in significantly better stability and gate driving current that came at the expense of increased difficulty, and thus cost, of manufacture.[82]

2.5.3 Organic TFT

Organic TFTs, which are TFTs made with organic polymers have opened up many potential applications involving flexible electronics.[83]–[85] On top of flexibility, organic TFTs can be fabricated in a low temperature process, and in fact can be printed by inkjet processes enabling cheap fabrication on even difficult to fabricate electronic substrates such as plastics. Additionally, while not quite as efficient as polycrystalline silicon TFTs, their mobility of up to 10 cm^2/Vs makes them better than even hydrogenated amorphous silicon TFTs, though they tend to be less structurally stable particularly on flexible substrates.[86]

2.5.4 Oxide TFT

Oxide TFTs are TFTs that have their active channel consist of a semiconducting oxide. A number of semiconducting oxides have been explored for the use of such devices including oxide compounds of silver, cadmium, zinc and indium, though recently there has been a great deal of interest in the Indium oxide compound Indium Gallium Zinc Oxide (IGZO).[87]–[95]

The first amorphous IGZO transistors were developed in 2004 by Dr. Nomura. [94] Their device had a mobility of 8.3 cm^2/Vs, was transparent and fabricated at room temperature. IGZO TFTs were first commercially demonstrated in 2006 when Sharp corporation fabricated LCD monitors with an IGZO back plane for the first time.[96]

2.5.5 TFT Comparison

Table 3: Comparison of TFT Technologies

Channel Type	Hydrogenated Silicon[80]	Poly-crystalline Silicon[81]	Organic Semiconductor[86]	Indium Gallium Zinc Oxide[94]
Mobility	4.7	46	10	8.3
Leakage Current	10^{-12}	10^{-12}	10^{-12}	10^{-13}
Substrate	Wafer/Glass/ Hard Plastics	Wafer/Plastic	Glass/Plastic	Glass/Plastic
Feature Size	1μm	50μm	50μm	5μm
Donor Type	N	N	N/P	N
Lifetime	Months	Years	Days(air) Months(vacuum)	Years
Process Temperature	350C	600C	100C	300C

2.6 Other Research on Similar TFT Devices

There has been a variety of research on both the analysis and manipulation of cells and materials done on our device. This is important to keep in mind, because our research is intended to integrate with other work to perform a universal analysis and manipulation platform on a single monolithic device.

2.6.1 DiElectroPhoresis(DEP)

DiElectroPhoresis(DEP) is the induced force upon a dielectric particle when it experiences an electric field gradient. Unlike electrophoresis, it does not require net charge, and in fact all particles exhibit dielectrophoretic activity, albeit to varying degrees. One aspect that makes it an extremely effective mechanism is that both the magnitude and direction of the force depends on the particle. If it is attractive to the stimulating electrode it is called positive DEP (pDEP), and if it is repulsive it is called negative DEP (nDEP). The equation behind the force, assuming a roughly spherical particle, is

$$F_{DEP} = \pi r^3 \epsilon_m \Re \frac{\epsilon_p^* - \epsilon_m^*}{\epsilon_p^* + 2\epsilon_m^*} \nabla (|E|)^2$$
$$\epsilon^* = \epsilon + \frac{j\sigma}{\omega}$$

Where F is the force, r is the radius of the particle, E is the electric field, ε^* is the complex permittivity, ε is the real permittivity, σ is the conductivity, and ω is the frequency.

But the part that determines the directionality, known as the Clausius Mossoti factor is

$$CM = \frac{\epsilon_p^* - \epsilon_m^*}{\epsilon_p^* + 2\epsilon_m^*}$$

Because this value is frequency dependent, at certain stimulating frequencies some particles will be attracted, some will be repulsed, and some will be barely affected. This means that the differentiation and sorting of objects by DEP is possible. Additionally, it is possible to extract information about the medium as well.

A demonstration of the attraction of yeast cells and the repulsion of micro-beads using our device performed by Dr. Tixier-Mita is shown in Figure 23.[21]

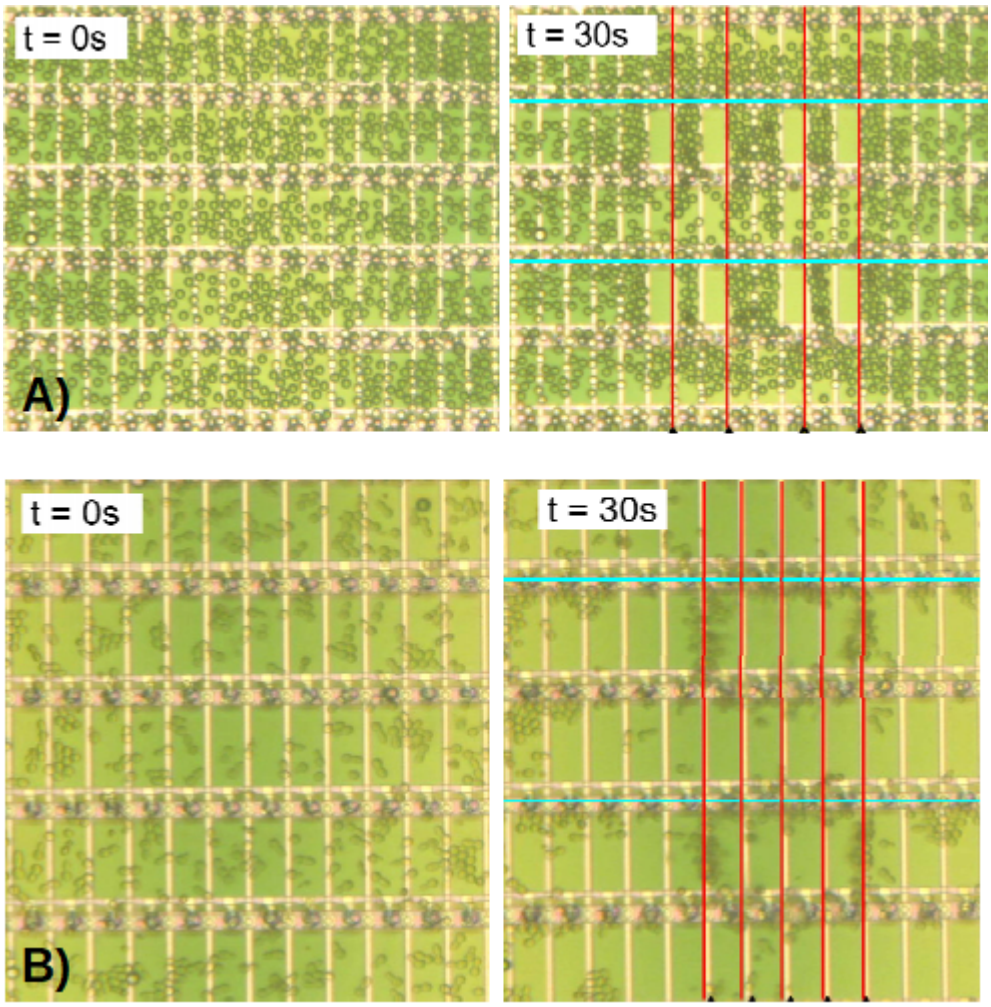

Figure 18: Demonstration of Negative(A) and Positive(B) Dielectrophoresis[21]

2.6.2 Electrowetting

Electrowetting is the modification of the wetting properties of a fluid droplet, physically presenting as changing the angle it contacts the surface. This requires a

high voltage, and as such cannot be done with most materials on a bare electrode. This issue is solved by depositing a dielectric film on the electrode with the resulting application being called ElectroWetting On Dielectric(EWOD). The equation governing the change in contact angle in EWOD is

$$\cos(\theta)=\frac{\gamma_{Electrode}-\gamma^{0}_{Electrode}+\frac{CV^2}{2}}{\gamma_{Fluid}}$$

Where θ is the contact angle, C is capacitance, V is voltage, and γ is the surface tension at various interfaces.

By doing this on adjacent electrodes in sequence it becomes possible to move droplets from one electrode to the other gradually moving it across an electrode array. Dr. Shaik performed these experiments on our device to move droplets and mix them together as shown in Figure 19.[22]

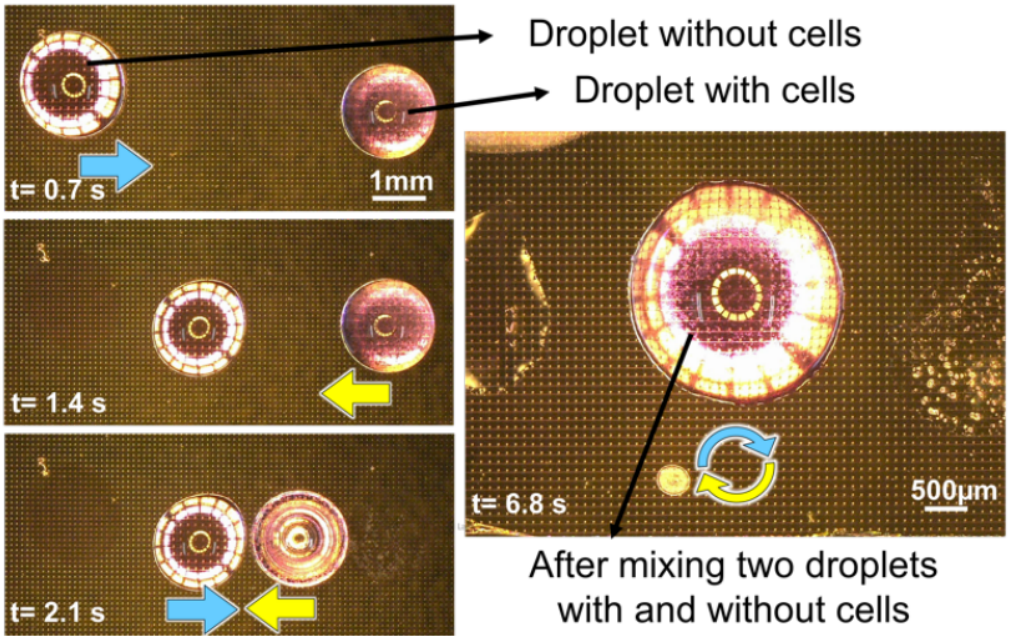

Figure 19: Movement and mixing of droplets using EWOD on our device[22]

2.6.3 Cell Potential Measurement

Another class of measurements that have been performed on our TFT device is that of the voltage measurement of electrogenic cells, specifically neurons. When neurons are stimulated with an electrical signal they respond by activating their ion channels causing an ionic pulse that is detectable as a voltage spike. Dr. Shaik performed experiments measuring such signals on our device, the results are shown below in Figure 20.[19]

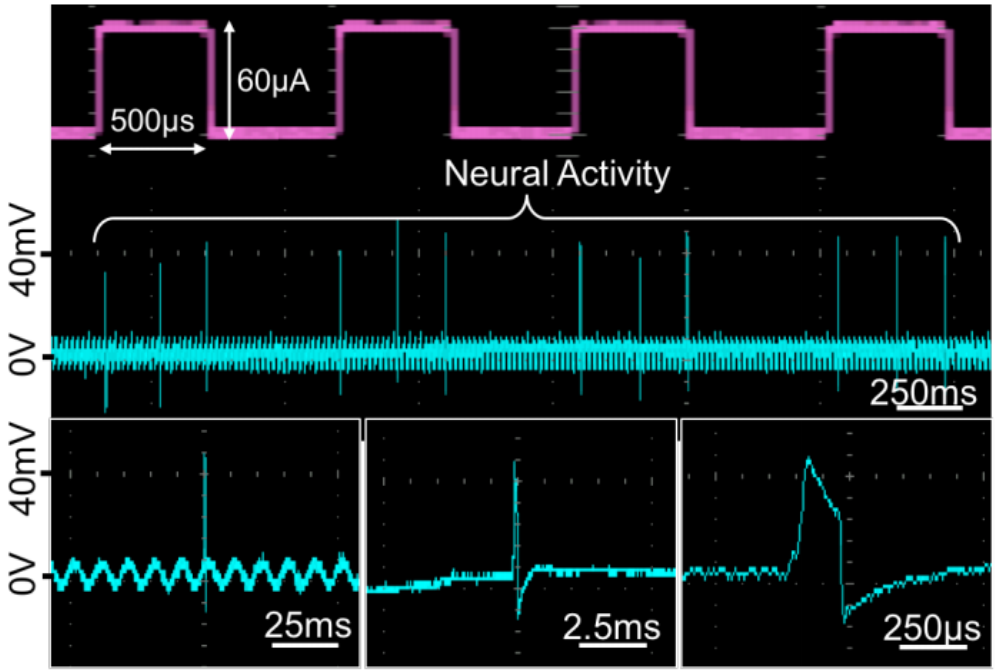

Figure 20: Neural activity recorded on our device with the stimulating signal in pink and the recorded response in cyan.[19]

2.7 Chapter Summary

In this chapter we explained the theory behind impedance spectroscopy and the various experiments we aim to complete on this device. We explored the

mechanics and electrical properties of the various biological structures, namely cells and antibodies, that we plan on measuring in our experiments. Furthermore, we discussed the nature of the noise we expect to encounter in our measurements and how we plan on mitigating it. Afterwards, we discussed the different types of TFT and why we decided on an IGZO TFT. We also gave an overview on several of the techniques performed on a tTFT substrate that would benefit from being monolithically integrated with our research.

Chapter 3:Device Design

In this chapter, we will explain the specifics of the design of the device. We will start with a discussion of how the device used in our TFT experimentation has evolved into its current state. Then we will discuss the structure of the transistor, and continue with a discussion of the electrode layout of the device. We will conclude with a characterization of the device.

3.1 Transistor

Our TFT plate was optimized and fabricated by Sharp Corporation.[97] It possesses a staggered bottom-gate design. The surface electrode upon which the biological experiments were conducted, was connected to the drain of the transistor by a through-via. In order to electrically insulate the surface electrode from any possible interference from the source/ gate lines the initial SiN insulative layer sandwiched a structural polymer layer as the creation of thick high quality SiN is non-trivial. The gate, source, and drain were constructed of aluminum while the semiconducting channel was Indium Gallium Zinc Oxide (IGZO), so chosen because of its nearly transparent optical properties. The transistors we used on our experimental devices had a 5 micron channel length and channel widths that varied from 5-15 microns. A wider transistor interferes less with the source-drain transmission, but it lowers the transparency of the device.

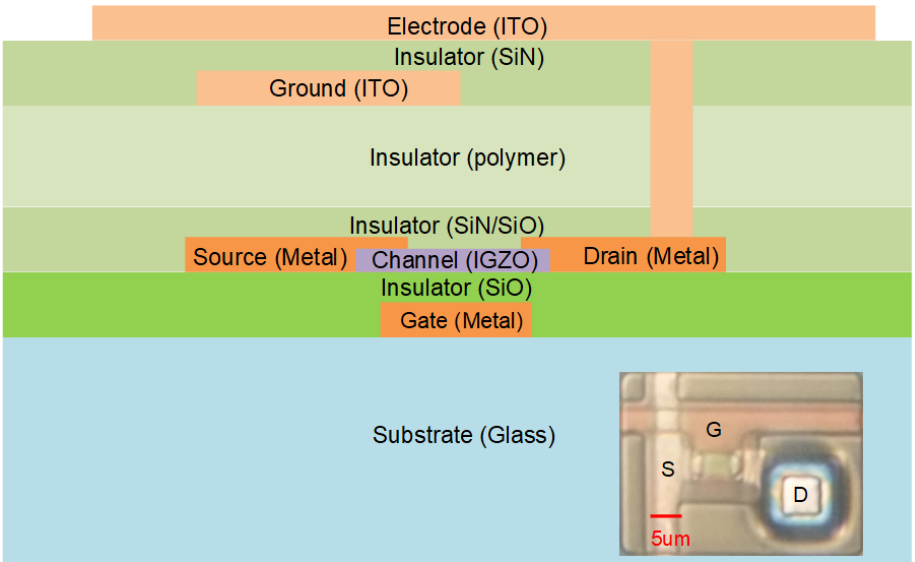

Figure 21: Transistor Design

3.2 Device Evolution

Over the course of this project, we have adapted the TFT platform to better suit our needs. In this section we will be detailing how our device has evolved over time and the variations which were produced. All of these devices were optimized and had their transistors designed by Mr. Ihida, and were fabricated by Sharp Corporation using their LCD back-plane fabrication process. All of the devices were made of the same materials and process. The semiconducting layer is crystalline Indium Gallium Zinc Oxide(IGZO) chosen for its high field mobility ~10cm^2/Vs. The surface electrodes are Indium Tin-Oxide(ITO) a transparent conductor and vary in size from $(45\mu m)^2$ to $(95\mu m)^2$. The transistor semiconducting channel cross section varies from $(4\mu m)^2$ to $(8\mu m)^2$. The primary application for the different electrode sizes is controlling the measurement specificity, experimentally we try to match the gap between the electrodes to the size of the cell being studied.

3.2.1 Gen 1 Device

The first device we experimented with consisted of 30,000 electrodes that ranged from $(45\mu m)^2$ or $(95\mu m)^2$. An image of the device is shown in Figure 22.

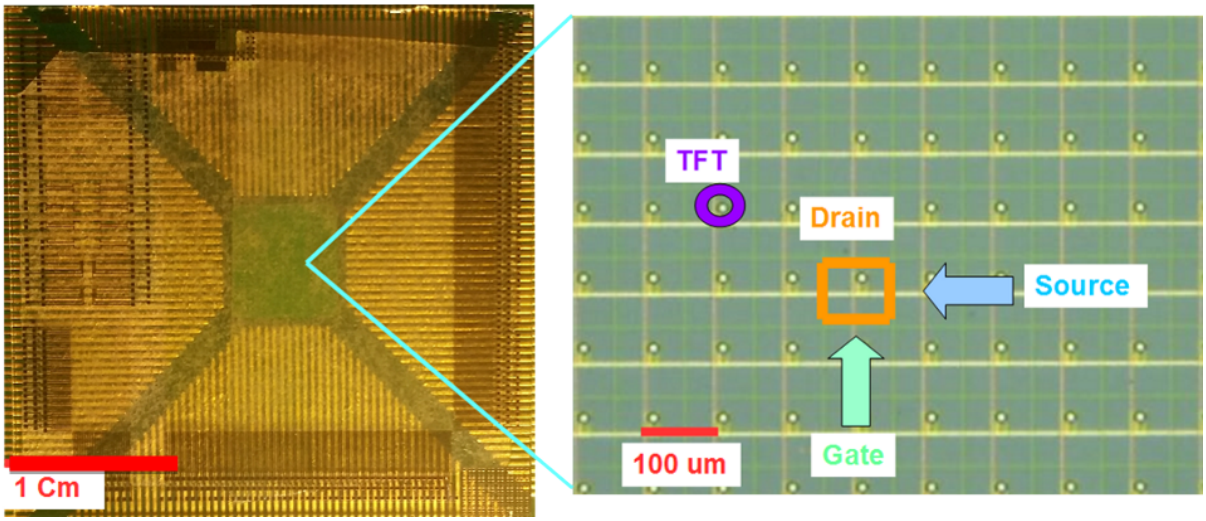

Figure 22: TFT Device and closeup

The electrodes were distributed into 9 different zones which consisted of different electrode sizes, gaps, and shapes. This was done so that ensuring the presence of a given type of electrode could be easily determined by the position of the enclosing Poly Di-Methyl Siloxane (PDMS) chamber. PDMS was used due to its ease of use and biocompatibility.

Additionally, the device contained a large number of test transistors and structures such as those intended for on-surface capacitors and other miscellaneous structures. The primary structural downside to this device is that it was extremely sensitive to electrostatic discharge. Due to the ground plane's structure, such a discharge would end up burning out the whole device making it useless. Furthermore, many of the experimental electrode designs proved impractical for experimentation. Additionally the presence of a ground plane is a common source of

parasitic capacitance, and given its limited functionality its removal was also done to improve signal quality.

3.2.2 Impedance Specialized Design

In order to improve results, we designed our own variation of the device for impedance measurements. Specifically we wanted to minimize the effect of the transistor by increasing the channel width. We also wanted to experiment with having a wide variety of electrode gaps and geometries to perform measurements. For reference for potential experiments, we also used the same fabrication process to fabricate a non-transistor gated device to operate similarly to an MEA. Additionally, we varied the transistor channel width in order to have a variety of different transistor properties to explore. Each of these variations are spatially isolated from one another to enable ease of control and multiplicity. The layout of the device is shown below in Figure 23.

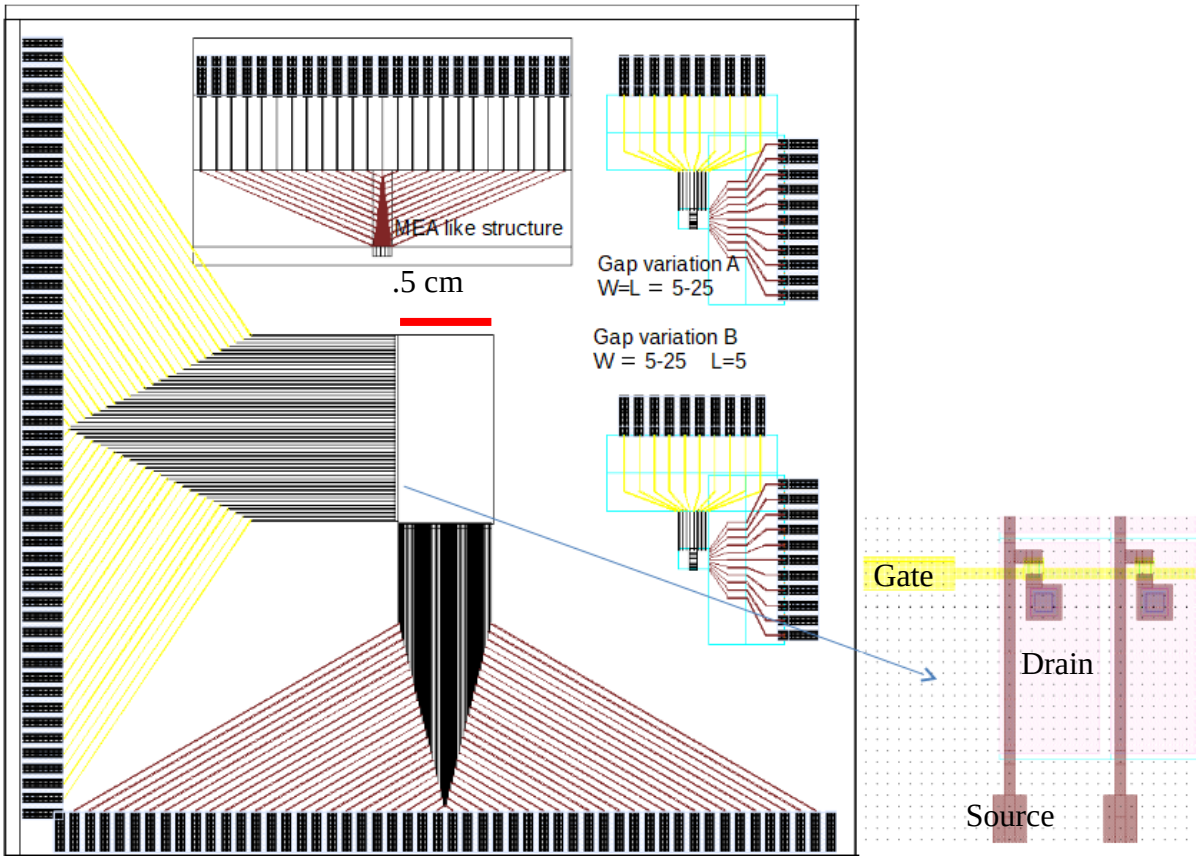

Figure 23: Second generation TFT device

Due to the opacity of the wiring, each of these structures is optically differentiable and it is a straightforward process to deposit the PDMS chamber in a manner such that the array needed for a given experiment is enclosed. One major structural deviation from the first generation is the removal of the ground plane. Often times the ground plane would induce parasitic capacitative effects fouling experiments, and using the ground plane as one would a conventional ground plane resulted in the device burning out. We designed the electrode layout of the device and the specifications for the various electrode arrays, but all of the transistor design, pathing, and fabrication process considerations were performed by Mr. Ihida of

Sharp Corporation who also fabricated the device along with several other varieties used for other types of experimentation.

3.3 Device Characterization

One of the primary methods of determining the functionality of a transistor is monitoring how the gate voltage affects the transfer of electrons flowing through the semiconducting channel. This is because the primary defining characteristic of a transistor is its ability to modulate that flow as the gate voltage increases. By monitoring how the current at a constant drain-source voltage is changing with respect to the gate voltage we can determine how effective the transistor is. The equivalent circuit is shown in Figure 24.

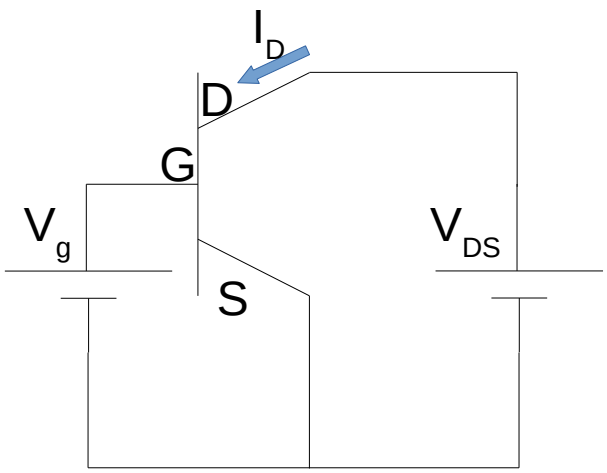

Figure 24: Equivalent circuit for determining transfer function

This is variable depending on the properties of the transistor, most notably the width of the semiconducting channel. By looking at different morphologies we can

determine which transistors are most suitable for a given application. The results for a 5 µm and 10 µm width transistor are shown below.

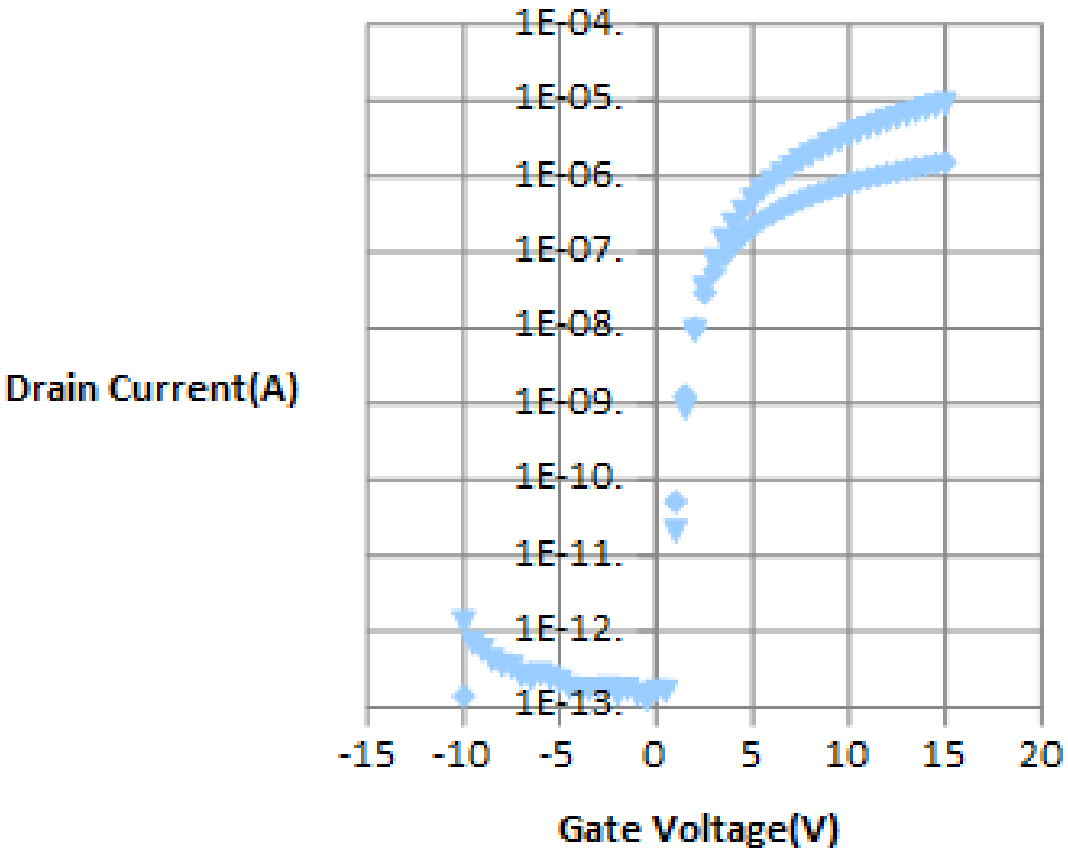

Figure 25: Transfer function of several of our transistors

As expected, the larger transistor had a significantly higher drain current at the same voltage. At operating voltages of V_g=15V this accounted for a 10x difference in the drain current. Suffice to say, in situations where electrical sensitivity is paramount larger transistors should generally be used, however the transistor

tends to be the least transparent part of the device, and as such it is a trade-off specific to the particular application of interest.

While an ideal transistor is often modelled as a device with variable resistance depending on the gate voltage reality is not that simple. There is inherent capacitance and inductance that induce a great deal of frequency dependent components. A Bode plot of the signal attenuation of our transistors is shown below.

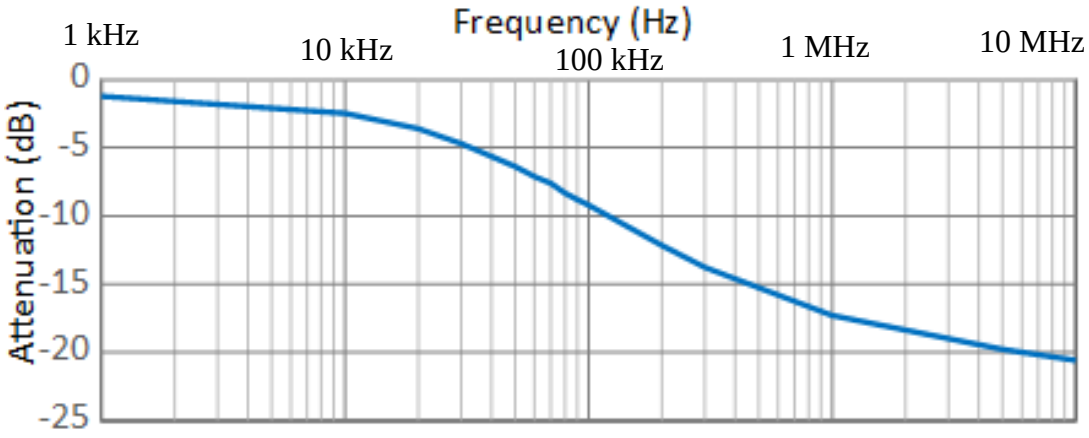

Figure 26: Bode plot of our device.

As the frequency increases, particularly as it increases beyond 100 kHz, the signal attenuation across the transistor becomes drastic. This is the primary limiting factor of the operational range of the transistor, and as such applications that require frequencies in the megahertz range such as certain fine dielectrophoretic sorting becomes rapidly unfeasible.

3.4 Chapter Summary

In this chapter we explained the functionality of the transistor as well as the fabrication process used to manufacture it. We explained why the original design was insufficient for our impedance measurements and how and why we laid out the

new generation of devices. We also gave some characterization data for our device and explained the frequency limitations.

Chapter 4:Experimental Setup

In this chapter we will discuss the experimental setup we used in our experiments. We will start with a general discussion of the equipment we used in our experiment. Then we will discuss how we used them to cell and antibody impedance measurements. We will then explain the setup we used for 2D impedance scanning on our device.

4.1 Equipment

In this section we will describe the equipment and materials used in our experiments. We will start with the electrical hardware, and continue with a discussion of the equipment needed for fluoroscopy. We will then discuss the control board for multiplicity, and finish with a discussion of the control program.

4.1.1 Electrical Equipment

4.1.1.1 Lockin Amplifier

To sense the exident current from the device, we used a lock-in amplifier. A lock-in amplifier is an amplifier that extracts a signal of the same frequency as an input reference signal even in the presence of noise several orders of magnitude larger. It does this by taking advantage of the orthogonality of sines to accurately extract only a specific frequency. By convolving the exident and incident signals it is capable of rapidly extracting both the relative magnitudes as well as the phase lag between the reference and the signal. The lock-in amplifier that we used was a NF LI5655 Wide-band Digital Lock-In amplifier.[98] We chose this device because it is capable of operating at frequencies up to 3 MHz as well as directly measuring a current signal without an external conversion chip.

Figure 27: LI5655 Lockin Amplifier[97]

4.1.1.2 DC Signal Source

To drive the gate lines of our device, we used a standard DC power supply. The specific DC power supply we used in our experiments was a Matsusada PK-80H High Precision switching power supply.[99] We used this power supply because it was capable of operating at over 25 V providing optimal gate activation.

Figure 28: Matsusada PK-80H DC Power Supply[98]

4.1.1.3 AC Signal Source

To drive the voltage on our device we used an AC signal source. The specific AC source we used was an Agilent 33220A Arbitrary Waveform Generator.[100] We used this signal generator because it is capable of operating at up to 100 MHz, and is controllable by GPIB which will be described later.

Figure 29: Agilent 33220A AC Signal Source

4.1.1.4 General Purpose Input Bus

A General Purpose Input Bus (GPIB), also known as IEEE 488 is a peripheral serial bus commonly used for automating test equipment. In order to interface with the controlling computer, we used an Agilent 82357A GPIB/USB interface. This allow us to send serial commands directly to any device connected to the GPIB chain

Figure 30: Agilent 82357a USB/GPIB interface

4.1.1.5 Faraday cage

A Faraday cage is a metal structure designed to cancel out external electrical fields and thus protect devices inside of it from being affected by them. The Faraday cage we used was a Technical Manufacturing Corporation Type 2 Faraday cage. [101] We chose this because in addition to operating as a Faraday cage it can be integrated with vibration canceling equipment to eliminate mechanical noise as well.

Figure 31: Technical Manufacturing Corporation Faraday Cage

4.1.2 Fluoroscopy Equipment

4.1.2.1 Fluorescent Dye

The caged fluorescent dye we used for our experiments was Propidium Iodide(PI)($C_{27}H_{34}I_2N_4$). Propidium iodide becomes uncaged when it bonds with DNA. This makes it an ideal dye for detecting dead cells because living cells will exclude PI preventing it from contacting the DNA containing nucleus. PI emits light at 670 nm when excited at 488 nm.[102] As demonstrated in Figure 32 the stimulated emission of PI is significantly different depending on the state of the cell.

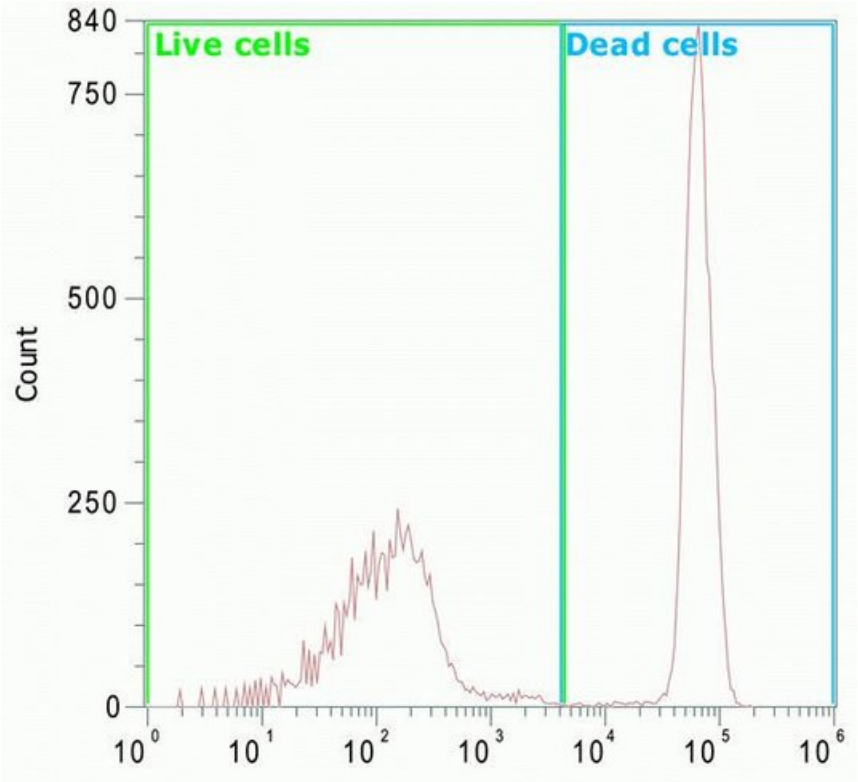

Figure 32: Emission spectra of Propidium Iodide for living and dead cells[101]

4.1.2.2 Light Source

To provide a light source for the stimulation of the Propidium Iodide we used an Olympus Life Sciences U-LH100HG Mercury Burner[103]. As shown in Figure 33 its primary emission peak is between 460-490 nm, making it sufficient for excitation of propidium iodide which has an emission peak at 488 nm.

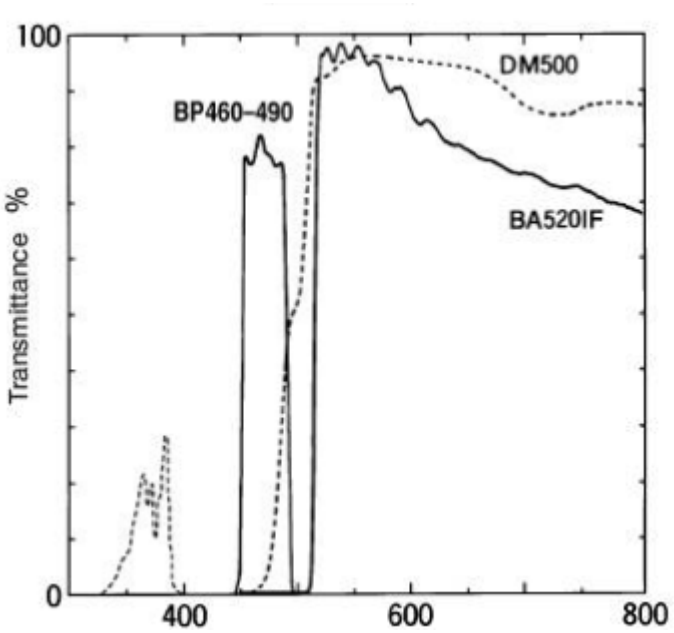

Figure 33: Emission spectra of Mercury Vapor Lamp[102]

4.1.2.3 Inverted Microscope

As previously mentioned to view a culture in-vitro an inverted microscope must be used to avoid image warping at the fluid/air interface. The microscope we used was an Olympus IX71 Inverted Microscope.[104]

Figure 34: IX71 inverted microscope[103]

4.1.2.4 Camera

To acquire the image so it can be saved and processed, we attached a Cascade II 512 Camera to the microscope.[105]

Figure 35: Cascade II 512 microscope camera

4.1.2.5 Capture Software

The acquisition software we used to communicate with the camera and dynamically alter the camera properties was Metamorph.[106] It was chosen due to

its robust tool-set for maintaining consistent spectra.

4.1.3 Japastim

In order to manipulate multiple electrodes with the same connection setup, we needed a technique to handle the rasterization of the signal. We collaborated with Dr. Levi from the University of Bordeaux to design a board that would be between the signal source and the device capable of sending signals to arbitrary pins interfacing with the device. The device, hereafter referred to Japastim is shown in Figure 36.

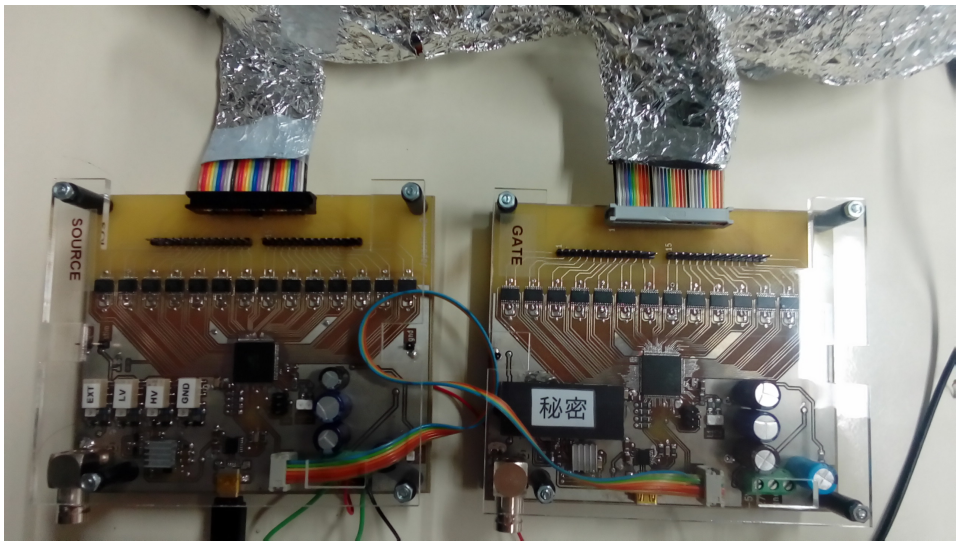

Figure 36: Japastim Device

It consists of 2 sub-boards, one for the gate, and one for the source, that possesses 28 output pins and is capable of outputting to an arbitrary number of them simultaneously. The chip is capable of outputting DC signals inherently, and can also output arbitrary signals passed through a BNC port on the outside. A full list of commands it is capable of executing is found in Appendix C.

4.1.4 Japasense

The Japastim device iss only capable of outputting signals and was unsuitable for sensing. However, by combining an Arduino microprocessor and several de-multiplexors, a programatically controllable sensing board has also been developed recently, and we hope to use this to enable full 2D impedance sensing on our device. This device is shown in Fig. 37.

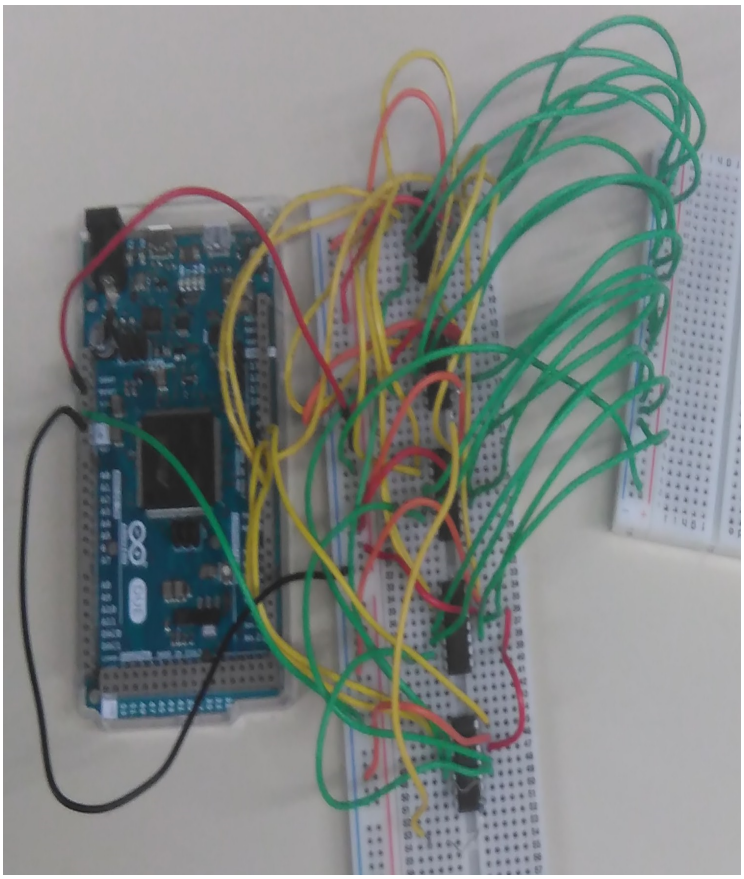

Figure 37: Japasense device

4.1.5 Labview™

In order to control the hardware, we used Labview™. Labview™ is a systems engineering focused graphical programming language based on C. Its main advantage over conventional environments is its ease of prototyping and its robust driver and device management systems.[107]

Communication with devices is done using the Virtual Instrument Software Architecture (VISA) protocol. VISA is a protocol abstraction designed to make communication over multiple different protocols, in this case USB and GPIB, straightforward. We also make use of the TULIP (The User-LAND Interface Protocol) to communicate between conventional VISA and Keysights iteration of VISA.

The primary purpose of the program we developed was to enable making a full impedance spectrum measurement as simple as possible. An image of the interface for the program is shown in Figure 38.

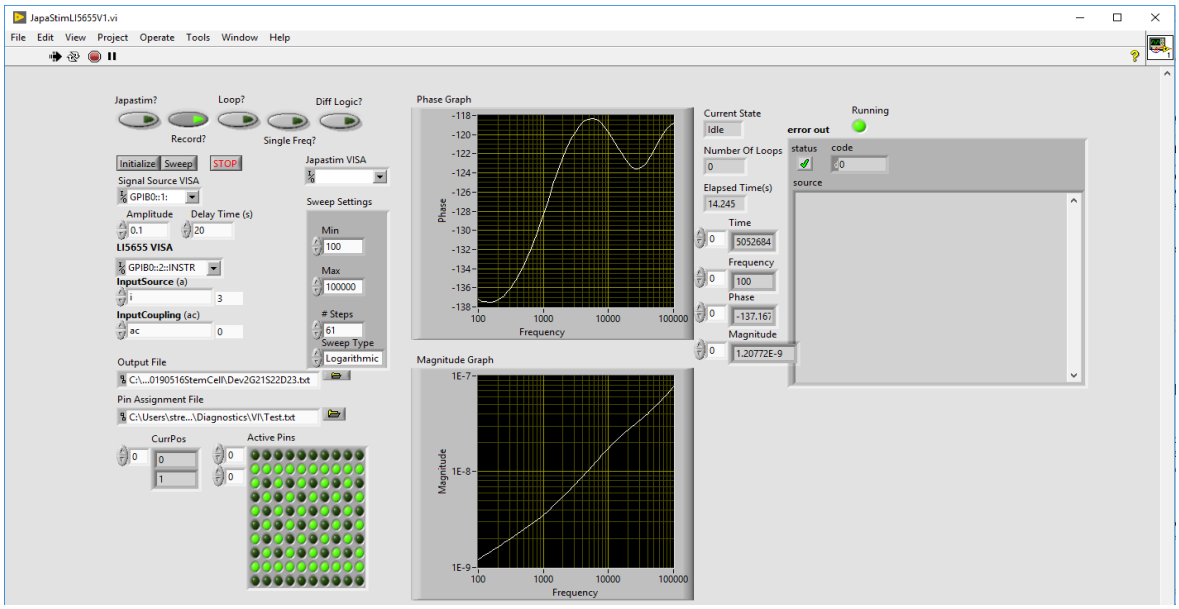

Figure 38: User Interface for our Labview program

To perform a measurement we simply enter the starting frequency, end frequency, number of step and whether we want linear or logarithmic frequency spacing. It will then iterate through the entire spectrum saving the magnitude and phase information. The full code and a more in depth explanation of the program is found in Appendix A.

4.1.6 ImageJ™

To extract quantitative data from the fluoroscopic images we post-processed the images programatically with ImageJ™, which was developed by the NIH for biological analysis.[108] We used the built in edge finding, contrasting, and cell counting functions to get the approximate number of cells per image. One of the major advantages of doing this programatically is that they are far more sensitive than the human eye. An example of this kind of measurement is shown in Figure 39.

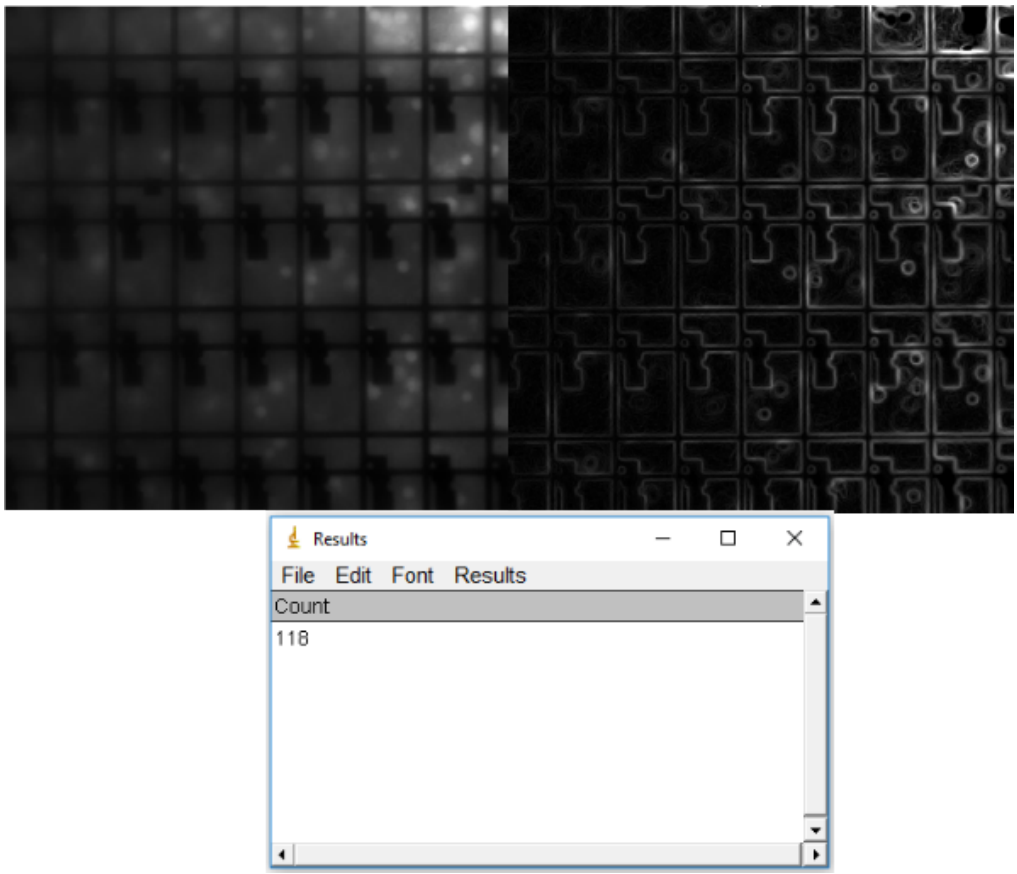

Figure 39: a)Raw image b)Edge processed Image c) cell count

4.2 Experimental Setup

4.2.1 Electrical Interface

The most critical part of our setup is the interfacing of our device with external electrical inputs and outputs. In order to do so we used a commercially available 0.65mm pin pitch silicon Printed Circuit Board from Sun Hayato (QFP112). To make the device optically accessible we manually drilled out a hole above which we placed our tTFT device. We adhered our tTFT device to it via the use of thin strips of double sided tape. To connect the PCB to the tTFT we used a 20 μm diameter 1% silicon aluminum alloy wire. We bonded it to both the PCB and the tTFTs aluminum pads

through the use of a West Bond wire bonder (Product # 10267) set to 0.4 W ultrasonic power and 20N bonding force. This process is shown below in Figure 40.

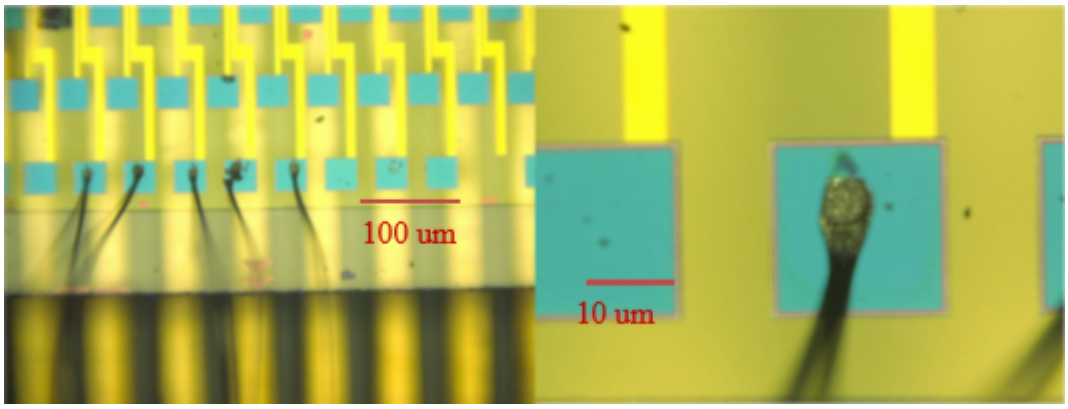

Figure 40: Wire bonding on our device at different scales

The external electrical connection was done by soldering a set of 2 row header pins to the PCB.

4.2.2 PDMS Integration

In order to hold fluids or a viable cell culture, we needed a means by which to contain fluids on the device without using any cytotoxic compounds. To this end we utilized a Poly DiMethyl Siloxane (PDMS) chamber. In order to have a strong bond with the device as well as maintaining flexibility so as to maintain that bond, we utilized a 10:1 ratio of PDMS monomers to curing agent.[109] Then it is placed in a vacuum chamber so that any bubbles in the mixture can be evacuated. The mixture is then poured into a mold and baked at 90°C for 30 minutes to harden. Once it is solid, it can be cut using a punch biopsy so as to create chambers of arbitrary size. In some cases it is additionally modified by an exacto knife. Additionally, liquid

PDMS can be poured onto the bonding wires so as to increase structural durability. The device after PDMS integration is shown below in Figure 41.

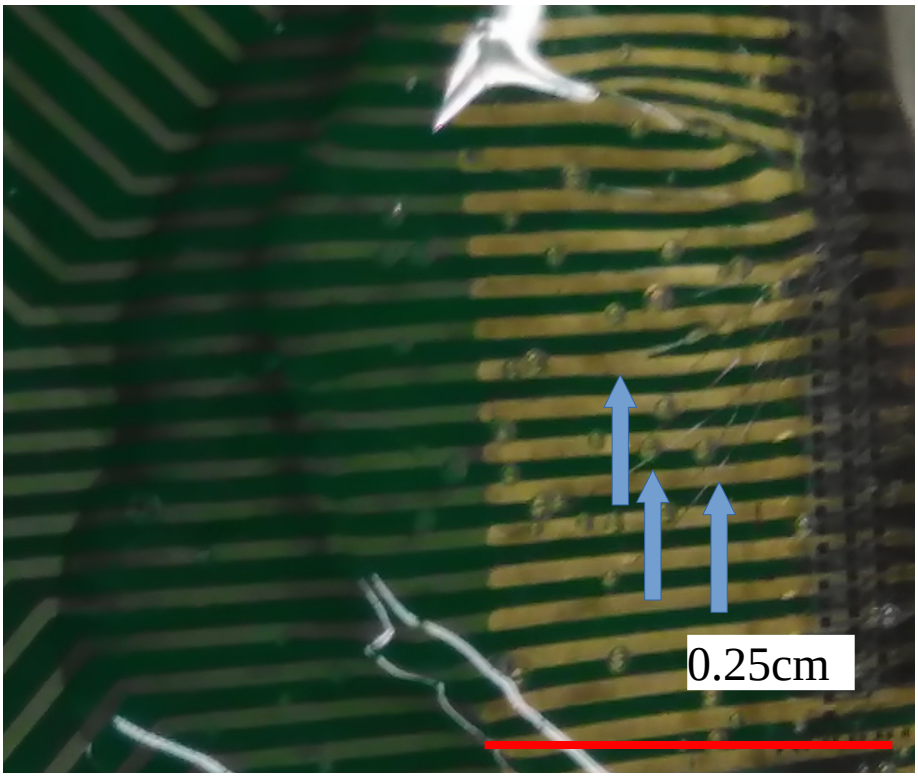

Figure 41: PDMS enclosed bonding wires

4.2.3Basic Cell/Medium Setup

To perform experiments we now combine the electrical pin accessible tTFT device described in the previous section with the electrical equipment described in 4.1. The basic principle of the experiment is to stimulate an electrode on the surface of our tTFT device, take in the current from an adjacent source line, and thus electrode, and pass it through the lock-in amplifier.

A DC signal source (Matsusada P4K36-1) set to 12V is connected to a pin that sends it signal to one of the gate lines of our tTFT device. This activates all the electrodes in a column on our device. The stimulating signal is a 0.1 V_{pp} signal sent from an AC signal source (Agilent 33220A) and is connected as a reference to the lock-in amplifier (NF LI5655) to serve as a baseline for the noise reduction and phase measurements. The AC source is also connected to a pin that sends its signal to one of the source lines of our tTFT device, which combined with the gate signal sends it to a single electrode on the surface of the device. An adjacent source line is connected to the current input of the lock-in amplifier completing the setup. A picture of this setup is shown below in Figure 42.

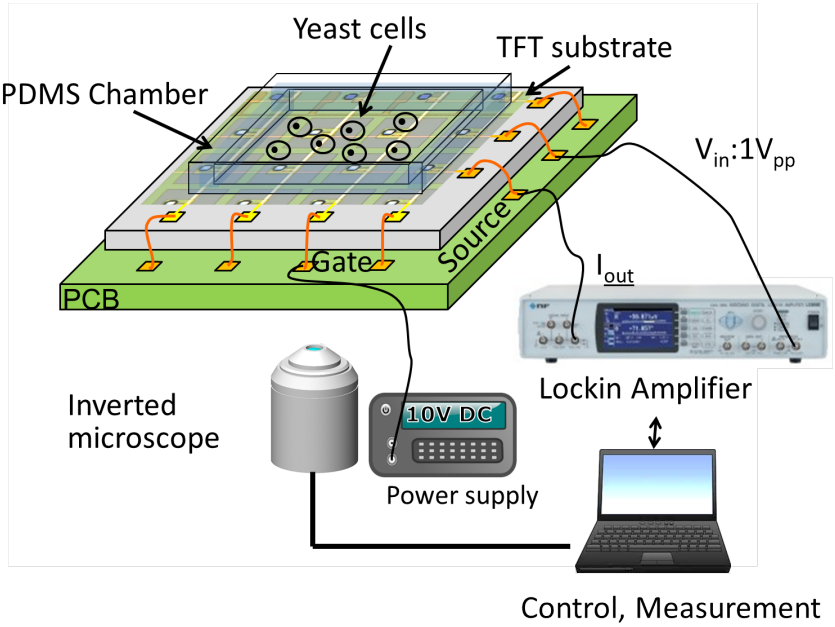

Figure 42: Conventional Cell Experiment Setup Diagram

4.2.4 Fluoroscopy setup

In order to integrate the imaging with the setup, the basic setup is still used, but it needs to be integrated with the microscope and assorted paraphernalia. The device is placed on top of the main stage of an inverted microscope (Olympus IX71). A magnification of 10-50x was used depending on the particular application. A mercury vapor lamp (Olympus Life Sciences U-LH100HG) was used to create the stimulating light for the fluoroscopy. 1 gram of Propidium Iodide(PI) dissolved in 1mL of DIW was used to mark cells for fluoroscopy. A camera (Photometrics Cascade II 512) was attached to the inverted microscope in order to capture the images, digitize them and send them to an adjacent computer. A computer running Metamorph was used to control the exposure, light magnitude, etc. to guarantee image quality.

4.2.5 Microfluidic Pumping Setup

In order to perform the electrogenic cell experiments on our device, we needed to integrate a basic pumping apparatus with the setup explained in the previous section. Two peristaltic pumps (Tokyo Rikakikai, MP-2010) were used to perform the fluid pumping. One pumped medium, and potentially an odorant, at 140uL/minute while the other pumped it out at the same rate to maintain parity. PDMS tubing was used to connect them to the chamber, and a metal tip was applied to the ends of them to reduce discharge noise from the ionic medium flowing in the tubing. A diagram of this setup is shown below in Figure 43.

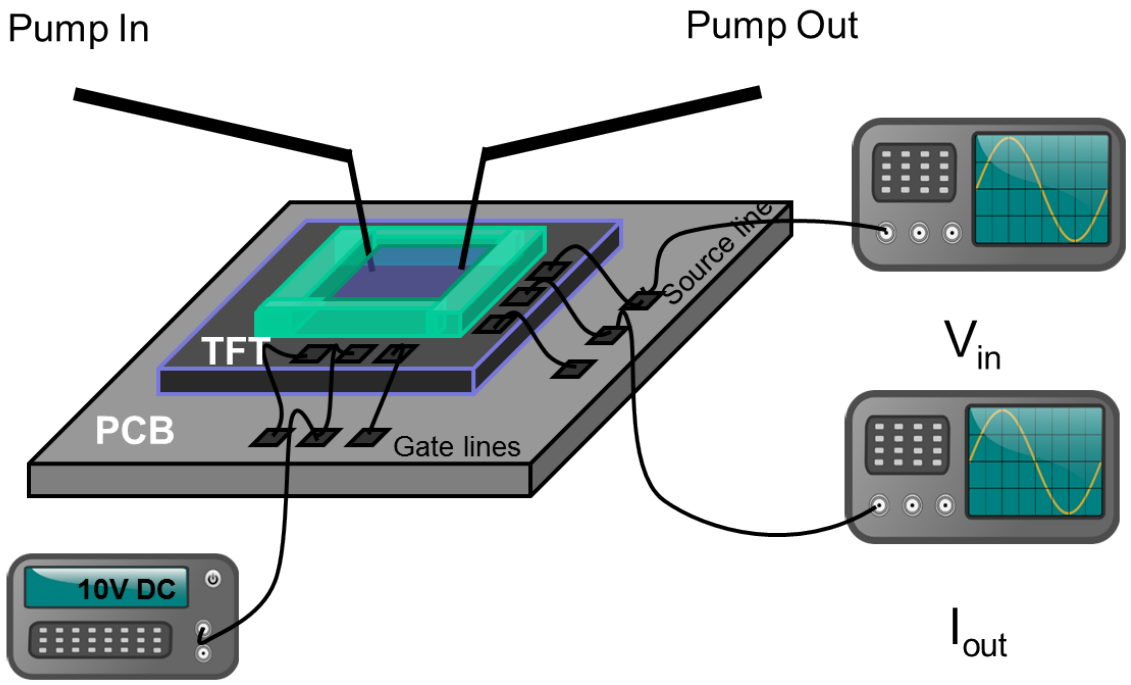

Figure 43: TFT peristaltic pumping setup

4.2.5 2D setup

To perform 2D sensing using our device we need to modify the basic setup slightly to account for the Japastim control board developed by the University of Bordeaux. For our purposes the device was used to intercept the gate voltage and distribute it programatically. Like the other equipment, it was controlled via micro-USB from the main computer through Labview's VISA protocol. Other than that the setup is unchanged as shown below in Figure 44.[110]

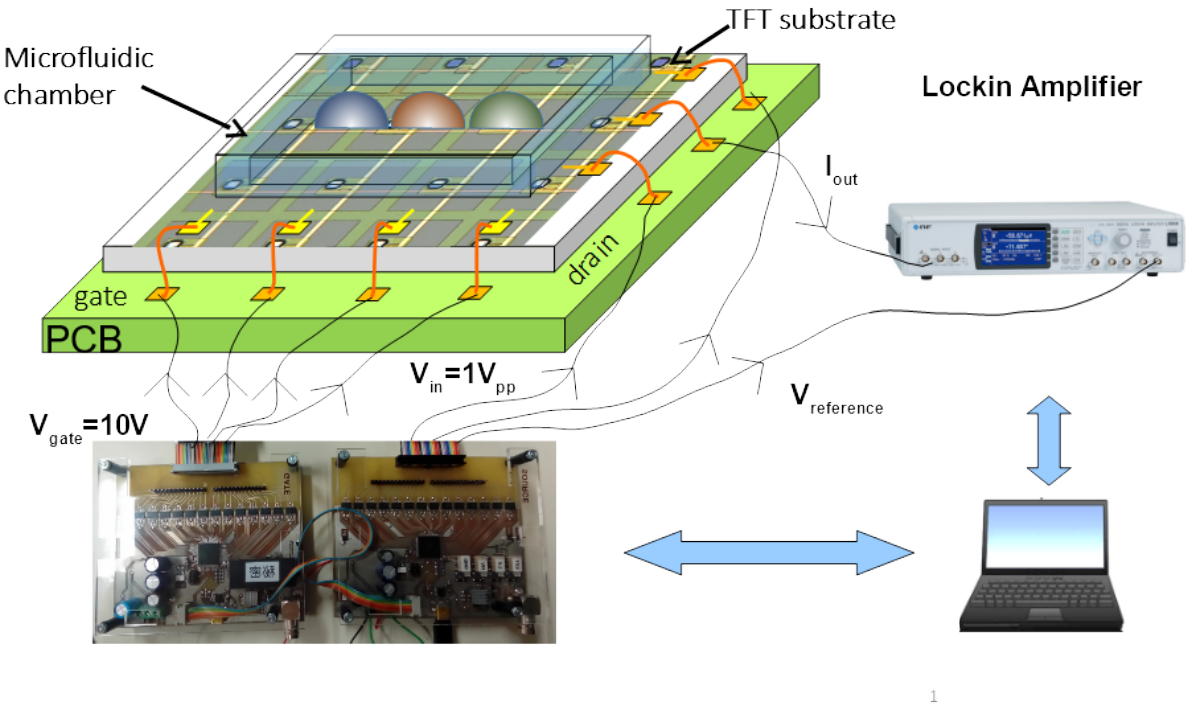

Figure 44: 2D TFT impedance spectroscopy setup[109]

4.3 Chapter Summary

In this chapter we described the equipment used for the electrical measurements, how they are used and why we selected the ones that we did. We also discussed the equipment for the fluoroscopic measurements including an analysis of the spectrum of the dye as well as that of the mercury vapor lamp. We furthermore discussed how we captured the optical data so that it could be processed. We also discussed how we used ImageJ to process those images and extract numerical information. We then discussed how these components were combined in order to create the various equipment setups used in our experiments.

Chapter 5:Experiments

In this chapter we will explain the specifics of the experiments we performed as well as deriving models from them. We will commence with a discussion of the progression of experiments to explain why we did these experiments in the manner we did. Then we will discuss the media differentiation experiments as well as the cell detection experiments. We will proceed with the cell viability experiments, and extend that principle to the creation of a simple cellular chemical sensor. The next experiment discussed will be the detection of antigens and marked compounds by monitoring antibodies. We will then conclude with a discussion of the experiments extending the multiplicity of the measurements.

5.1 Experimental Road-map

The general progression of experimentation in this work follows the basic principle of Minimum Viable Product (MVP), wherein the goal is to first attain the minimal building blocks of a functional system and then gradually expand that into more and more complicated analysis that create create incrementally more complicated systems.[111] We were uncertain of the specificity of our device and as such were uncertain as to what degree we could measure phenomena.

Our initial experiments were done in order to determine if we could differentiate between media of different bulk conductivities, as this is the most fundamental exploration of electrical properties using impedance. Doing this would enable the detection of different media and chemicals as well as enabling the detection of mass release of ions into the media by cellular organisms.

Once we had demonstrated the differentiation of bulk media on our device, we proceeded to perform experiments to see if we could detect gross cell state through impedance. Due to the inherent dyshomeostatic nature of cells with respect to their environment, there is an inherent capacitance across the cell membrane. We wanted to determine if this was detectable by our impedance measurements.

Once we had demonstrated the differentiation of living and dead cultures, we used that as a proof of concept for a more mathematically robust modeling of the health of the culture. By correlating the electrical impedance measurements and fluoroscopic measurements, we hoped to be able to build predictive models of how many cell are alive by performing solely electrical measurements.

We then wanted to explore whether we could detect more fine measurements such as those produced by electrogenic cells in response to a stimulus. Unfortunately the detection of the penultimate electrogenic cell, neurons, would be exceedingly difficult due to the short time of their pulse. As such, we decided to explore the response of moth olfactory cells to odorants due to their prolonged activation time.[36] This would give us an electrical cell based non-mutative chemical sensor that could be easily tuned to a wide variety of volatile organics.

Another parallel project we worked on was the utilization of antibodies in a similar manner. By bonding antibodies to the substrate we hoped to be able to detect the bonding of antigens due to their strong dipolar nature. This would enable a wide variety of medical diagnostic applications as well as the detection of purposefully marked compounds.

Our final set of experiments dealt with the expansion of our heretofore localized measurements to a much wider area of the device. While localized measurements may be useful in a tightly controlled environment it is a crippling deficiency when it comes to analyzing a large number of cells and detecting aberrations. To this end we coordinated with colleagues at the University of Bordeaux to develop a control card capable of this multiplicity. To test this device, we explored whether or not media and cells could be differentiated using it.

5.2 Medium Differentiation

In order to verify that impedance differentiation was even possible on our device we first experimented with seeing if we could detect the differences between

media of different conductivities. As explained in Chapter 4, the setup for this experiment consists of a DC signal source connected to the gate line of a transistor array, an AC source connected to the source line of the same array and a lock-in amplifier, and a connection from another source line to the lock-in amplifier as well. The lock-in amplifier convolves the AC signal with the exident current to eliminate noise and calculate the phase lag between the signals. A picture of the setup is shown in Figure 45.

Figure 45: Experimental setup for medium differentiation experiments.

The media we tested our device with for this experiment were Deionized Water (DIW), which we expected to have a high impedance due to its low conductivity. We also measured human serum and Phosphate Buffer Solution (PBS), both of which have higher conductivities and as such were expected to have lower impedances. This experiment was performed with a gate voltage of Vg=12V,

and with a stimulated voltage of .1Vpp from 10-100kHz with log decimal frequency distribution with 10 samples per decade.

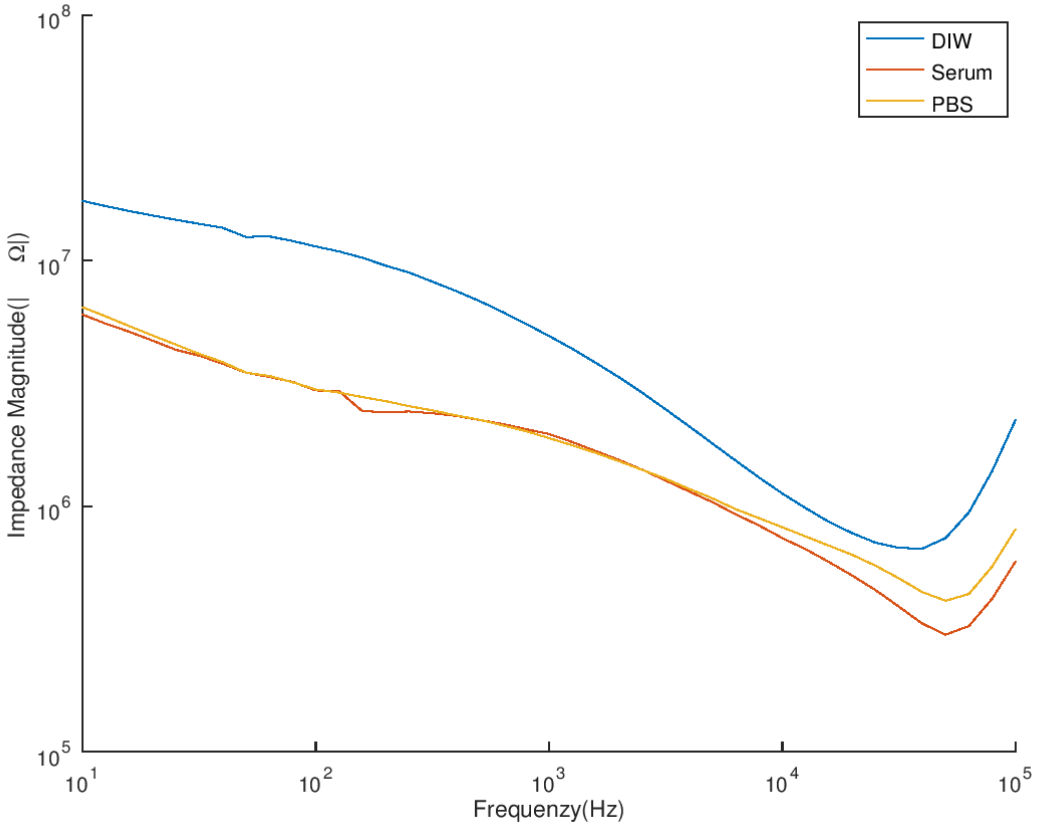

Figure 46: Measured Impedance Spectra on our device for various materials.

By modelling the system as a network of parallel resistors and capacitors we can extract information about the materials and prove that it correlates with expected values.

$$Z_{Individual} = R \| C = \frac{RC}{R+C} = \frac{\frac{\epsilon_0 \epsilon_r}{\sigma}}{\frac{1}{\sigma}\frac{d}{A} + \frac{\epsilon_0 \epsilon_r A}{d}} = \frac{\epsilon_0 \epsilon_r A d}{d^2 + A^2 \epsilon_0 \epsilon_r \sigma}$$

$$C = \frac{\epsilon_0 \epsilon_r A}{d}$$

$$R = \frac{1}{\sigma} \frac{d}{A}$$

Now that we have calculated the expected results from first principles, we can compare them with those calculated from first principles using an octave script to perform the calculations at each measured frequency point. The results are shown in Figure 47.

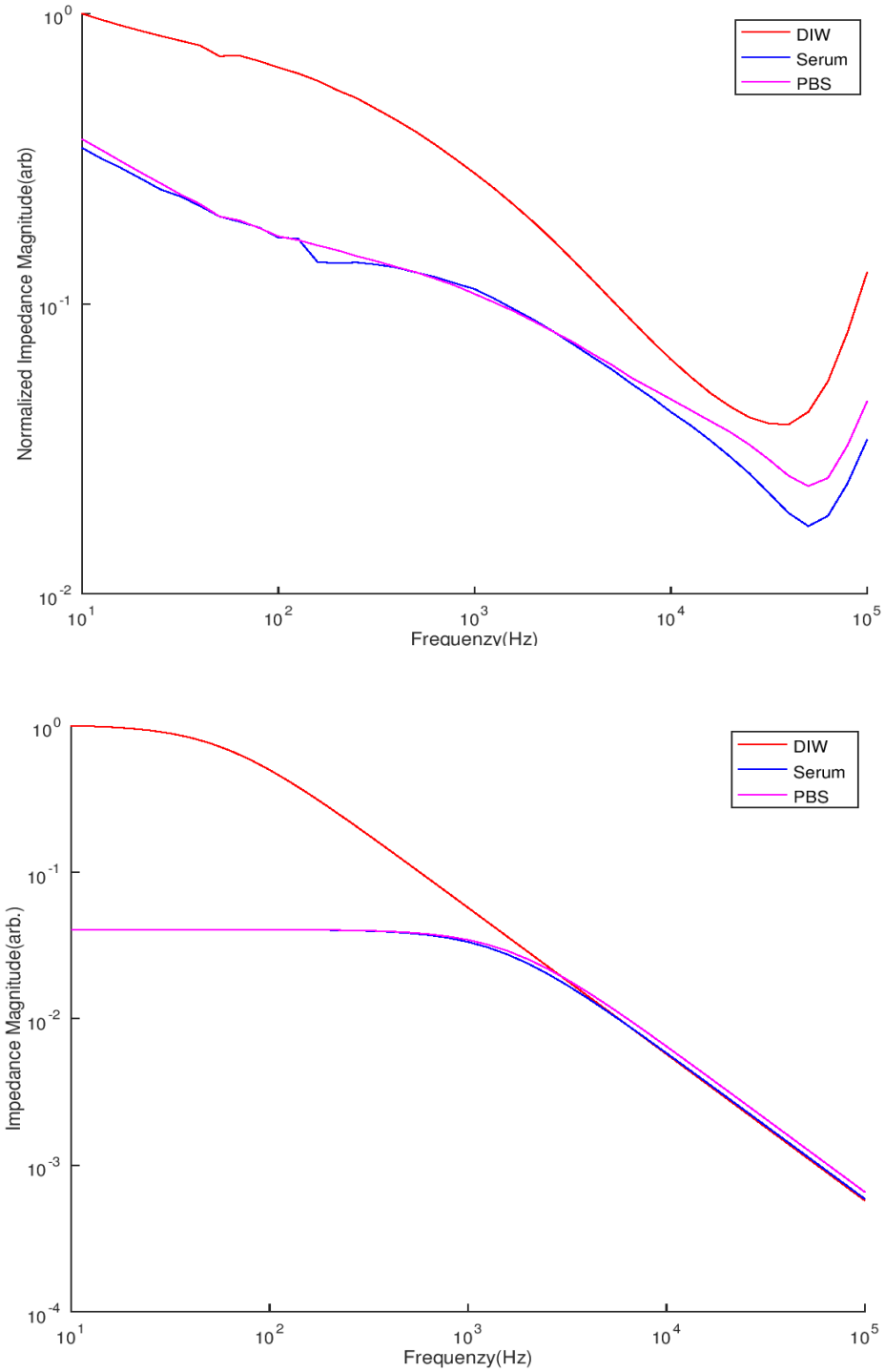

Figure 47: Real Data(top) vs. Modeled Data(bottom)

Structurally, the basic model and the experimental data match up quite closely at lower frequencies. Most notably, the impedance of the DIW is significantly higher than that of the PBS and serum especially at lower frequencies, and that while the PBS and serum have quite similar values, though the serum has a slightly smaller impedance at higher frequencies. The one major structural deviation from the model is that the measurements taken at high frequency showed a very large increase in impedance. This is due to the high frequency effects of the transistor, and is a factor consistent across all experiments and will be explained in more detail in Chapter 6. Additionally the scale differs drastically due to the networked impedance throughout the electrode array. A signal will not travel exclusively directly between adjacent electrodes and can conceptually thought of as an infinite series of parallel impedances with magnitude proportional to path length as it traverses the array of electrodes.

$$Z = \sum_{\|} L * Z_{Individual}$$

Additionally, there are series of parallel 3 dimensional paths due to fringing effects caused by the extremely thin nature of the electrode. All of these factors however, are frequency independent and as such will only be a linear scaling factor and thus will have no effect on the structure of the system and can be safely ignored.

5.3 Discrete Cell State Detection

5.3.1 Background

The next set of experiments were seeing if it was possible to differentiate between medium and medium containing cells, as well as detecting whether those cells were living or dead. A cell can be modelled as a region with a high concentration of ions encompassed by a lipid membrane that isolates it from the environment. Eukaryotes also have a second electrically relevant region, the nucleus. These are both shown in Figure 48.

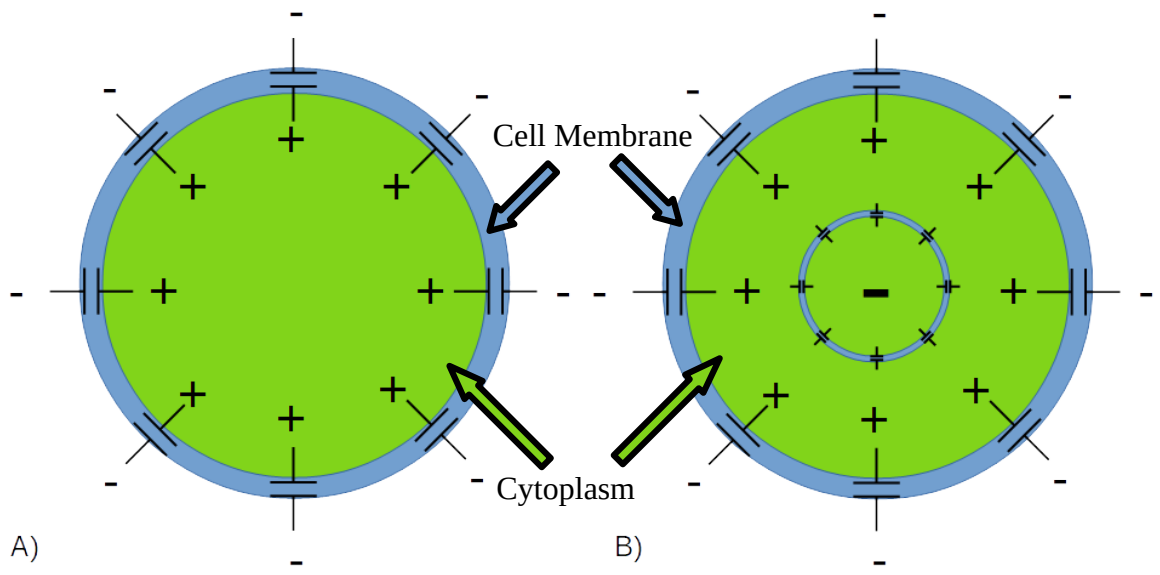

Figure 48: Electrical schematic of a)Prokaryotic and b) Eukaryotic cells.

The reason we initially explored the effects of cell death are to a property known as lysis. Lysis is the rapid degradation of the lipid membrane encompassing the cell. This results in the near complete loss of membrane capacitance caused by

the varying concentrations of ions as they are now free to move as the cytoplasm leaks out of the cell as shown in Figure 49.

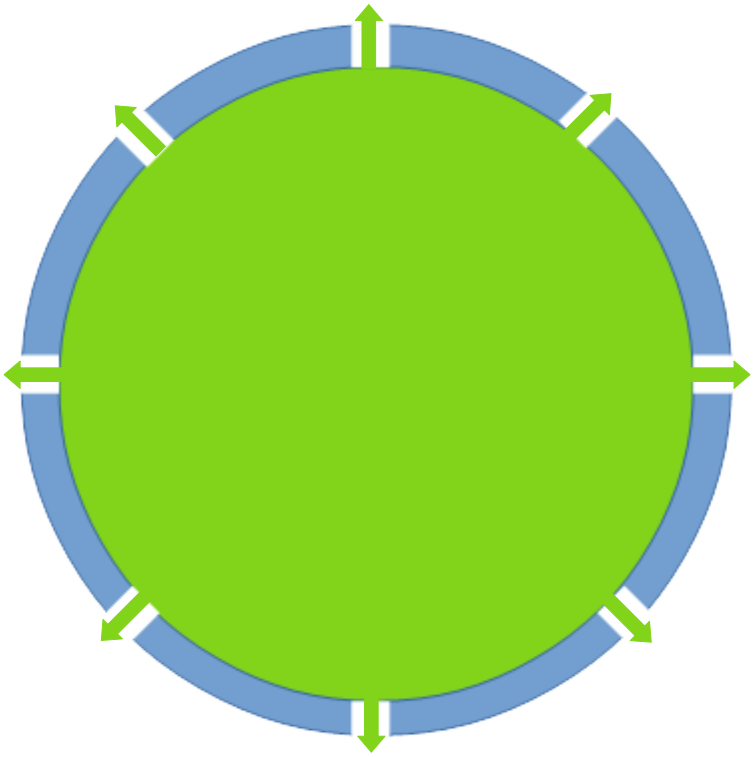

Figure 49: Lysis of a eukaryotic cell

5.3.2 Yeast

The first experiments were performed with Saccharomyces Cerevisiae(Baker's yeast, hereafter referred to as yeast) cultures. Yeast were chosen for this experiment due to their cell wall, which should result in a higher measured capacitance and thus signal, as well as their robust nature and ease of culture. The results are shown on the next page in Figure 50.

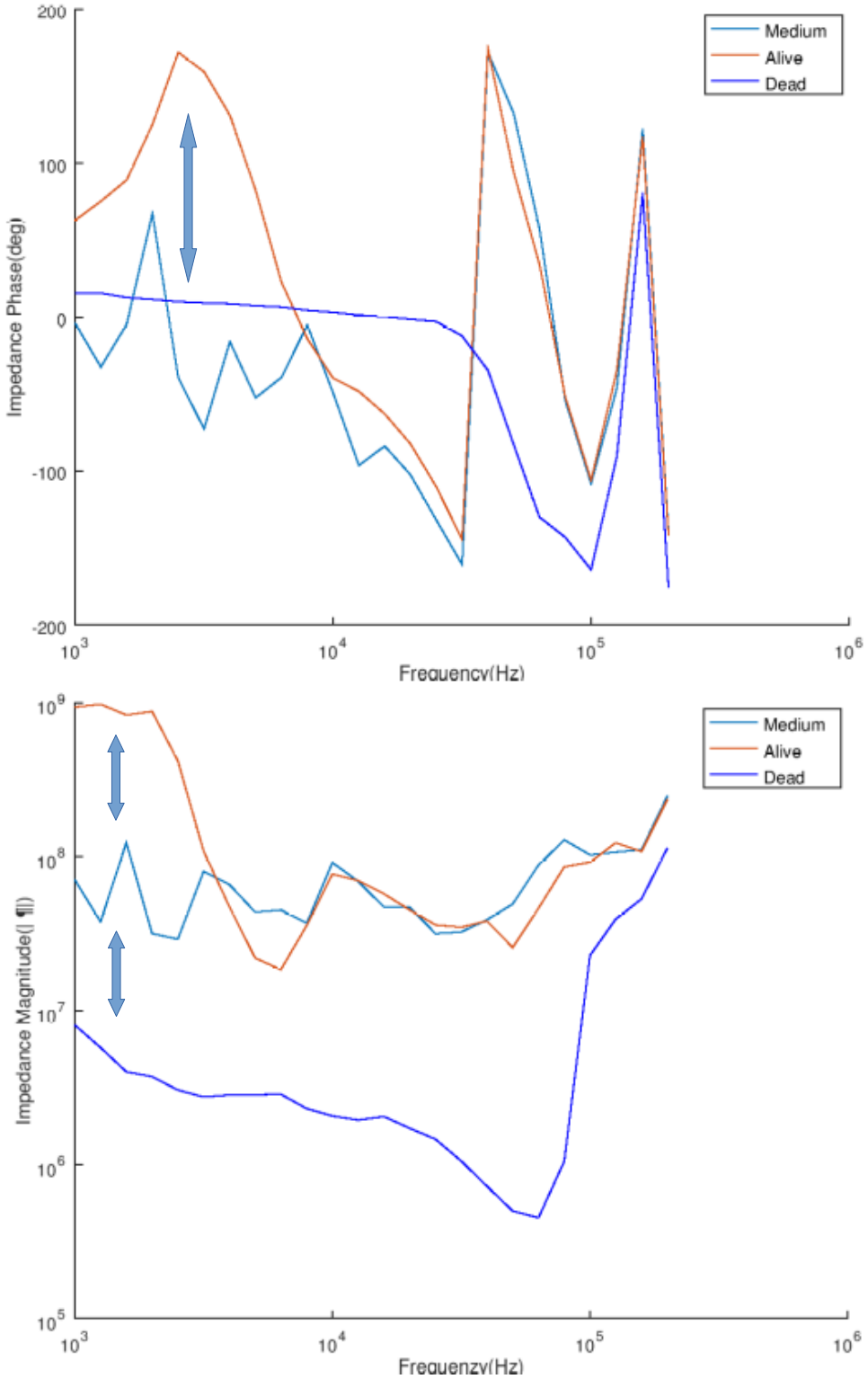

Figure 50: Yeast Impedance Spectra

There was a clear differentiation at lower frequencies between all three states at lower frequencies, as this was primarily dominated by the cell wall capacitance. While initially unexpected the drop in impedance of the dead cells with respect to the relatively high conductivity can be explained by the lysis of cells increasing the local ion concentration. While the volumes involved would not be enough to significantly alter the bulk concentration, the measurements are only over a localized area.

In order to compare these results with the bulk of prior art, most of which do not use transistors, we decided to a differential analysis. By using the medium impedance as a baseline we can minimize the effects of the transistor on the result getting the results shown in Figure 51.

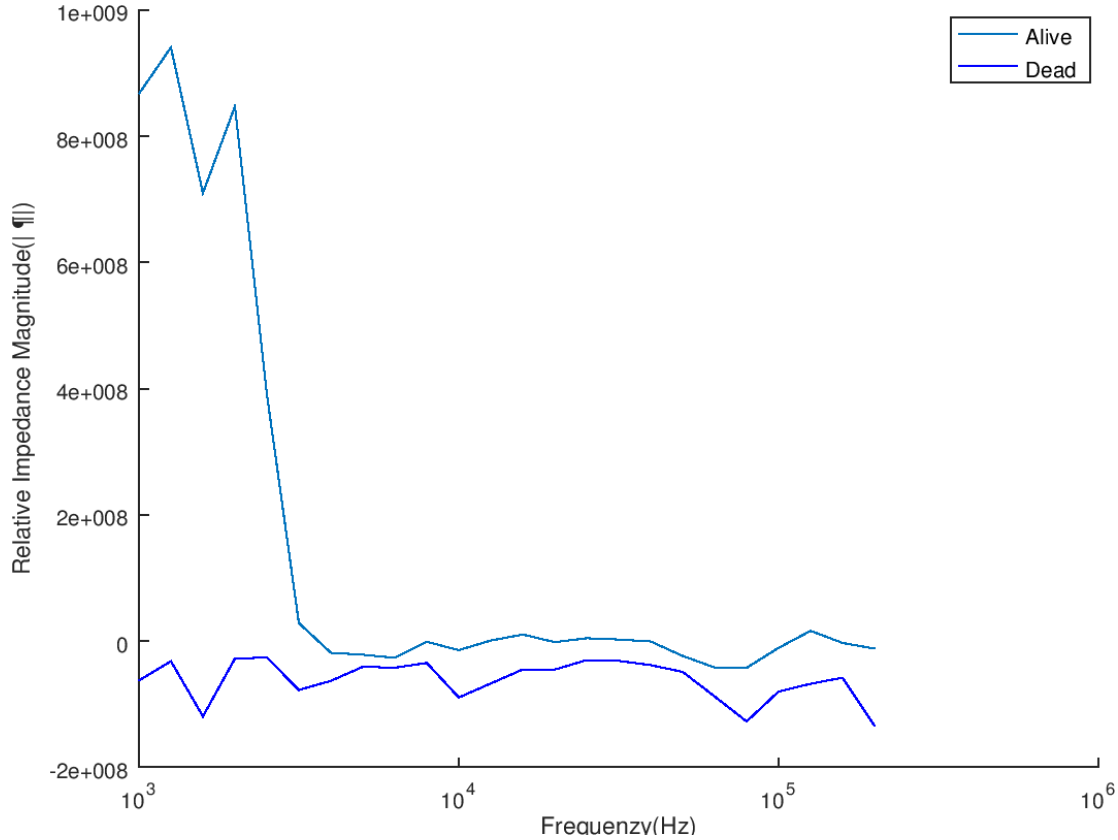

Figure 51: Relative impedance magnitude wrt medium of yeast cells.

This is in confirmation with prior research on yeast cells which determined that there was a strong capacitative drop-off between 1 and 10khz between living and dead cells.[112]–[115].

5.3.3 Neurons

Once we had performed these experiments with yeast we wanted to verify that similar differentiation could be performed on animal cells. These would lack a cell wall resulting in a smaller measurable difference. We first chose to study rat primary neurons due to their unique electrical properties including the high

conductivity of axons and their tendency to form advanced networks. An image of the neuron culture on our device is shown in Figure 52.

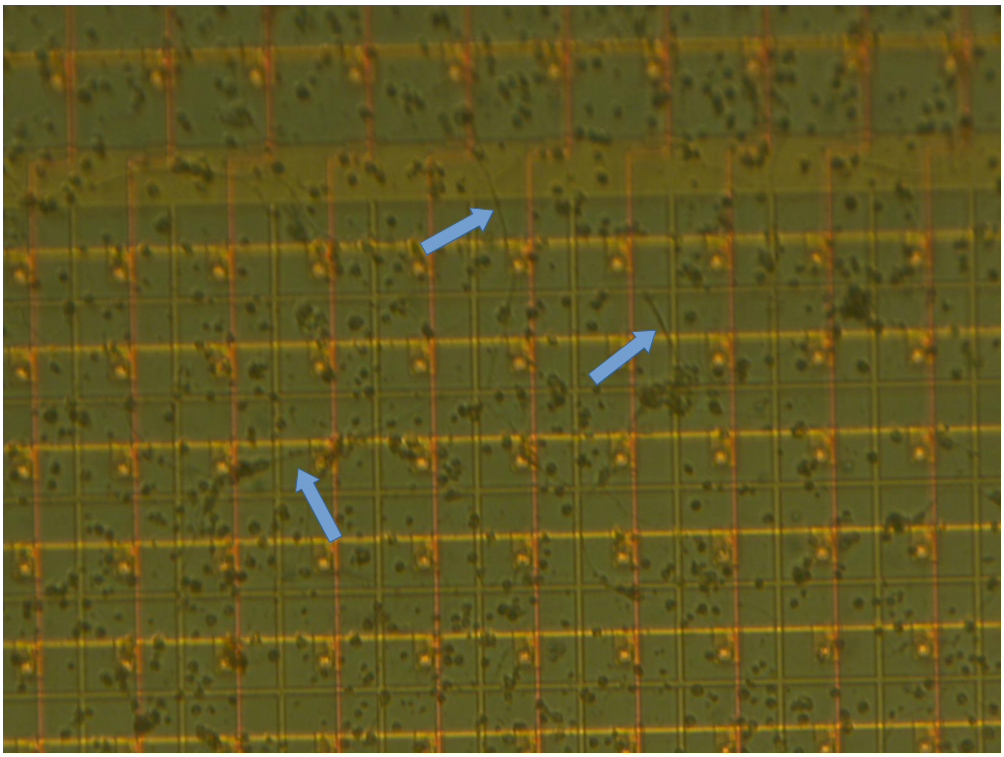

Figure 52: Neuron Culture on our device with arrows pointing to axons.

Due to the highly conductive nature of axons as well as their tendency to form networks bridging electrodes, we expected them to present as a lower impedance than that of the medium at higher frequencies. At lower frequencies we would expect the impedance results to differ slightly due to the sparse nature of the culture as well as the low parallel resistance. We measured and three separate locations in order to get a better analysis of the culture, and as such were required to normalize the results to compare them. This is due to the inherent variance in transistor properties. These experiments were performed with a gate voltage of Vg=12V, and with a stimulating voltage of 0.1V pp from 1kHz-100kHz with samples taken on a log

decimal scale with 10 points per decade. Our results are shown in Figure 53 with the different sampling areas labelled G2,G3, and G6 corresponding to activation of gate line 2, 3, and 6 active respectively, and normalized to compensate for transistor and culture variation.[116]

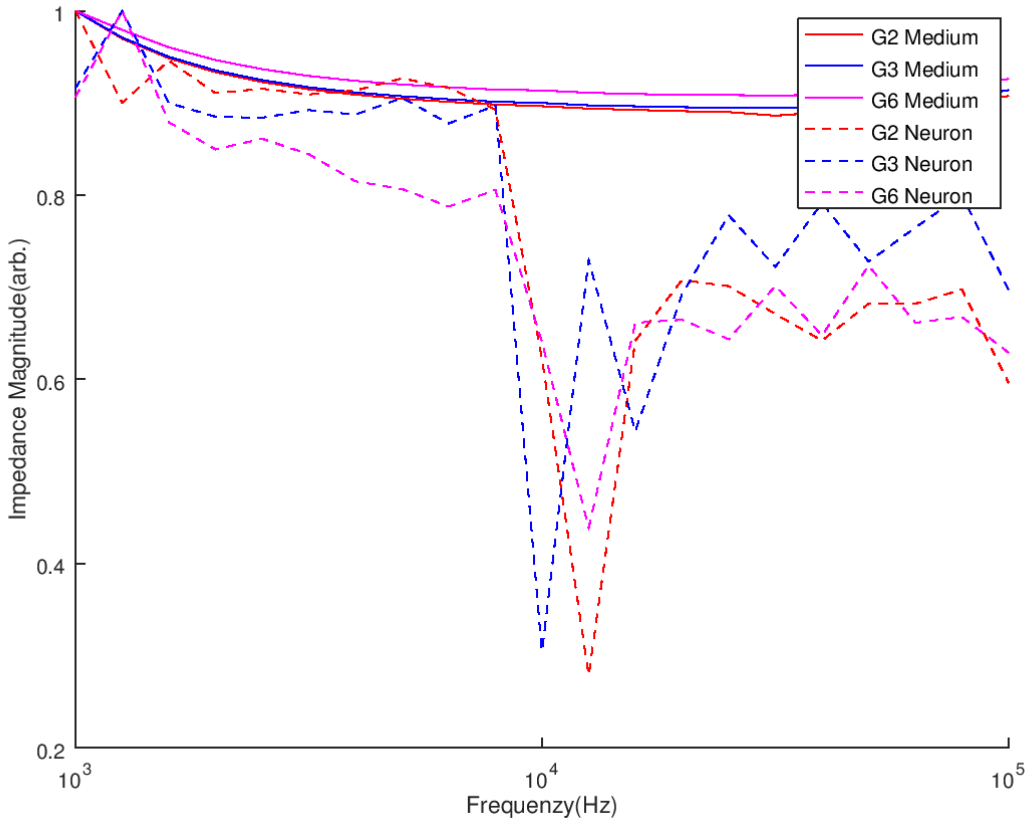

Figure 53: Normalized impedance spectra of neuron culture on our device

This was the first detection of neuron growth on a transparent transistor gated electrode array. Both primary predicted effects were present in the impedance spectra of the neurons as compared to those of the medium. The capacitance was minimally affected to the sparseness of the culture as demonstrated by the minimal

change of the normalized impedance at lower frequencies for all except for G6 which had some minor deviation. Higher frequencies had a lower impedance corresponding to a lowered resistance from the axonal networks bridging electrodes. One unexplained point of interest is the rapid drop in impedance at around 10kHz experienced at all three locations. It is probable that this localized spike was due to more complicated RC networks than were accounted for in the basic model presenting as a band-pass filter through a structure similar to that shown in Figure .

Lending credence to this hypothesis is the fact that the exact frequency of the drop in impedance of the neuron cultures differs based on location, G3 drops a single frequency step earlier than the G2 and G6 locations.

5.3.3 HEPG2

Due to the difficulty and length of time involved with culturing Neurons, when we wanted to analyse eukaryotes more in depth, we used HEPG2 liver cancer cells instead.[117] Additionally, we felt that cancer cells were more relevant for culture state analysis.

Due to not being electrogenic, HEPG2 cells have far more conventional insulative properties than neurons. Additionally, due to the conductive nature of the medium the leaking of ions during cell death should minimally affect both local and global concentrations. As such, we would predict that the difference in living and dead cells would be due wholly to the capacitative effects resulting in the living cells having a significantly higher impedance than the dead cells at low frequencies,

followed by convergence at higher frequencies. These experiments were performed with a Vg of 12V, and with a stimulating voltage of .1Vpp from 100-100khz with 10 samples per decade on a log decimal scale. The experimental results are shown in Figure 54.

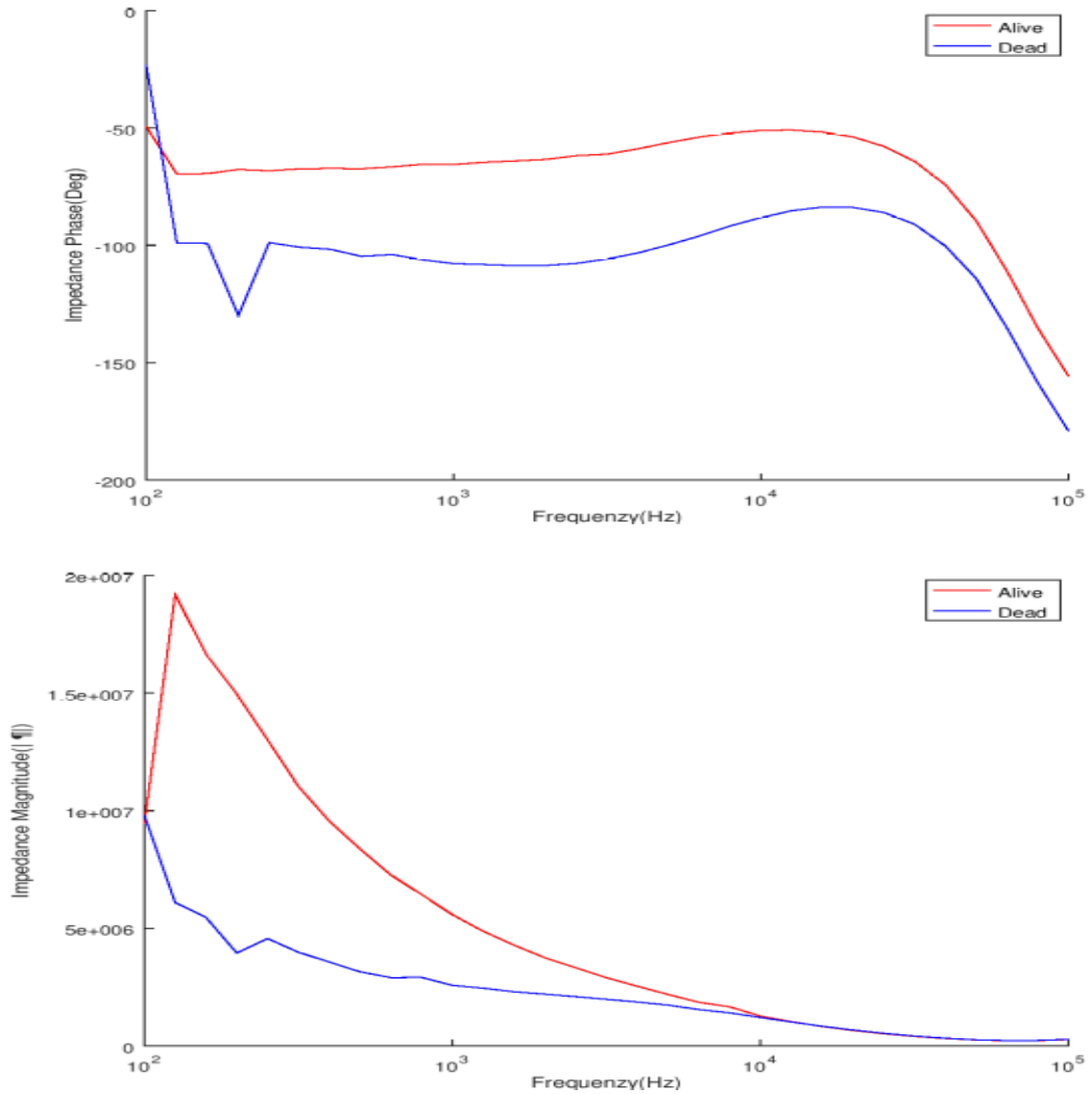

Figure 54: Impedance spectra of HEPG2 liver cancer cells

Outside of the anomalous data point at 100 Hz, the results were very similar to that which we expected. This is unfortunately likely due to a quirk in the measurement apparatus, the lock-in amplifier has a tendency to give strange readings for its first couple of measurements.

5.3.4 Summary

In this section we have demonstrated the differentiation of different media a well as the living/dead status of various cell cultures. It is important to keep in mind that these are very limited in applicability due to their reliance on a given culture being either mostly alive or dead and with limited granularity. With the next set of experiments we aimed to ameliorate this flaw.

5.4 Continuous Cell State Detection

5.4.1 Background

While differentiating between wholly alive and dead cell culture has a few applications, finer granularity would enable significantly more utility. Often-times contamination, and medical testing is not that drastic and a gradual and slower rate of decay is expected. Being able to determine this rate opens up a window into the specific type of contamination or the mechanism of action of a given treatment. Thus our next set of experiments was focused on developing a continuous predictive model so as to provide the desired granularity.

5.4.2 Yeast

Much like in the binary state detection experiments, we first experimented with yeast due to its ease of culture, robust nature, and cell wall. The experiment will be similar to the binary differentiation, but locked at one frequency, 1 kHz, and performed on top of an inverted microscope so that we can garner simultaneous optical data. This will enable us an independent measurement of cell state to give us far more precise measurements of cell state. We used Propidium Iodide to mark the dead cells resulting in pictures from the inverted microscope similar to those shown in Figure 55 with dead cells emitting light and appearing white.

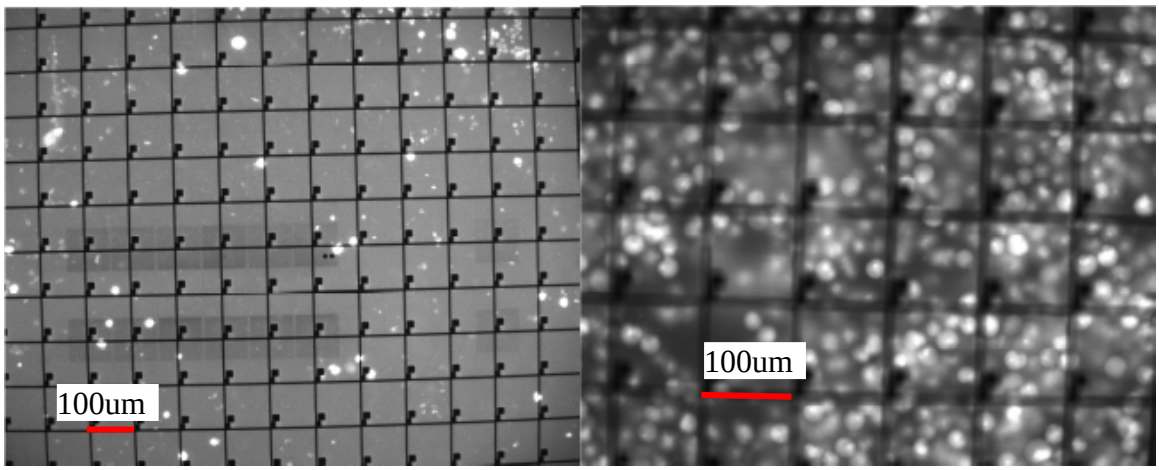

Figure 55: Propidium Iodide stained yeast cells under inverted microscopy

We also made sure to perform the experiment at different cell concentrations in order to explore the resistive effects of non-viable yeast cells. We drove the gate line with a Vg of 12V, and used a stimulating voltage of 0.1V pp at 1 kHz. Our results are shown in Figure 56.[118]

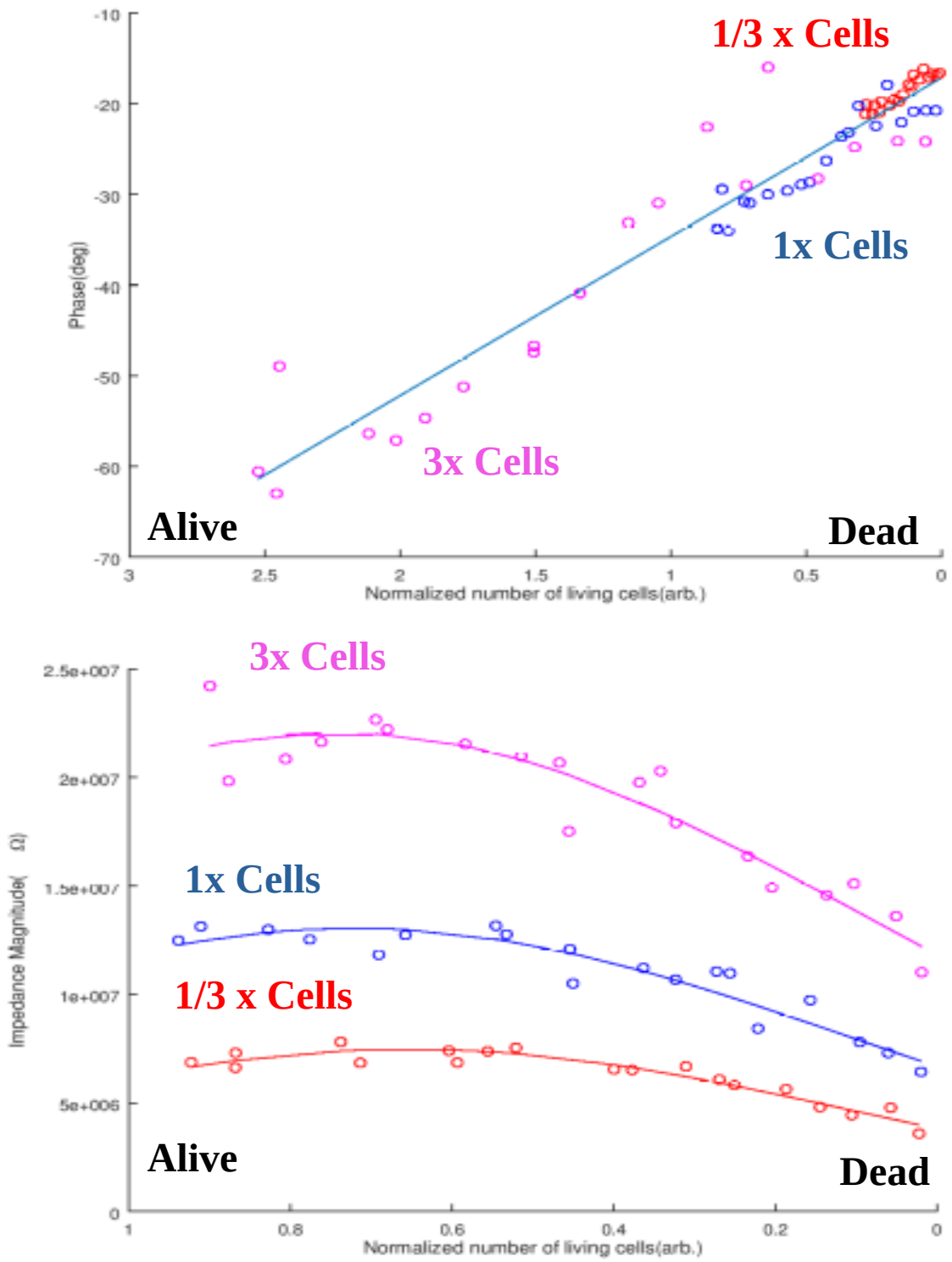

Figure 56: Continuous Impedance Modeling of Yeast

The same general trends were exhibited as in the discrete differentiation scenario with a few caveats. The magnitude of the impedance was highly concentration dependent at all cell states. At the living states this was due to the combination of resistive and capacitative effects near the electrode, at 1 kHz both are major contributing components. As the cells died, the dead cells continued to contribute to the resistance due to the shards of their membrane and the organelles and internal ions leaking into the environment near the electrodes.

The Impedance phase seemed to offer significantly more prospects a predictive measurement. Due to its physical basis being the separation of different ionic gradients, the membrane fragments and organelles have a minimal effect on the capacitance between electrodes leading to more consistent measurements between electrodes. This is mostly due to dead cells having almost no effect on the capacitance, enabling a strong linear relationship between the number of living cells, calculated by multiplying the proportion of living cells by the cell concentration, and the phase lag. Because of the transistor variation as well as the inherently stochastic nature of biological systems, absolute determinations can be complicated and thus self referential effects are easiest to predict. As shown in the model, outside of the electrochemical and transistor effects, the phase is the primary effect modified by cell death. So long as the cell concentration is neither sparse nor concentrated this model can be further simplified to a straightforward linear relationship by taking advantage of the effect that parallel capacitances sum. This allows us to have a predictive phase model for calculating the number of living cells in a given measurement area given below.

$$\angle Z = -17.524(Living) - 17.144$$

The best fit line was a very strong fit as determined by the coefficient of determination (R^2) given by the equation.

$$R^2 = SS_{Res} / SS + Total$$
$$SS_{Res} = \sum (y_i - \bar{y})^2$$
$$SS_{Total} = \sum (y_i - model_i)^2$$

Where SS is the sum of squares, res is the residuals, and model are the modelled values. The closer this value is to one, generally the stronger the fit, in this case R^2=0.925 indicative of an extremely strong fit between data and this simplified model. It's important to stand that this relation is only true for linear models.

By extracting the capacitance directly using the complex exponential we can build a more robust description of what exactly we are measuring that is correlated with the number of living cells. The results are shown in Fig. 57.

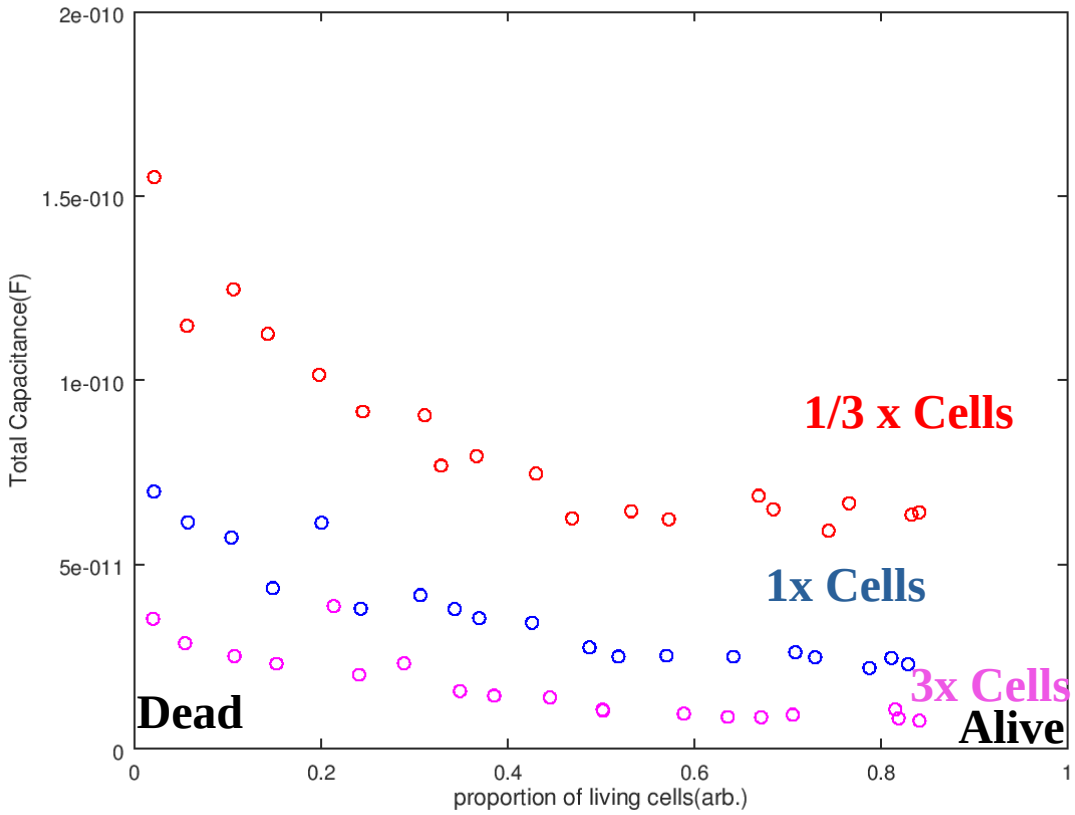

Figure 57: Extracted capacitance of yeast cells

Contrary to initial expectations, the net effect is not dominated by the inherent capacitance of the yeast cells, but in fact by the electrochemical effects of the randles circuit. While other works had shown measured capacitances due to the cells themselves in the pF range, these were performed with sandwiched electrodes and thus the plate area was significantly larger.[115] Thus, while they would have an effect on the system their direct effect would be smaller than what would be observed. Additionally, the magnitude of the capacitance was decreasing rather than increasing as the cells died, which would be expected from the purely capacitative effects of the cells.

More specifically, the physical phenomenon being measured is the increase in double layer capacitance, and Warburg impedance, and the decrease of the charge transfer resistance as the cells lyse and release their ions in the local area. When the cells die they release their ions into the surrounding area and due to the constant AC stimulating voltage are effectively trapped causing a higher relative concentration when compared to the bulk content. This leads to an increase in capacitance from the double layer formed by the ions adhering to the surface of the electrode and the symmetrical reduction and oxidation of ITO into ITO black.

5.4.3 HEPG2

Once we had demonstrated that continuous differentiation with yeast cells was possible we wanted to verify we had the sensitivity to monitor similar relationships with eukaryotes. We had made significant upgrades to the control software in the interval between the experiments and as such we were able to garner significantly more data points to compare. We had also become more familiar with the image analysis software enabling the application of the counting algorithm automatically rather than manually executing it for every image. While it is possible that this added some level of noise to the results, it enabled the analysis of hundreds of images that otherwise would have been impossible. Additionally, due to the sensitive nature of eukaryotes we did not use external toxins to control the rate of cell death. The results are shown in Figure 58.

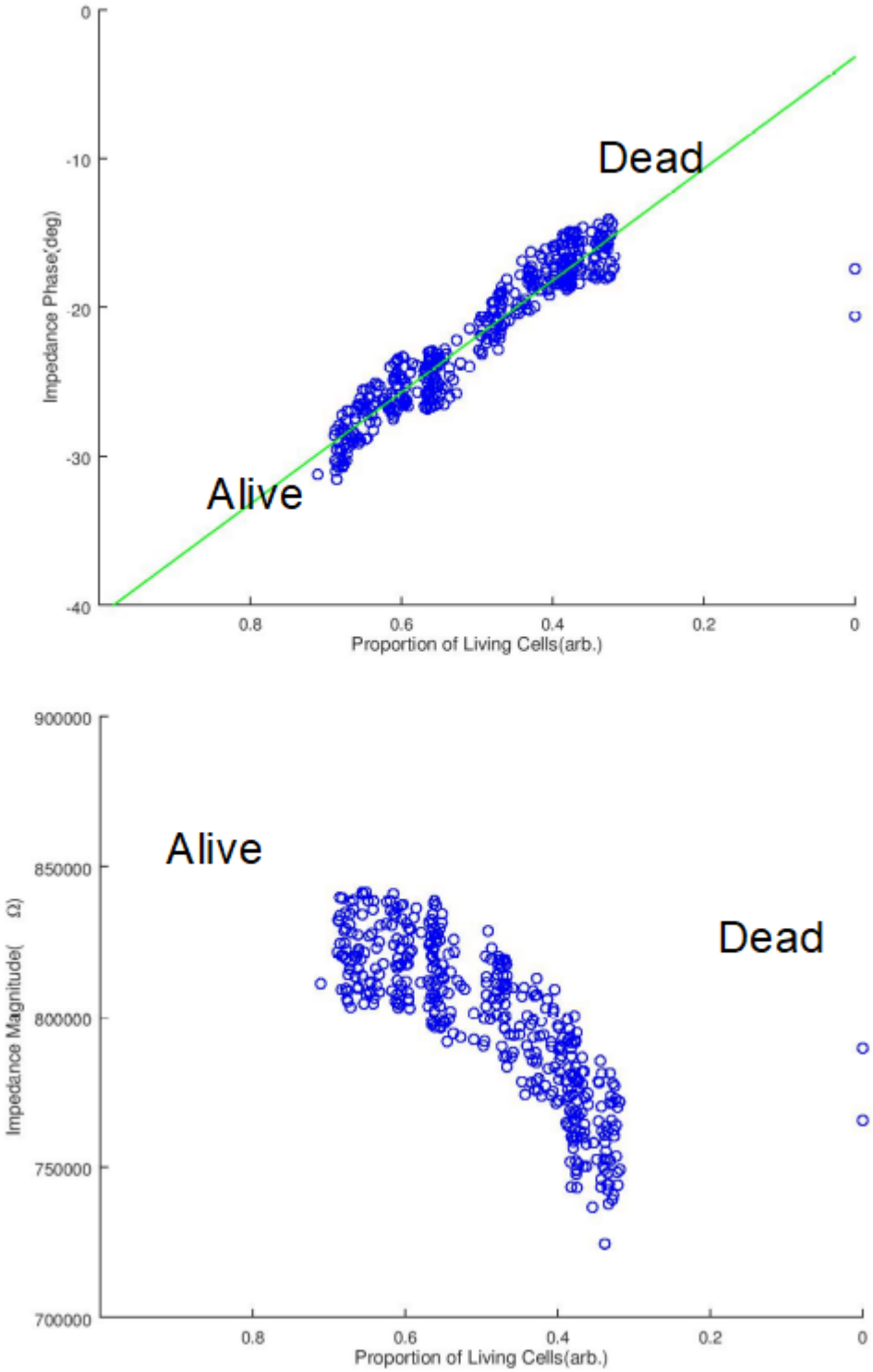

Figure 58: HepG2 Impedance Spectra and model

The results obtained by the impedance spectra were structurally similar to those obtained in the yeast experiments but to a differing degree. Because we did not use a toxin in this experiment because of the more sensitive nature of eukaryotes, we had less control over the death of the cells and as such the culture was not as completely killed over the course of the experiment as the yeast cells. Additionally, there were two data points where the acquisition software failed to properly acquire the inverted microscope image resulting in the two anomalous data-points on the right edge of both graphs.

The phase model for these cells at this location gave a result quite similar to that of the yeast experiments with a phase model of

$$\angle Z = -37.5540 * Alive - 3.1818$$

This similarity, *ceteris paribus*, would be an anomaly due to the expected lower capacitance of eukaryotic cells, but there are several factors unaccounted for. This was caused primarily by the difference of the relative concentration of cells, which was ~3 times more concentrated than the baseline yeast concentration, meaning a comparison to the base model would be an equivalent slope of ~12. Additionally, because the conductivity of the medium was significantly higher, the resistance between the electrodes was smaller as well, making the relative effect of a given unit of capacitance significantly larger.

Much like with the yeast experiments, by extracting the Capacitance we can verify the physical phenomenon that is occurring. While we would expect the capacitative change to follow the same general pattern as that of the yeast cells, the

scale will likely be different due to the differing media and relative ion concentration. The extracted capacitance is shown in Fig. 59.

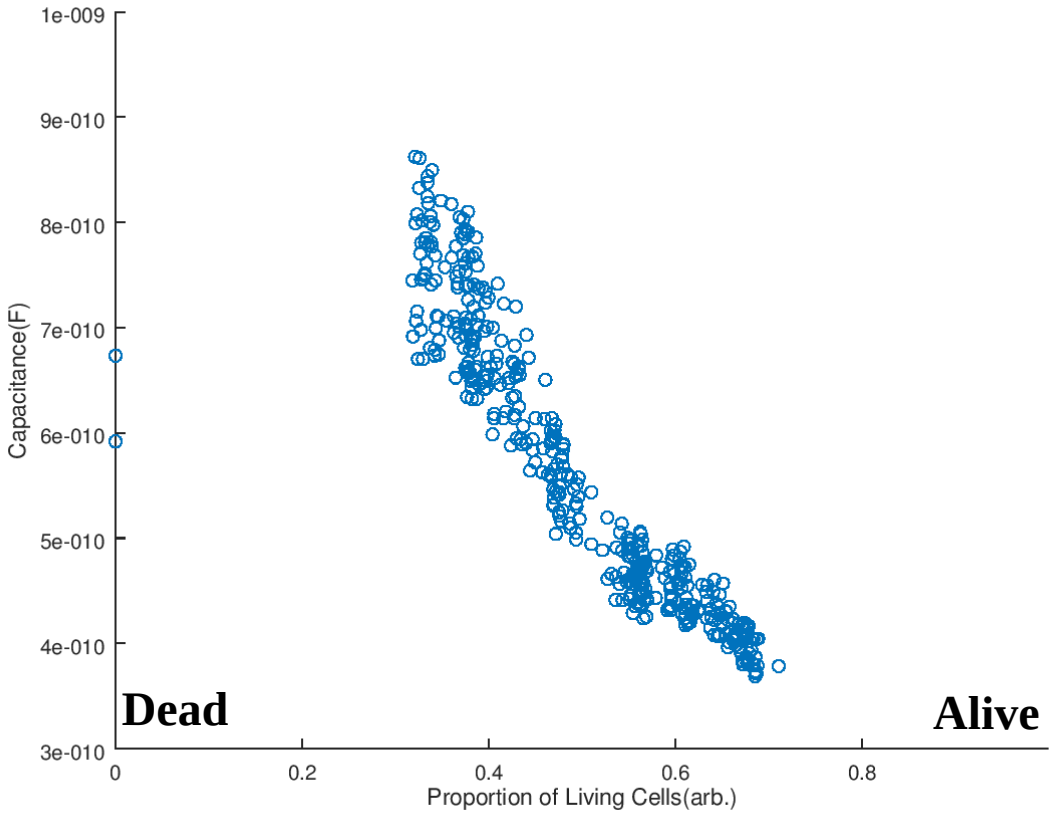

Figure 59: Extracted HepG2 Capacitance

As expected the same general pattern occurred, and the system was dominated by the electrochemical effects. It's important to note that with the yeast cells, due to the increased ion concentration in both the medium and the cells themselves the base double layer capacitance and the change as the cells died both increased at ~10 times that of the yeast experiments.

5.4.4 Summary

We have demonstrated the use of a TFT platform as an electrical sensing methodology capable of continuous differentiation and prediction of cell cultures in real time. We independently verified these results optically using fluorescent dyes, but this method does not necessitate any dyes or other marking mechanisms making it ideal for long term analysis of cell cultures.

5.5 Moth Bio-Sensor

5.5.1 Background

While cell death is one of the more drastic ways to change the electrical properties of a cell, many do so naturally, albeit in a less extreme manner. These cells are called electrogenic cells and in response to a stimulus pump ions either in or out of the cell to create a localized potential differential. These are called electrogenic cells and are commonly found in the nervous system, and with system that interact with it.

By using these cells on our substrate, we plan to electrically detect the presence of these stimulii. The particular cell type we are interested in are olfactory cells, found in the nose, and respond to the presence of various volatile organics and pheromones that correspond to scents, emitting a signal so as to inform the brain of the presence of these compounds. Insects tend to have a significantly better sense of smell than mammals, even those known for their sense of smells such as dogs. [119] These cells have already been shown to work on gate mediated ISFET systems by Dr. Terutsuki, who collaborated with us on this experiment, providing the cells, pumping apparatus, and expertise.[36] However, as explained in Chapter 2

ISFET systems are inherently opaque limiting their applications, by utilizing our tTFT substrate we hoped to expand the utility of such sensors.

5.5.2 Experiment

For our experiments we are using SF21 moth olfactory cells[120] modified to express the gene BMOR3[121] that causes them to respond to a pheromone called bombykal (BAL). [122] While measuring the impedance continuously at 1kHz, we will first activate the peristaltic pumps moving Di-MethylSulfOxide (DMSO) medium into and out of the chamber at equivalent rates. Then we will pump the chemically similar compound bombykol (BOL)[123] as a control which we don't expect to cause a reaction. Finally we will pump two different concentrations of BAL (10 μM and 30 μM) to determine if we can detect both concentrations on our device. The gate voltage was Vg=12V, and the stimulated voltage was .01Vpp at 1 kHz. The results are shown in Figure 60 with red lines indicating the different pumping stages.

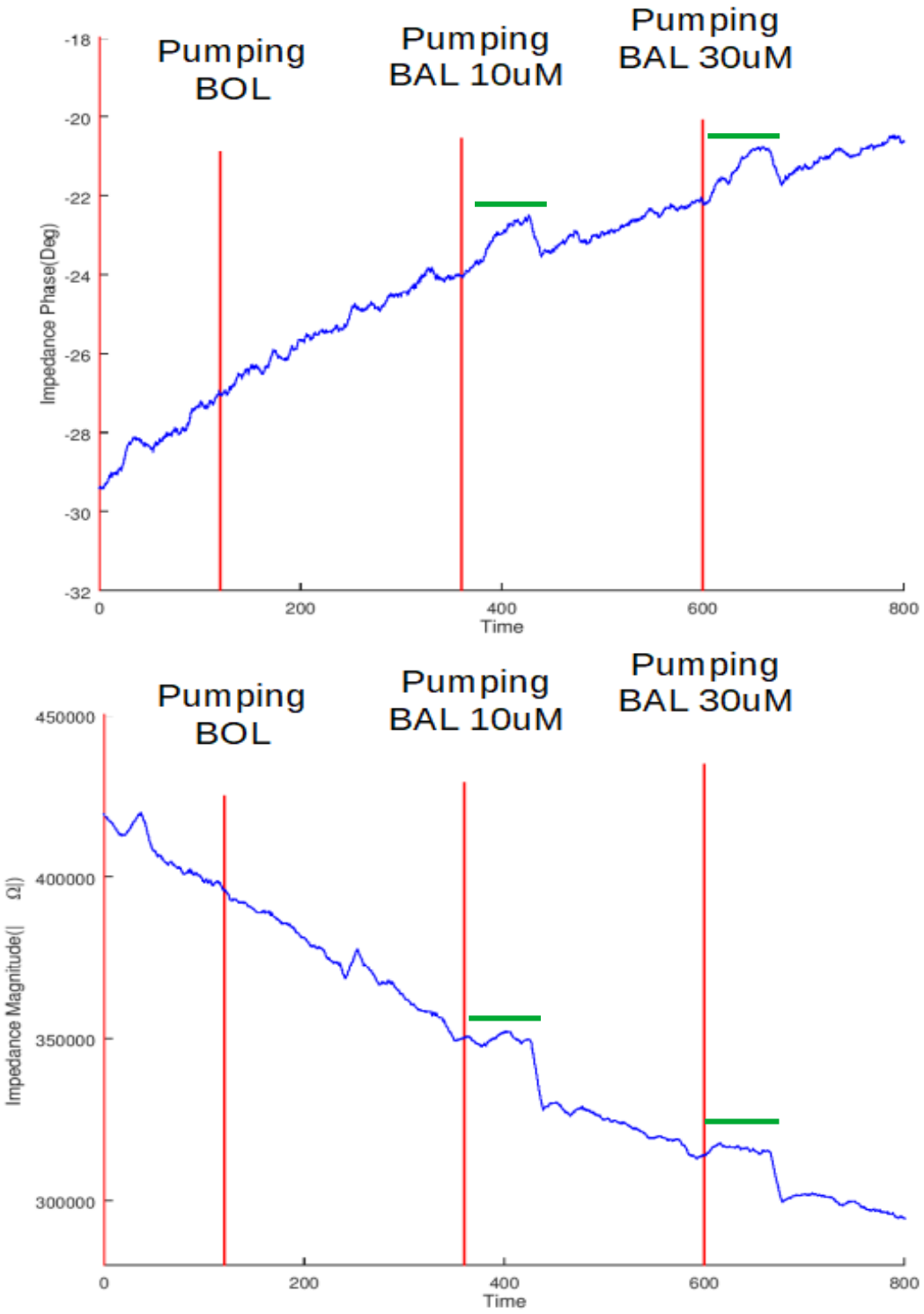

Figure 60: Sf21 Impedance chemical sensor with signals overlined in green

One issue we have consistently encountered in setups involving pumping are a consistent bias due to the mechanical disruption of stabilization and the inability to have a medium reference without mutating the results. Most notably it exacerbates noise from the electrolyte transfer of the pumping mechanism causing secondary peaks. It does obviate the drift quite effectively. This is explained more in depth in Chapter 6. However, there is a strong deviation from this in both magnitude and phase ~30 seconds after the introduction of BAL, and no deviation from DMSO and BOL pumping, which is in strong agreement with prior research on sf21 cells. [36] The drop in both phase and impedance caused by the SF21 cells is indicative of the pumping out of ions matching the physical phenomenon we would expect.

By utilizing the number of ionic channels, as well as the pumping rate of the ionic channels, we can estimate the amount of channel activation in a given animal cell by a given analyte using the equations below. The only significant variation between cells would be the number of cells, the number of channels, and the charge of the ion being pumped, all of which can be accounted for by a linear scaling factor.

$$\Delta\sigma = \Delta\sigma_{channel} N_{channel}$$
$$\Delta\sigma_{channel} = \Lambda * \left(\Delta \frac{Ca^{+2}}{mol}\right)/V$$
$$\Lambda = 119 \frac{S\,Cm^2}{mol}$$
$$V \approx 10^{-8}\, cm^3$$
$$\Delta Ca^{+2} = 2.5 * 10^7/s$$
$$\Delta\sigma_{channel} = 119 * 2.5 * 10^7/\left(6.22 * 10^{23} * 10^{-8}\right) = 4.78 * 10^{-7} \frac{S}{Cm\,s}$$
$$Nchannel \approx 10000$$
$$T \approx 30\,s$$
$$\Delta\sigma \approx 4.78 * 10^{-7} * 10000 * 30 \approx .14\, S/cm$$

[124]–[126]

Given that animal cells have a base conductivity of ~1 S/cm[124], we would expect an approximately 14% increase in conductivity, and thus capacitance due to the change in frequency dependent complex permittivity if all ion channels are activated. Given that the cells used in our electrogenic sensing studies were modified to almost exclusively react with a single compound, this is a reasonable base assumption, though of course genetic variation, as well as cell viability and defect rates will lower this value in practice. It is also important to know that there was no information of the exact number of ion channels, and pumping rates of those used in the SF21 cells we used so general values for neurons which are far more studied were used instead.

The primary difference between the theory and experimental results is a matter of scale. Given 100% activation of ion channels, we would expect an approximately 14% increase in impedance magnitude due to capacitance, however the measured results were on the order of 5%, which is in reasonable agreement with the theory given the nature of the assumptions used. There was a paucity of information on the ion channel characteristics of the SF21 cells used and as such some of the difference is likely due to variation between them and electrogenic neuron cells. Additionally, there are losses within the transistors even at the relatively low measured frequency of 1kHz, and secondly it is likely that 100% ion channel activation is unachievable due to both the state of the cells themselves as well as asynchronous activation of ion channels. Altogether however, the peaks are clearly extractable and are in the same order as predicted values.

5.5.3 Summary

We have demonstrated the use of intermediate cells as a means to create a primitive chemical sensor using our device. While there are some long term stability issues with the current setup, the results are consistent with those found by other researchers.

5.6 Antibody Based Antigen Sensor

5.6.1 Background

While cells are useful in the creation of intermediate chemical sensors, any system reliant on them will have inherent instability issues as well as necessitating regulation of medium and environmental factors in order to ensure viability. By using alternate biological compounds to form a sensing system we can obviate the need for such controls. We decided to use antibodies to their inherent medical diagnostic applications. Antibodies are a key component of our immune system and function by binding with marker proteins known as antigens to attach to cells and compounds of interest. In our immune system this serves as a means of marking them for destruction by white cell, and if the relative concentrations are high enough, tearing bacteria apart by rupturing their cell membrane. Both antibodies and antigens are highly dielectric, and as such we wanted to explore if we could detect the bonding of antigens to antibodies using our device. A schematic of bonding is shown in Figure 61.[127]

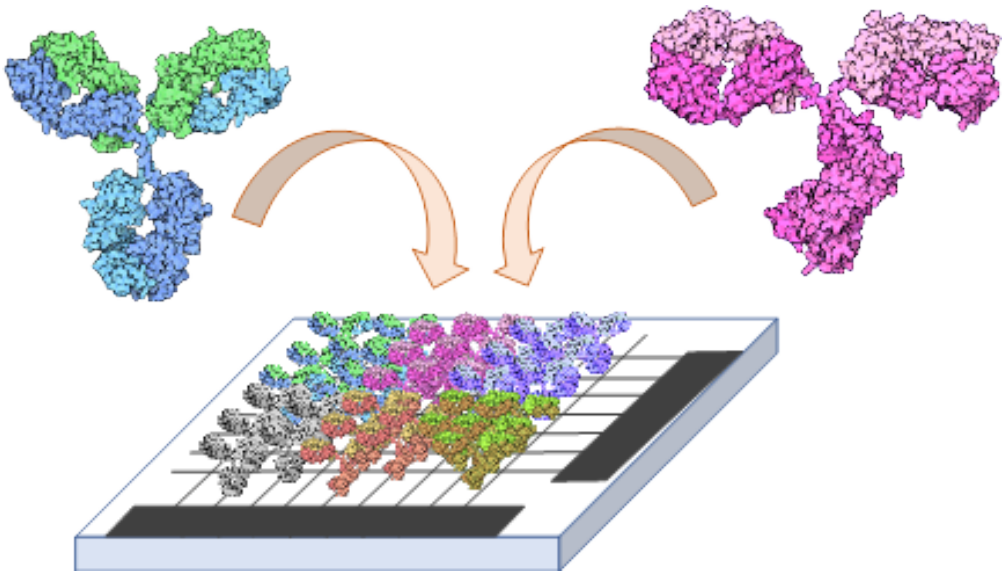

Figure 61: Antibody Adhesion to device[127]

5.6.2 Experiment

These experiments were performed with the help of Sakai Laboratory, with the antibody bonding process, and device treatment performed by Mr. Zhu, a Masters student in Sakai Laboratory. The experiments were performed on several isolated PDMS chambers on the device, half with antibodies bonded within them, and half without to serve as controls. After a period of measurement with PBS, we then manually pumped the PBS containing antigens into the chambers and monitored the results over time. If the difference in dielectric properties is measurable, we would expect the end state impedance to differ significantly between the control and antibody laden devices. The results are shown in Figure 62. Much like the previous experiments a Vg of 12V and a stimulating voltage of 0.1 Vpp was applied at 1 kHz with a sampling rate of 4 Hz.

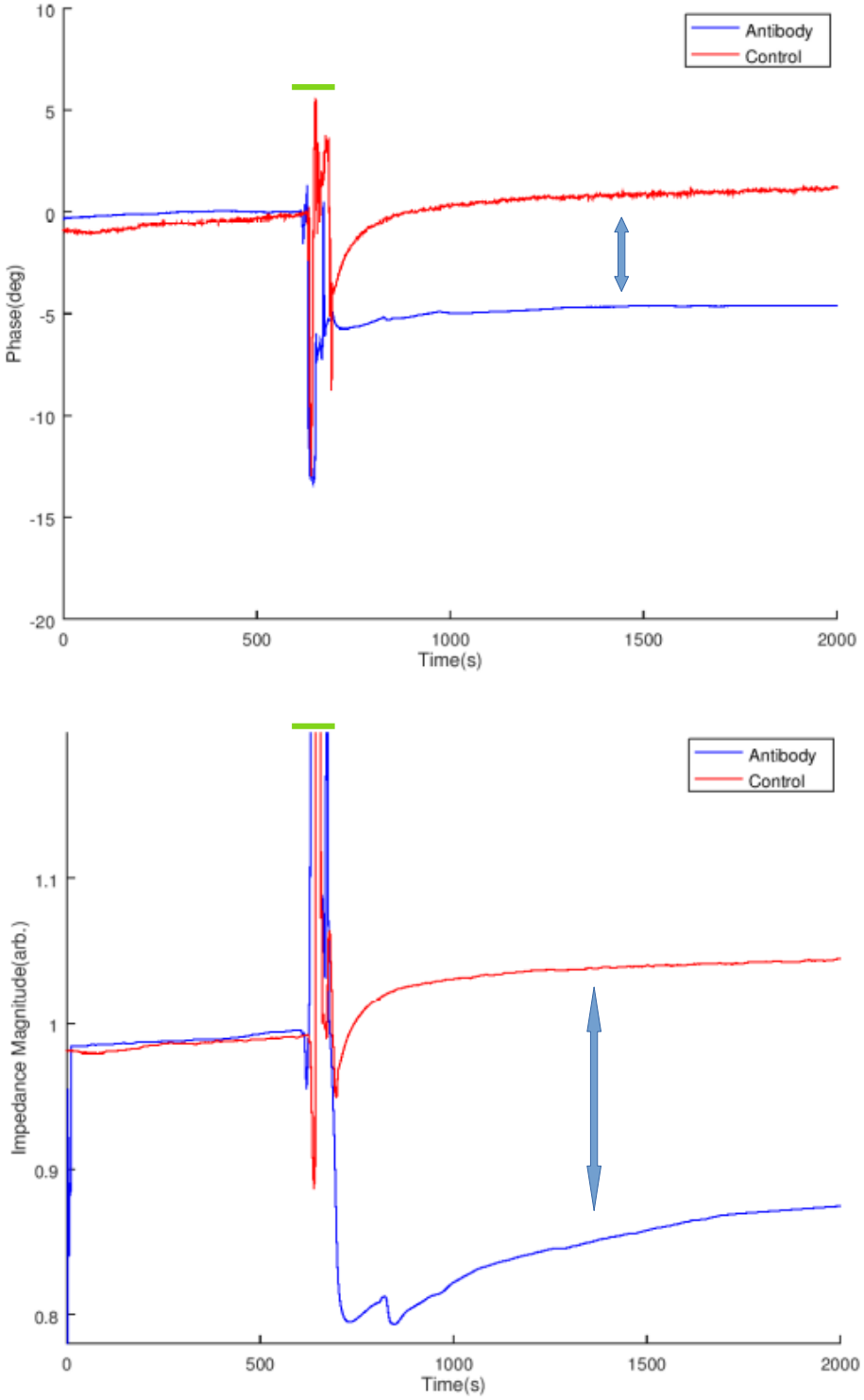

Figure 62: Impedance analysis of antibody seeded and untreated devices with the pumping stage overlined in green

The effect of the antibody pumping on the impedance, both phase and magnitude, is clearly visible in the results of the experiment. The reason for the extremely high noise around the pumping of the antibody is due to the physical disruption from the pumping action, due to logistical constraints we were unable to use a peristaltic pump and as such had to do so with a syringe. There are two physical results indicated by the impedance, firstly that the phase lag increase corresponds with an increase in capacitance, and the drop in magnitude corresponds with a larger relative drop in resistance simultaneously. The capacitance is, as expected caused by an increase in the dielectric constant of the antibody/antigen compound with respect to that of the antibody. This directly explains the increase in capacitance because the equation for capacitance is $C = \epsilon \frac{A}{D}$. However, *ceteris paribus* this would cause an increase in impedance magnitude. Thus there must also be a simultaneous decrease in resistance. Physically, like other electrochemical phenomena, this can be explained by the Randles electrochemical circuit, and more specifically a change in charge transfer resistance. Other works, albeit on relatively non-reactive platinum electrodes, found that a change in charge transfer resistance of 30kOhm.[128] This is similar in scale to the results found in our experiments.

5.6.3 Summary

We have demonstrated the use of antibodies as an intermediate compound for the detection of antigens on our device. This can be trivially expanded to a large

number of potentially useful medical diagnostic applications, as well as having potential uses in drug treatment experimentation.

5.7 2D Differentiation

5.7.1 Background

While we have demonstrate a wide variety of impedance analysis experiments on our device, they all have one major limitation; they are performed with the sampling of one electrode pair at a time. Our device has tens of thousands of electrodes, but if we only use a couple that multiplicity is meaningless. In order to take advantage of the full device, clearly the control system needs to modified to use a large number of electrodes.

5.7.2 Experiment

In order to control a large number of electrodes simultaneously on our device we partnered with the University of Bordeaux through the LIMMS program. They designed and produced a device called Japastim, pictured below in Figure 63.

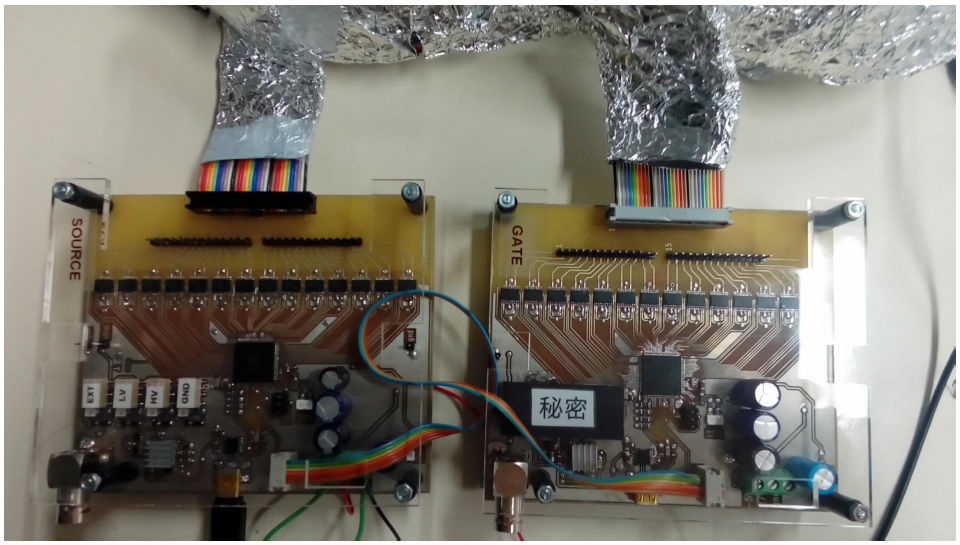

Figure 63: Japastim Device

The device consists of two cards, each of which can be used to stimulate 28 pins that can be connected to lines on the device enabling the control of 784 electrodes simultaneously. All of this is controlled through a serial terminal, which we integrated into Labview through the VISA protocol. Unfortunately, the current device cannot be used for current sensing in its current iteration. Specific details about the device can be found in Appendix D.

For this experiment we deposited droplets of DIW, medium, and medium containing yeast cells. We performed two different frequency measurements to determine which was on each measured electrode pair. We used 100 kHz to differentiate between air, DIW, and medium and then a second interrogation at 10 kHz in order to differentiate between medium and medium containing yeast. The results are shown in Figure 64.[110]

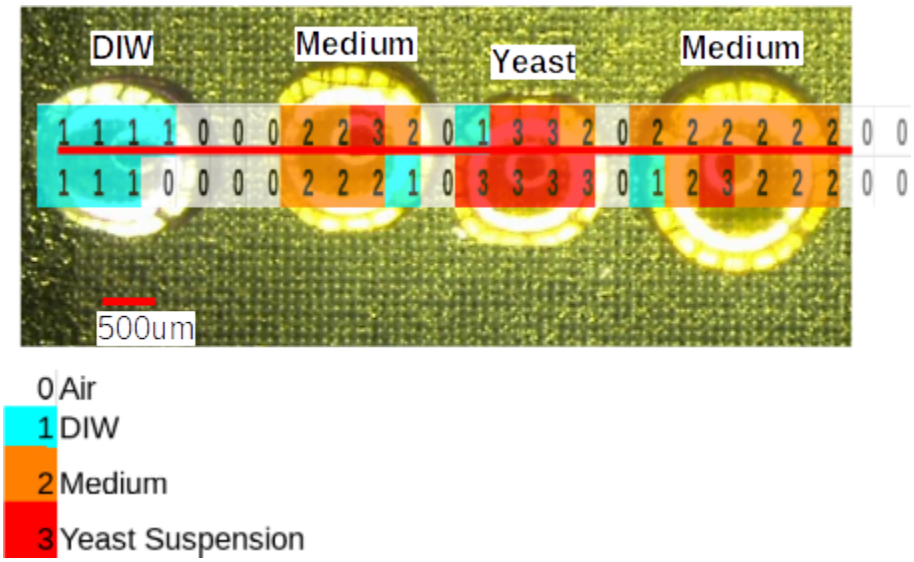

Figure 64: 2D Impedance detection of droplets[110]

Out of the 50 measurement points, only 7 were misidentified giving a total accuracy of 86%. By increasing the frequencies measured on the device, this can be increased, though that would result in a corresponding increase in the time to perform the total measurements.

5.7.3 Summary

Despite only taking two data points we managed to get 86% accuracy with determining the content of a given electrode pair using only impedance. This can be abstracted to differentiating between any experiment demonstrated on this device. Accuracy can in theory be arbitrarily increased at the expense of time required to take measurements.

5.8 Chapter Summary

We have demonstrated a large number of differentiations are capable on our transparent thin film transistor gated electrode array substrate. We showed that different bulk media can be differentiated upon our device, and then demonstrated

that we could detect the differences between living and dead cell cultures. We then expanded upon this by building predictive models capable of determining the amount of living cells, both eukaryotic and prokaryotic, in a given region on the device. Once we had demonstrated those gross measurements were possible we built a primitive chemical sensor using moth olfactory cells as an intermediary measuring a 5% increase in impedance corresponding to the intake of ions. We then abandoned cells entirely and built a chemical sensor using antibodies bonded to the substrate. This demonstrated a 15% differential between the devices with and without the antibody. Once we had demonstrated a variety of potential applications for impedance sensing on our device we demonstrated 2D analysis of the device achieving 86% identification accuracy with only two measurements. Taking these all together we can create a large number of different chemical sensors and cell state analysis tools all on the same device.

Chapter 6:Discussion

In this chapter we will discuss several of the issues encountered with the device. We will first discuss issues of signal variation, and how we normalized the results, and continue with a discussion of bias and environmental leakage. We will then continue with an explanation of issue with the pumping setups and follow up with an explanation of the thermal characteristics of the device. We will finish up with a discussion of how the device is cleaned so it may be reused and a summary of where our device fits in with prior art.

6.1 Evaluation

As mentioned in Chapter 1, the primary device properties that are necessary to be fulfilled in order for this tTFT plate to function as a total analytical system are as follows. First the device must be bio-compatible, being minimally mutative to cells grown upon the device. Secondly, it must be transparent enough to enable optical observation through an inverted microscope. Thirdly it must be addressable so as to control as many electrodes as possible.

6.1.1 Bio-compatibility

Our device has shown remarkable bio-compatability. Even sensitive cells such as neurons, which are extremely sensitive to environmental contaminants were capable of being grown on our device for up to a month with minimal cytotoxic effects.

6.1.2 Transparency

The device, while not wholly transparent, is transparent enough to enable fluoroscopic measurement. We demonstrated this by performing Propidium Iodide staining and excitation in order to identify non-viable cells. The lit up cells where the PI had bonded to the DNA of the cells were clearly visible and countable.

6.1.3 Scalability

While this iteration of the device does not have the same number of electrodes as the first generation device. Having 50*50=2500 electrodes enabled 100 um resolution across a .5cm x .5cm area. This enables scanning of material over a large area as demonstrated by our droplet detection experiments.

6.1.4 Addressability

Due to the use of IGZO tTFT transistors to gate the electrodes we were able to utilize full 2D addressing to access the full array with a minimum of inputs. By utilizing the Japastim device we were able to further expand upon this addressability controlling up to 28 device inputs from a single source.

6.2 Variation/Normalization

As was briefly mentioned in the experiments where different locations, or different cultures or a control are utilized, normalization is a necessity when it comes to getting consistent results with experimentation. This is due to factors inherent to all biological systems, as well as factors inherent to the device itself.

Biological systems are inherently chaotic, and impedance measurements are extremely sensitive to many of the variations caused by such systems. Due to the reliance of impedance measurements on electric field line pathing, it is extremely sensitive to positioning of cells, extracellular matrix thickness, and other physical variables such as size and membrane anomalies. For example an electrogenic cell with a larger size, and thus smaller ion channel to volume ratio, would experience less of a shift in impedance than a smaller cell with a larger ion channel to volume ratio. Additionally, as mentioned in prior chapters, impedance analysis is highly dependent on electric field pathing which makes factors such as the positioning and mitosis state of the cells another variable that can be difficult to explicitly account for. While some of these can be stochastically mediated by looking at larger areas, this would still necessitate initialization and self differential measurements in order to

garner a consistent result. By looking at the relative shift, we can more accurately describe what is physically occurring in the system.

Furthermore, there are many device specific sources of variation, both due to our specific device constraints as well as universal device factors. One of the primary factors that causes variation in the impedance measurements is electrode geometry and spacing. Due to the dependence of the impedance on electric field pathing, research with different electrode geometry and spacing cannot be strictly compared although the general structural factors(a rise in phase and magnitude for example) will generally be consistent.

Due to the fabrication process of our device different regions on the device itself are not explicitly comparable. Due to variations in layer morphology during the deposition process, electrical properties of the transistors gating our electrodes can vary by as much as a factor of 5. Additionally the ITO layer on the surface of the device has a variable surface morphology, and in addition is deposited on a deformable polymer layer that can further cause variation in electric field pathing. Additionally, the frequency dependent characteristics of the transistor make high frequency operation unfeasible. To quantitatively analyze this a gold, chromium layer was deposited on the surface of the device through sputtering enabling the measuring of a two transistor structure as shown in Figure 65.

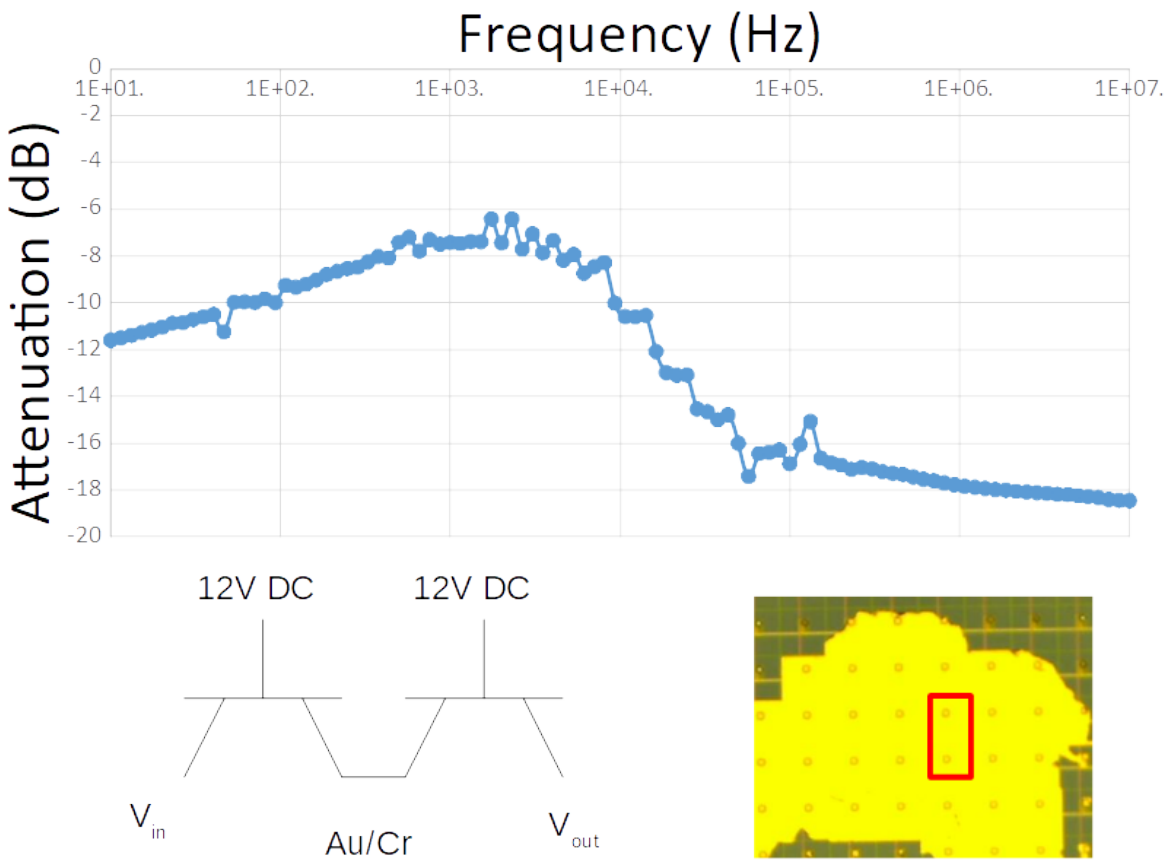

Figure 65: Bode diagram of Double Transistor structure on gold/chromium test structure

As can be clearly seen, the attenuation caused by the transistor peaks at approximately 1kHz, and rapidly decays at higher frequencies. This is the primary limiting factor of the operational frequency of our device.

6.3 Pumping Noise

Despite electrically isolating our system within a Faraday cage we have discovered that we still have a great deal of unmitigatable noise in our peristaltic pumping setup as shown in Figure 66. (t=0 is the start of pumping)

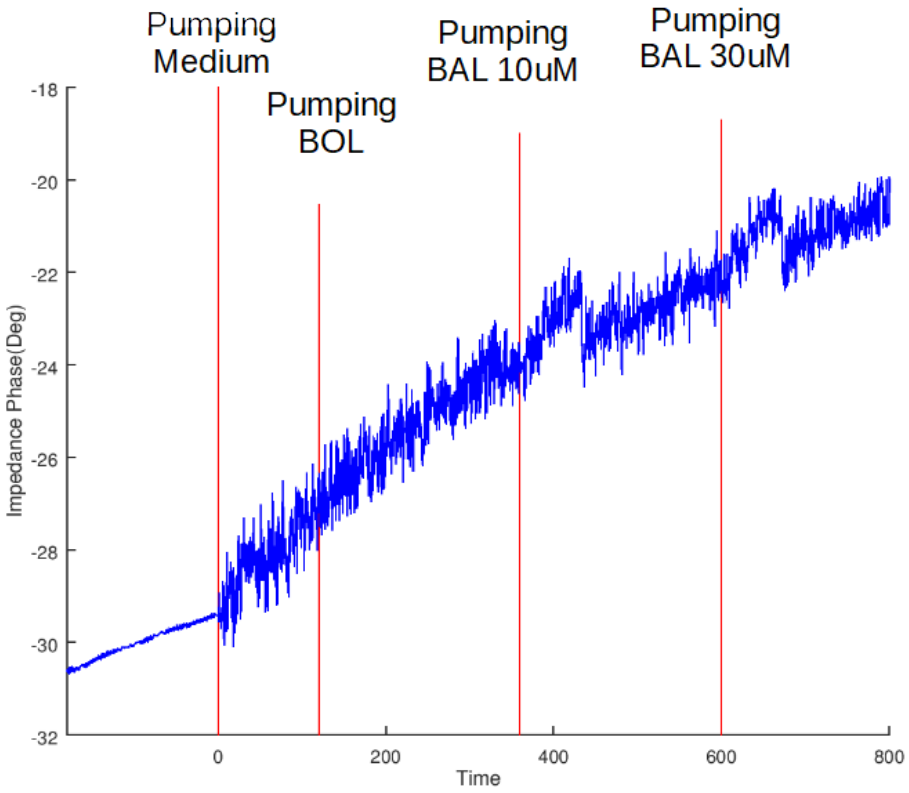

Figure 66: Impedance phase of Sf21 moth olfactory cells

As is clearly visible, despite the pump being outside of the Faraday cage there is a large amount of noise immediately upon the activation of the pump. The reason behind this is due to the plastic discharge of the rubber tubes containing the pumped fluids. As the highly ionic medium is pumped into the tubes it causes stochastic buildup of charge within the tube that it is unable to distribute due to its highly insulative nature. Thus it builds up to a certain point and discharges inducing chaotic potentials in the medium affecting the results. Thankfully this noise was zero mean noise, and as such could be largely mitigated by using a sliding window filter on the data. An example of this filtering, demonstrating the removal of the noise while maintaining structural characteristics is shown below in Figure . It is important to keep in mind that this can only be used on oversampled effects, because the peaks

in this case were tens of seconds long, and the sampling rate was 4 hz, it was applicable to our electrogenic experiments. Measuring more transient effects would require a means by which to mitigate this noise.

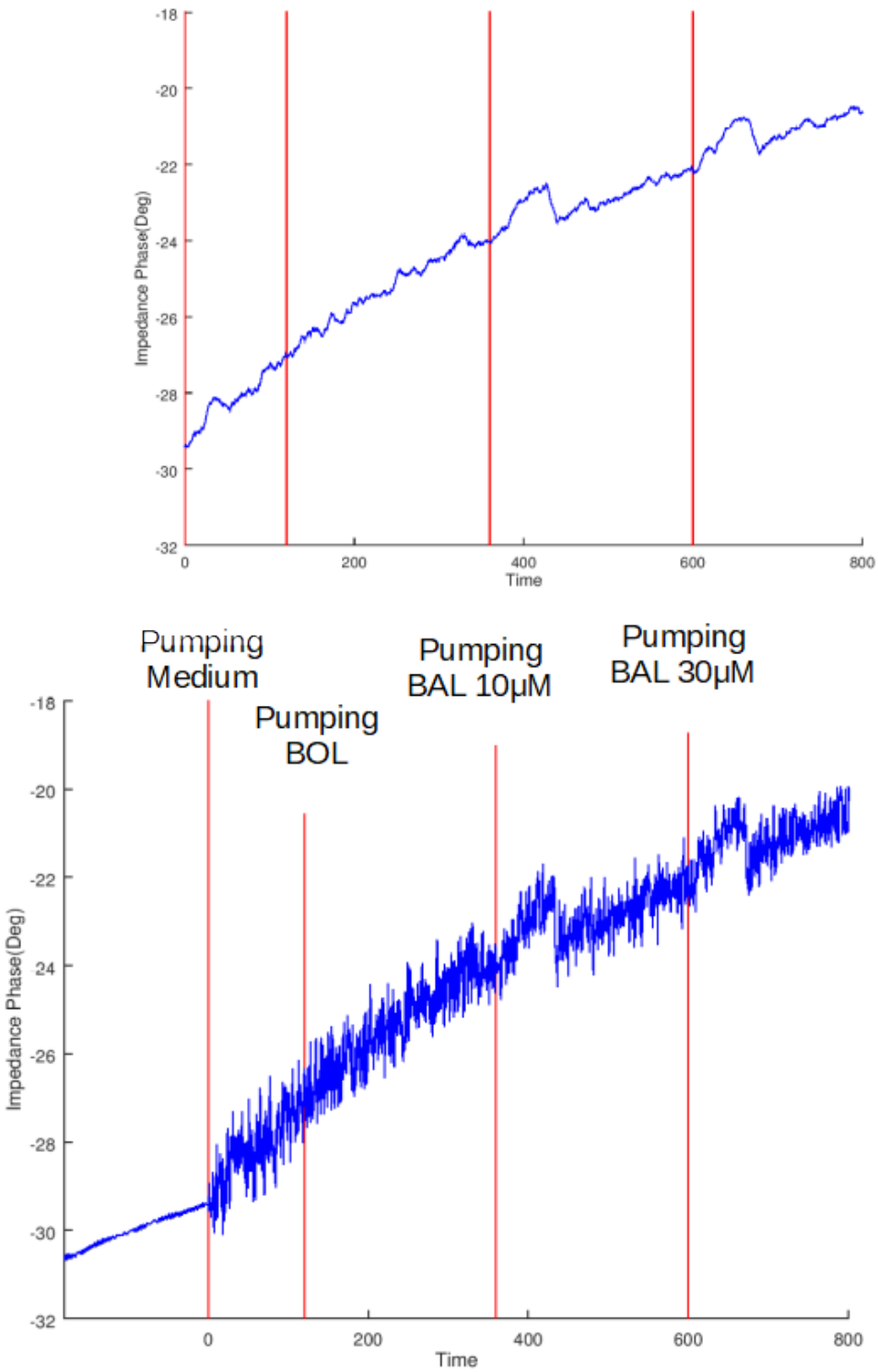

Figure 67: Demonstration of reduction of zero mean noise by sliding window

Additionally, in many of the experiments there was a non permanent secondary peak in the transitory period preceding the introduction of the medium into the chamber. This was present in both voltage and current measurements. The noise was somewhat mitigated by the introduction of a metal tip to the PDMS microtubule carrying the medium, but it is still found in about two thirds of performed experiments. Fortunately, even with this noise peak, the signal peak is still present at the expected time after the stimulated peak, however it is significantly more difficult to detect as shown in Figure 68. Eliminating this peak will be a key factor in making this type of experiment practically viable going into the future.

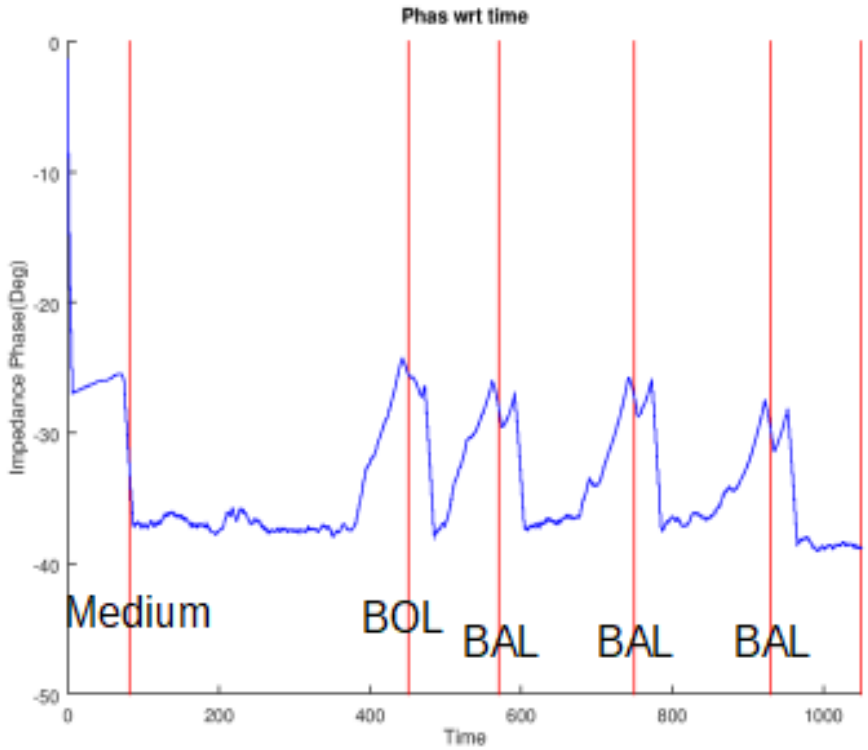

Figure 68: Demonstration of double peak behavior

6.4 Leakage/Reference

As is apparent in some of the experiments, most notably the electrogenic moth olfactory cell experiments there is a strong slope to both the impedance phase and magnitude over time. This is due to the necessity of stimulus in getting an impedance measurement, over time the voltage signal to the surface electrode results in the attraction of ions in the medium despite the pumping resulting in localized concentration despite the pumping. Unfortunately due to the nature of the measurements a conventional reference electrode in the medium is unable to counteract this effect, and in fact completely fouls the experiment. This is due to the preferential pathing of the electric field to the reference electrode due to not having to pass through the transistor on the device. This fouling is shown in Figure 69. As can be seen the resulting impedance is larger by a factor of 100, which given the same device and measuring location means that the signal received by the lock-in amplifier is 100 times smaller.

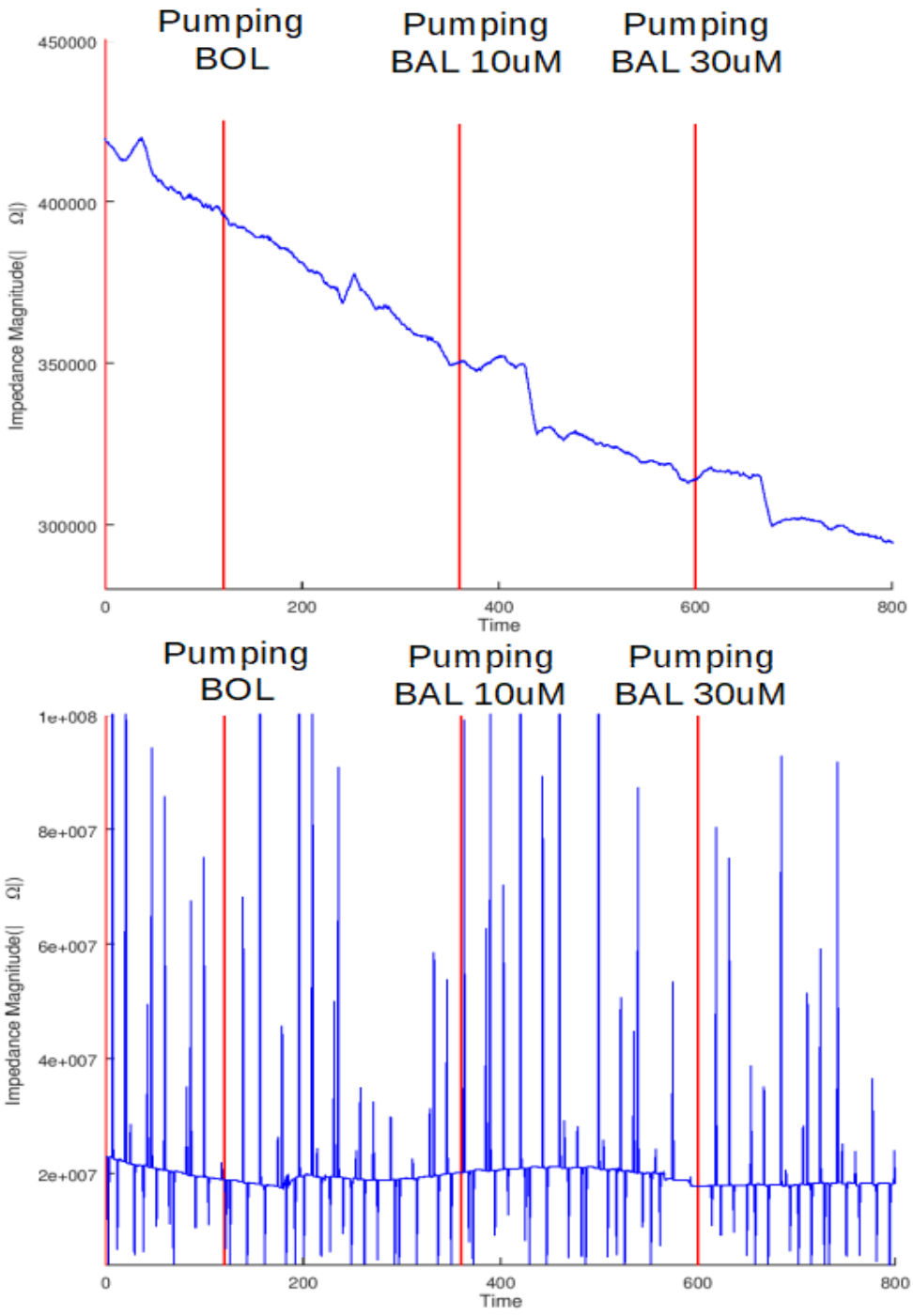

Figure 69: Comparison of impedance magnitude without(top) and with(bottom) a medium internal reference electrode

While a true reference electrode was unworkable, we have experimented with using a pseudo-reference electrode on the device itself in order to minimize temporal

drift. Unlike a true reference electrode which uses a stable electrochemical reaction to create a constant potential with respect to the medium, a pseudo-reference is a connection to a metal within the medium that is not expected to react. This was done utilizing the device itself, by connecting a source line far from the measurement and stimulation electrodes, this will have the effect of placing a neutral reference point on the surface of the electrode array far away from the interrogation region. While it did not significantly help with the net noise in the system, some of the resistive drift seems to have been caused by the pumping mechanism but the capacitative stability from the double layer is signficantly more stable than that without the pseudo reference as shown in Figure 70.

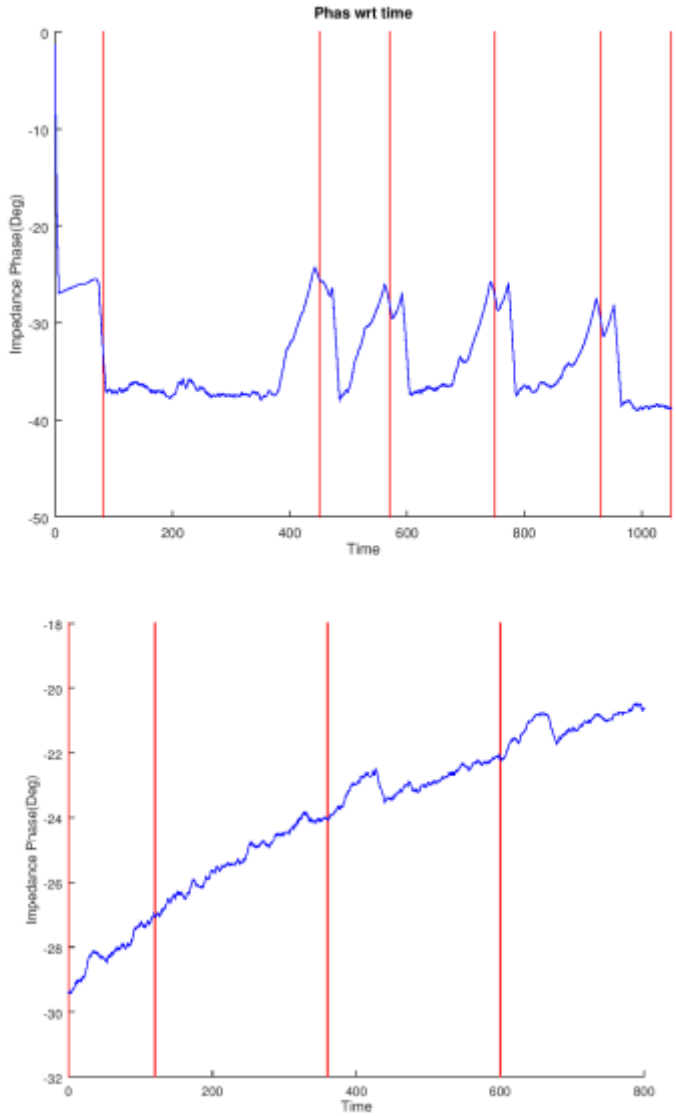

Figure 70: Comparison of pseudo-reference(top) and no reference(bottom)

6.5 Device Reuse/Cleaning

A single use device is limited in application due to its cost, additionally it limits reproducibility due to the necessity of using a different transistor for each experiment. There are a variety of different cleaning methodologies for biological contaminants,

and we used two for our device, trypsin and ultrasonic assisted ethanol and acetone baths.

Trypsin is a serine protease that is commonly used for cutting through enzymes and proteins.[129], [130] We use it to cleave the bonding proteins and extracellular matrix of cells cultured on our device enabling them to be free floating and thus easily removed. Once these bulk contaminants are removed we can use more through methods to eradicate the remnant contaminants.

Ethanol and acetone are both useful for removing organic compounds on the device. However due to the small feature size of the device conventional solvent baths are insufficient to adequately clean the device for reuse. Thus, an ultrasonic bath is used to facilitate more efficient cleaning. An ultrasonic bath operates by pulsing high frequency ultrasound into the device so as to induce vibration and enhance the cleavage by the ethanol and acetone. This results in a clean and reusable device that is not cytotoxic even to extremely sensitive cells such as neurons.

6.6 Chapter Summary

In this chapter we discussed several of the experimental design considerations we ran into. We explained the sources of variation and the necessity of normalization as well as several of the forms of bias we ran into. We also explained the process for cleaning the device so that it can be reused.

Chapter 7:Conclusion

This chapter summarizes the entirety of this dissertation, and then proceeds with a discussion of the types of applications we can institute with the experiments proven in this work. Afterwards, we will opine about the future projects already planned for this methodology as well as some of the larger goals this work is a part of.

7.1 Summary

Analyzing the health of cell cultures in real time is of critical importance to the medical industry, particular when it comes to diagnostics and drug development. Being able to do so over prolonged periods of time enables the rapid iteration of drug testing methodology on a single substrate that is unfeasible with current optical analysis techniques, while current electrical analysis techniques are limited in scope due to the choice between either high surface coverage or opacity.

In this work we have explored the novel application of an Indium Gallium Zinc Oxide(IGZO) transparent Thin Film Transistor(tTFT) substrate to perform electrical analysis of cell cultures and biological complexes both for determining viability as well as creating simple chemical sensors. We demonstrated strong agreement with capacitative predictions for homogenius media. We also demonstrated strong agreement with the frequency drop offs shown in prior experimentation. We were able to build predictive models for determining the number of living cells in a given culture, creating a large area transparent TFT planar culture impedance analysis setup for the first time. We demonstrated the first detection of animal odorant response on a transparent TFT electrode array substrate. We were able to detect a 5% change in the impedance of moth cells when introduced to an odorant corresponding to 20% of the theoretically optimal signal measurable on a bare un-gated electrode. We also measured the impedance change of antibodies as they bond with antigens for the first time on a transparent TFT electrode array. We measured a 20% drop in impedance upon the bonding of the antigen to the antibody. We have also built the first tTFT droplet detection system utilizing impedance. We

were able to correctly identify droplets with 86% accuracy through the use of only two measurements. While this technology has been used for decades in the usage of the lower glass of LCD screens, by applying it to biological systems we designed a device that can theoretically scale up to m^2 surface area with um resolution. We demonstrated not only that our device capable of performing such experiments, but that it can do so without interfering with conventional optical measurements. We have also demonstrated the simultaneous optical and electrical analysis of cell cultures to build predictive models of cell viability, and the expansion of the control system to 2D analysis of the entire substrate.

Most importantly, this device can function as a complete biological platform inducing motion, mixing, controlled lysis, rotation, and countless other proven electrical manipulations simultaneously. This work can function as a cornerstone of the sensing portion of a true micro total analytical system(uTAS) capable of performing almost limitless varieties of biological experimentation.

7.2 Theoretically Implementable systems

While the experiments expressed in this work may appear to be limited in scope, they form the cornerstone of a wide variety of potential applications. Medium differentiation enables significant enhancement to the already demonstrated ElectroWetting On Dielectric(EWOD) droplet motion system on our device. By being able to determine what specific droplets contain, can monitor them and ensure that droplet loss and spreading is compensated for. We could even combine this with

trypsin and other reagents in order to create a cell mobility aparatus, which could cleave cells in a localized area and move them to an outlet for other applications.

The cell detection experiments can be used to track a wide variety of medically relevant phenomena. Cancer migration, how cancer cells move throughout the body and metastasize is a poorly understood process and long term analysis of such motion could open up countless insights into the mechanisms and principles behind it. By differentiating between different cell forms it may even be possible to detect the differentiation of stem cells, a chaotic and difficult process with a high failure rate. Making such a differentiation electrically would enable the continued use of such post-differentiated cells unlike conventional optical measurements which would damage the cells or require complex microfluidic sampling mechanisms.

Finally, the electrogenic and antibody chemical sensor result could be trivially applied to vast chimeric sensing arrays. By depositing cells and or antibodies in specific spatial regions and detecting where impedance changes we can measure an arbitrary number of compounds simultaneously on a single substrate with arbitrary specificity and tweakable sensitivity. These assays are commonly used for a variety of diagnostic and research applications, but they typically operate either optically, or electrically. By integrating both optical and electrical measurements on our device we enable much greater specificity as well as the integration of the assays with conventional culturing.

This work opens up a large number of potential future applications, and our research group will hopefully continue to expand to even further applications in the years to come.

7.3 Conclusion

This work presents a novel application of an established substrate technology, IGZO channel tTFT gated electrode arrays to the differentiation of organic compounds. By reapplying this technology to the biological field we have constructed a large surface area electrical analysis platform that does not interfere with conventional optical analysis. We have proven the viability of material differentiation, cell detection, continuous cell state detection as well as antigen and electrogenic cell based chemical sensors. Given the prior work on this type of device by our research work, this will provide a powerful analytical tool for a micro total analytical system capable of arbitrary manipulation and analysis of any conceivable organic structure or compound.

Appendix A: Labview Programs

In order to implement our experiments in a reasonable amount of time it was necessary to have a control system capable of dynamically altering their parameters and controlling the timing between them. For this purpose we decided to use National Instruments Labview in order to control our experiments. This chapter will explain the general structure of the Labview programs we used to control our equipment.

A.1 Main Control Program

A.1.1 Introduction

In order to control the basic experimental setup, specifically the lock-in amplifier and the AC signal source, we developed a Labview program to automate the sweeping and experimental setup. We designed it to be plug and play, both literally in the device driver handling as well as in being easy to use to the untrained user. Structurally our program is a state machine sandwiched between opening and data handling routines.

A.1.2 User Interface

The user interface for our device is shown below in Figure 71.

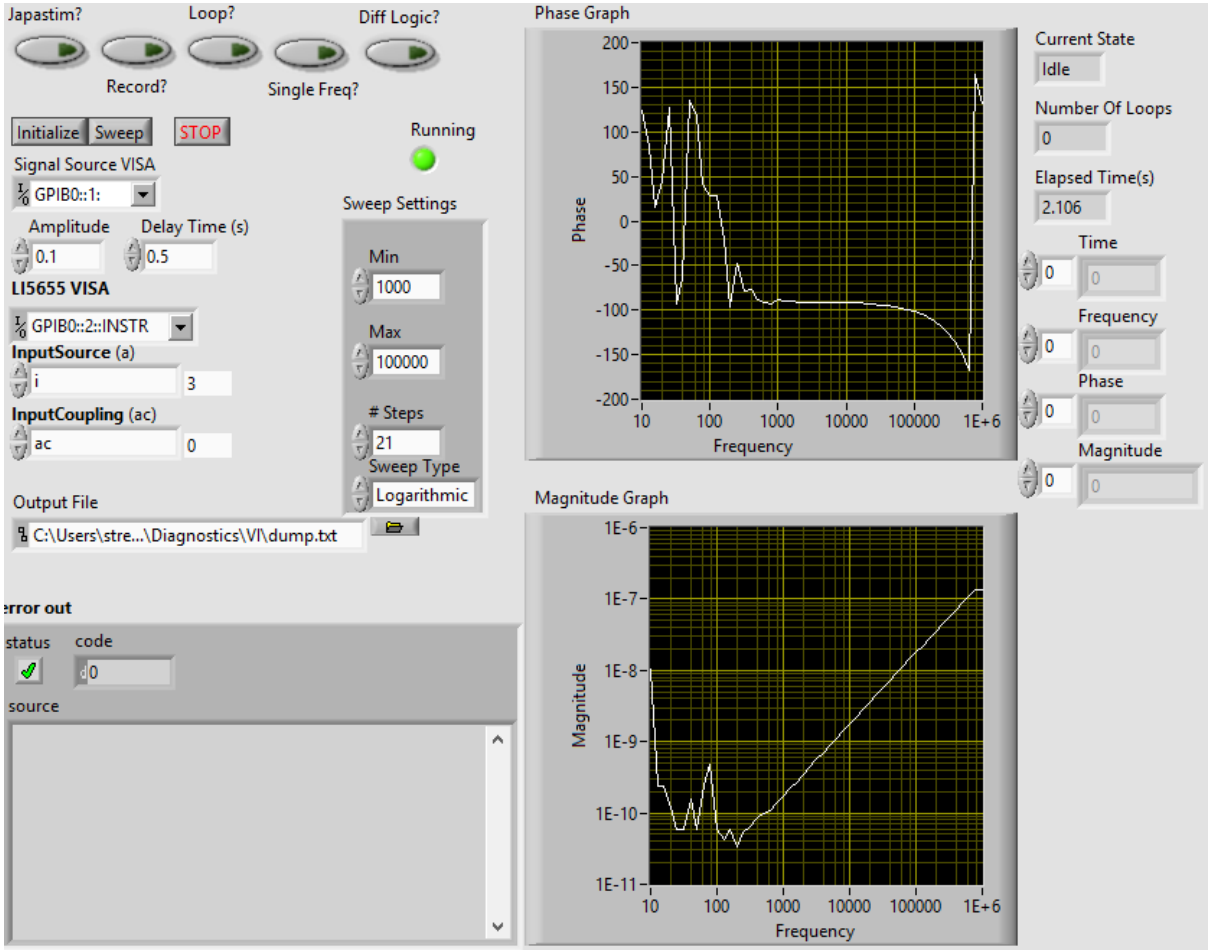

Figure 71: User Interface for our Labview Control Program

The top left consists of five function altering buttons, the first is the "Japastim?" switch talks with the Japastim control program discussed later, and in the future will be integrated into this program. The "Record?" switch determines whether or not the data is output to a file or simply shown on screen. The "Loop?" switch determines whether the program loops infinitely or only runs once. The "Single Freq?" toggle turns on/off optimizations to the program that rely on the AC signals frequency remaining constant. The "Diff Logic?" button enables differential logic and classification for multiple tiered analysis setups such as those described in our 2D Differentiation section.

Below those are three action button that directly control the states of the program. The “Initialize” button sets the state to initializing, which makes the program communicate with all the equipment and set them up to their designated initial states. The “Sweep” button starts the impedance spectroscopy frequency sweep according to the factors described in the following sections. It will either run once or loop depending on the “Loop?” buttons state and output to a file depending on the “record?” buttons state after every loop. The “Stop” button stops the program and runs garbage collection routines.

Below those on the left side are the device configuration settings. The VISA addresses through GPIB for the lock-in amplifier and the signal source are controlled there as are the voltage magnitude for stimulation, the coupling mechanism, and whether we are measuring current or voltage. Additionally, the time between measurements is controlled here, a key factor when frequency switching occurs as there is a time lag between sending a command and it being executed as well as a time lag between the frequency of the signal source being switched and the lock-in amplifier locking in on the new frequency.

To their right is a button indicating program operation as well as the settings for the frequency sweep for the impedance spectroscopy measurements. It consists of a starting frequency, an ending frequency, the number of points between measure and whether to distribute those points linearly or linear in logarithmic scale.

At the very bottom left are the address of the output file as well as the error information from program operation, most commonly showing either no error or

various device communication errors that help troubleshooting issues.

To the right of all the input fields and buttons are two graphs for the phase and magnitude of the current measured by the lock-in amplifier. They are updated at every point and display the results for each sequence, being rewritten on the start of each sweep if the program is set to loop.

To the far right are various status indicators. They include the current state of the program, the number of loops within the current spectrum that have been executed, time information as well as the recorded magnitude and phase information in numerical form.

A.1.3 Program Description

This section will show the functioning of the program as well as some basic descriptions of what each state or section of code does. We progress through 5 basic states. The standard state for the program is the idle state where it loops repeatedly checking every second or so if there has been a signal sent from one of the buttons to cause a state change. The initializing state initializes the equipment, the sweeping state performs an impedance frequency sweep, the exporting state outputs the data in a machine readable format, and the stopping state executes the garbage collection code.

A.1.3.1 Idle State

The idle state simply loops infinitely, only doing anything when a button state change is detected. It cedes control between these checks so as to avoid monopolizing processing power.

A.1.3.2 Initializing State

The Initializing State opens up the visa connection to the provided addresses for the lockin amplifier and the AC signal source. It also verifies and resets the devices and sets the values to the user indicated start value. Once complete it sets the program back to the idle state

A.1.3.4 Sweeping State

The Sweeping state performs the impedance sweep. It calculates the frequency for the next data point, tells the AC source to change its frequency, waits to give the lock-in amplifier time to lock in on the signal then reads our the magnitude and phase values storing them in a data structure and displaying the values on the graphs in the user interface. At the end it switches to the exporting state to output the data.

A.1.3.5 Exporting State

The exporting state is the state wherein the program outputs the stored arrays of timing information, current magnitude and phase are sent to a tab delimited output file. Then the system checks if it is set to loop, and if so returns back to the sweeping state for another cycle, otherwise it sets the program back to the idle state.

A.1.3.6 Stopping State

The stopping state, performs the data cleanup operations after the program is finished executing. It cleanly terminates all the visa connection freeing the devices for control by other programs as well as turning off the AC signal sources output

A.1.4 Source Code

Page 1

JapaStimLI5655V1.vi
C:\Users\stret\Dropbox\Diagnostics\VI\JapaStimLI5655V1.vi
Last modified on 4/16/2019 at 11:55 AM
Printed on 5/30/2019 at 5:52 PM

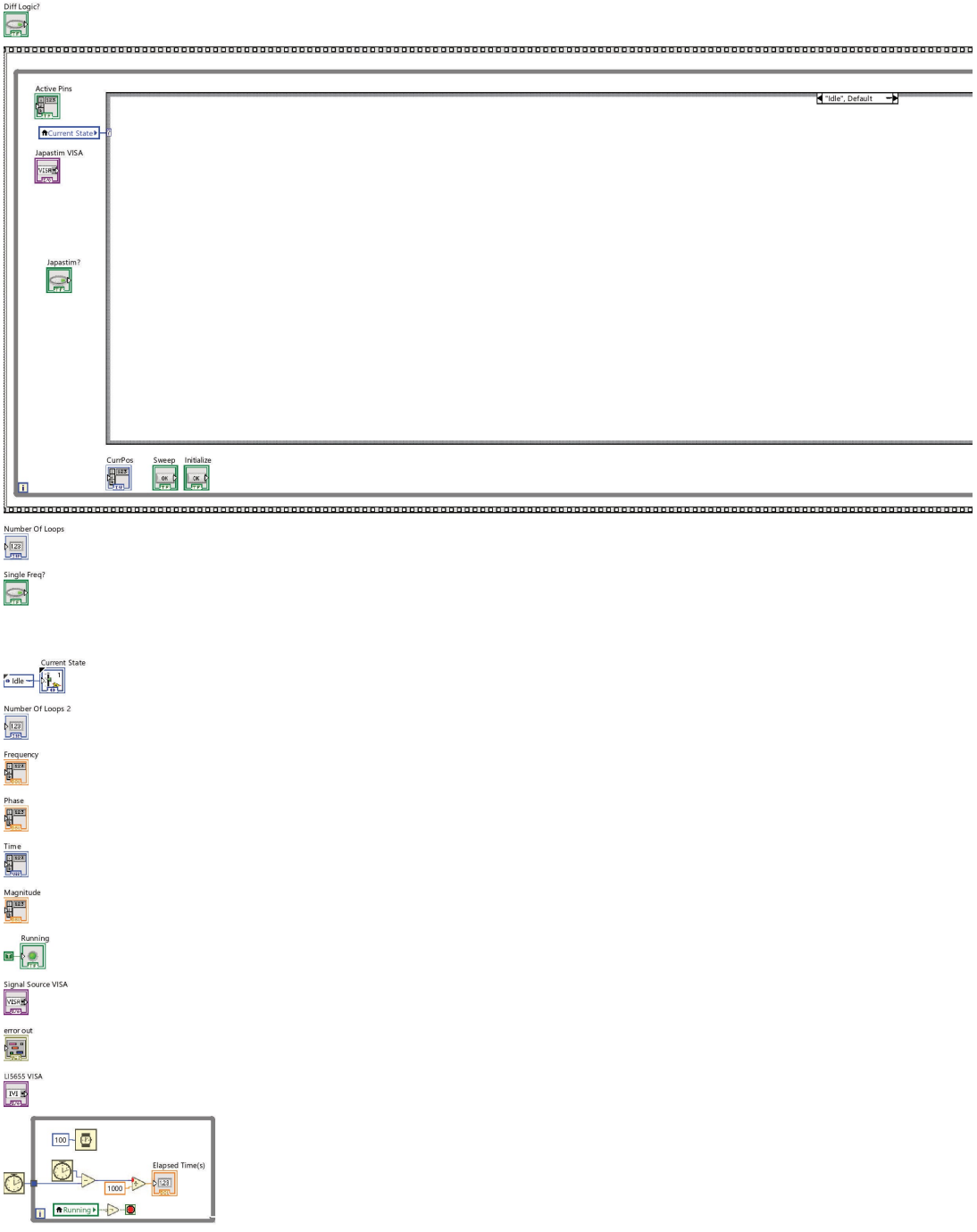

JapaStimLI5655V1.vi
C:\Users\stret\Dropbox\Diagnostics\VI\JapaStimLI5655V1.vi
Last modified on 4/16/2019 at 11:55 AM
Printed on 5/30/2019 at 5:52 PM

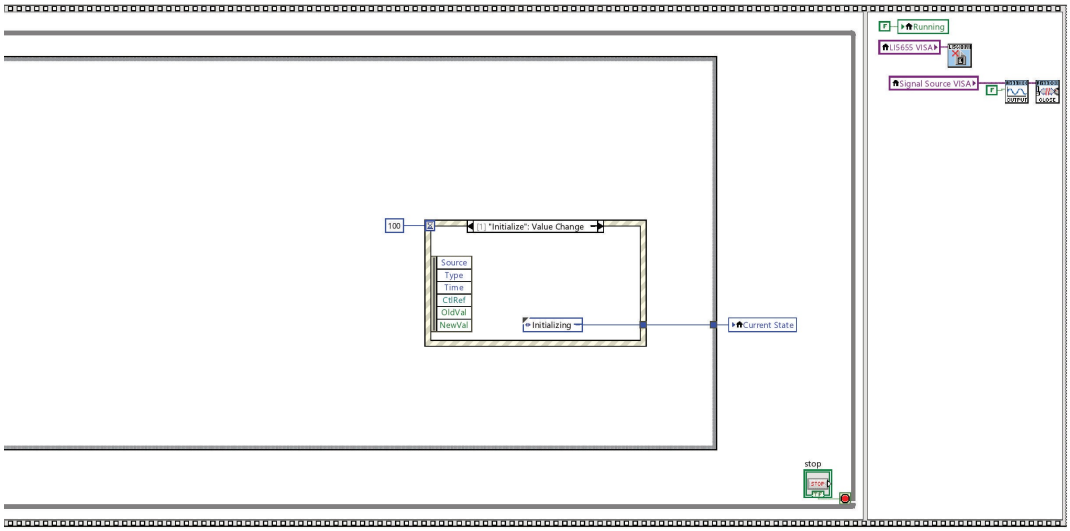

JapaStimLI5655V1.vi
C:\Users\stret\Dropbox\Diagnostics\VI\JapaStimLI5655V1.vi
Last modified on 4/16/2019 at 11:55 AM
Printed on 5/30/2019 at 5:52 PM

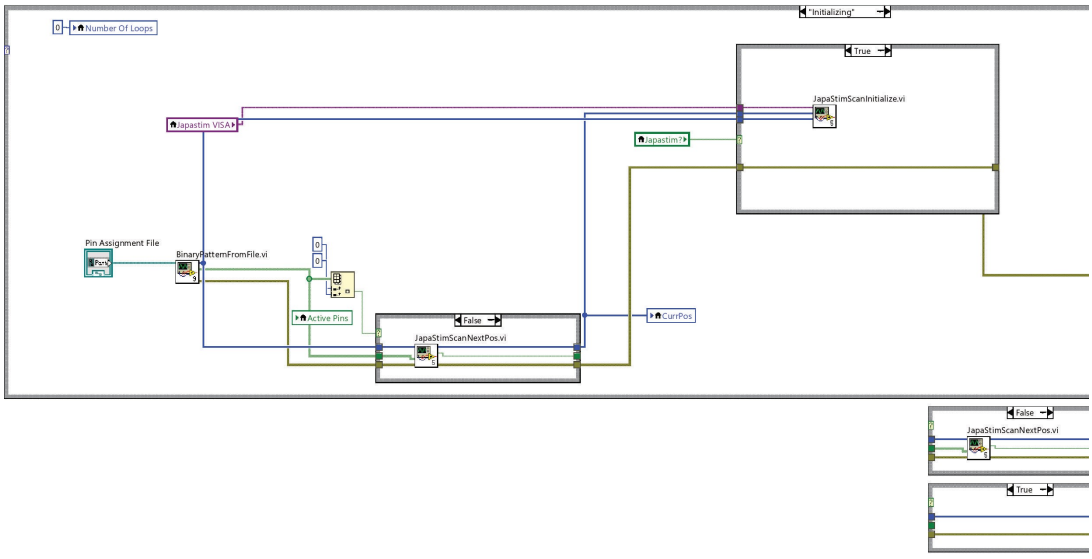

JapaStimLI5655V1.vi
C:\Users\stret\Dropbox\Diagnostics\VI\JapaStimLI5655V1.vi
Last modified on 4/16/2019 at 11:55 AM
Printed on 5/30/2019 at 5:52 PM

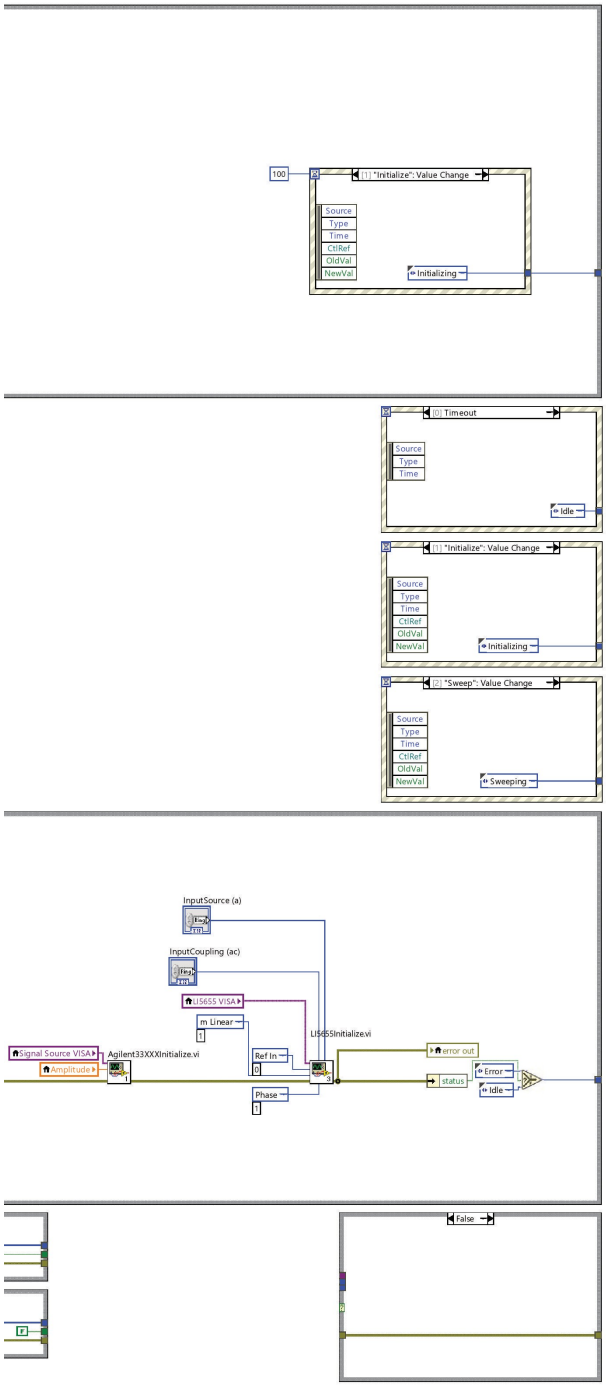

JapaStimLI5655V1.vi
C:\Users\stret\Dropbox\Diagnostics\VI\JapaStimLI5655V1.vi
Last modified on 4/16/2019 at 11:55 AM
Printed on 5/30/2019 at 5:53 PM

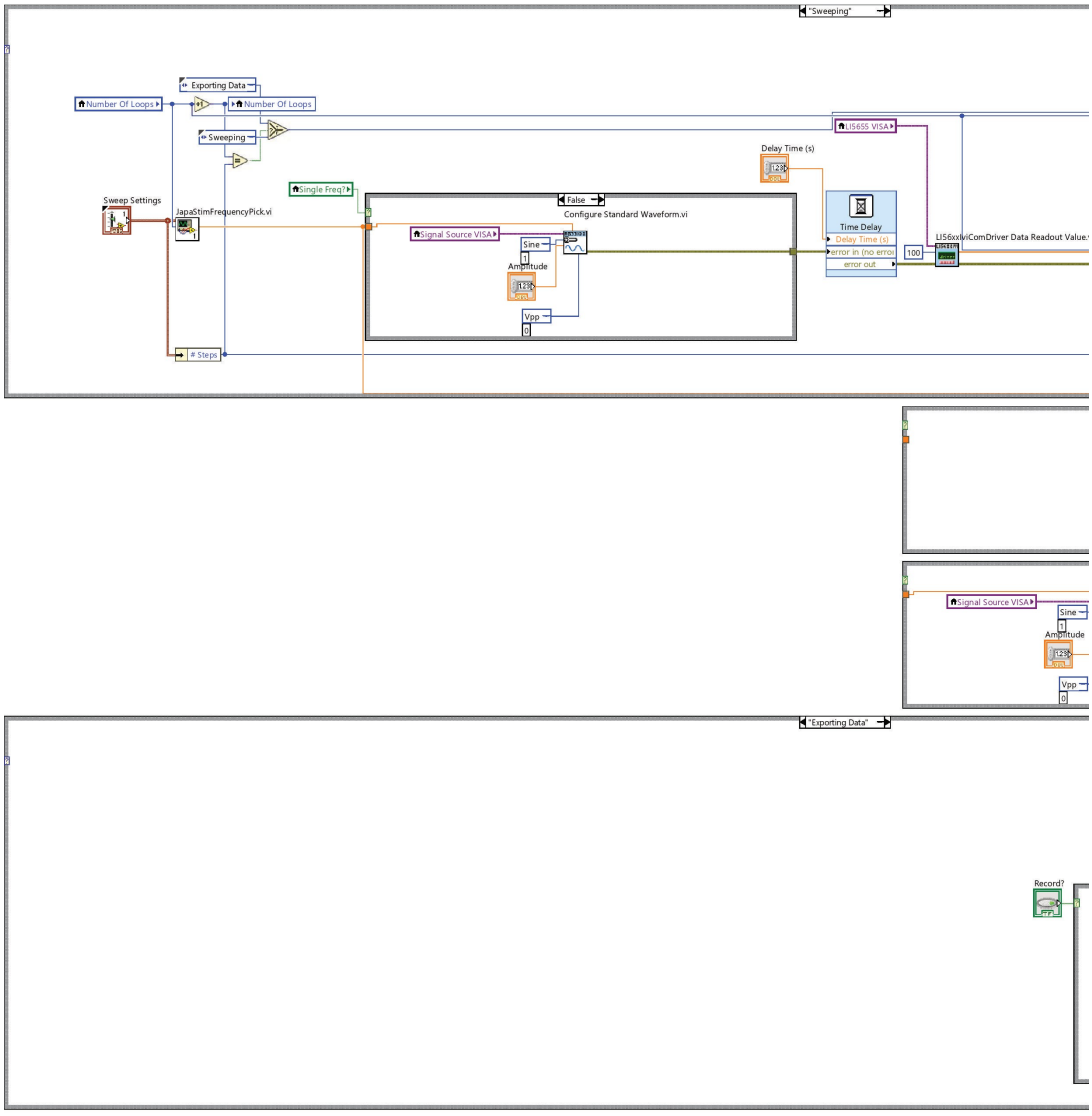

JapaStimLI5655V1.vi
C:\Users\stret\Dropbox\Diagnostics\VI\JapaStimLI5655V1.vi
Last modified on 4/16/2019 at 11:55 AM
Printed on 5/30/2019 at 5:53 PM

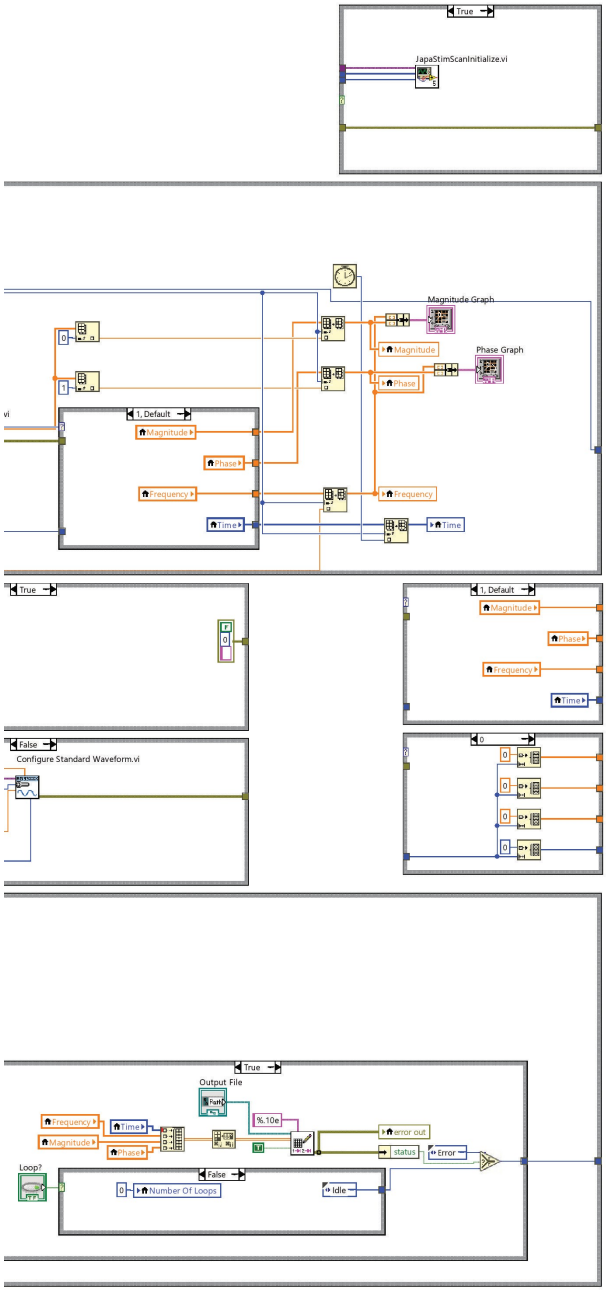

JapaStimLI5655V1.vi
C:\Users\stret\Dropbox\Diagnostics\VI\JapaStimLI5655V1.vi
Last modified on 4/16/2019 at 11:55 AM
Printed on 5/30/2019 at 5:53 PM

JapaStimLI5655V1.vi
C:\Users\stret\Dropbox\Diagnostics\VI\JapaStimLI5655V1.vi
Last modified on 4/16/2019 at 11:55 AM
Printed on 5/30/2019 at 5:53 PM

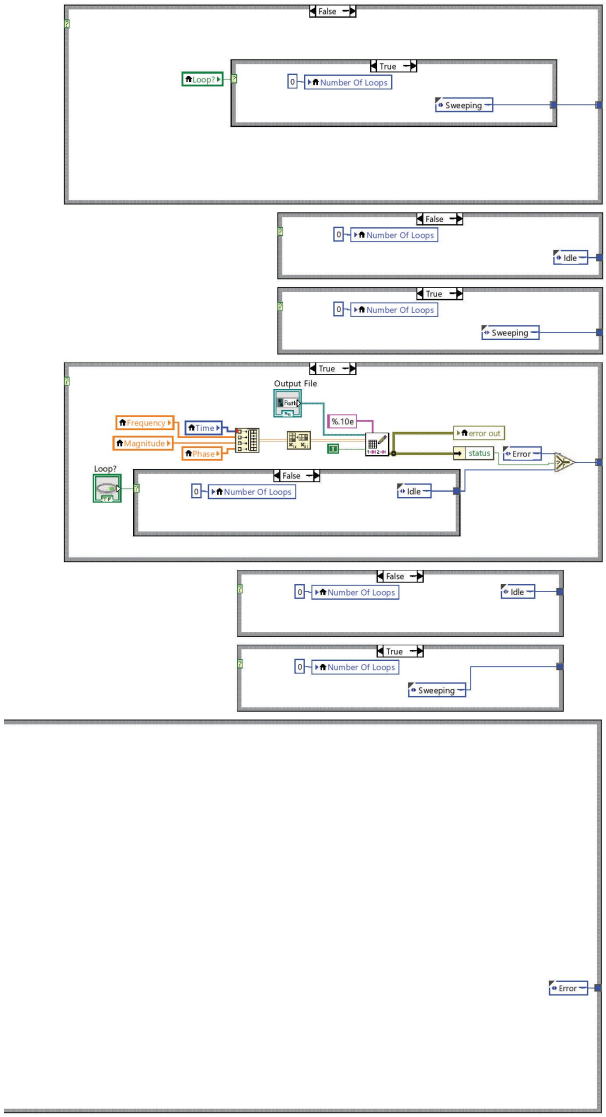

JapaStimLI5655V1.vi
C:\Users\stret\Dropbox\Diagnostics\VI\JapaStimLI5655V1.vi
Last modified on 4/16/2019 at 11:55 AM
Printed on 5/30/2019 at 5:53 PM

A.1.5 Summary

In this section we have described our control program. We have explained its operation and user interface as well as details about its state structure and source code.

A.2 Japastim Control Program

In order to control the Japastim device we developed a simple program in order to interface with it over visa. In this section we will describe the practical use of the program as well as its coding.

A.2.1 Source Code

This section contains an annotated version of the source code for the japastim control program

A.2.1.1 Main Program

The main program consists of a series of direct actions, first it initializes the Japastim device, reads any data waiting on the devices buffer and then writes a series of endline delimited commands. In order to vary functionality of the program, the list of commands concatenated to be sent to the write program should be manually altered. Details about the acceptable commands are shown in Appendix D.

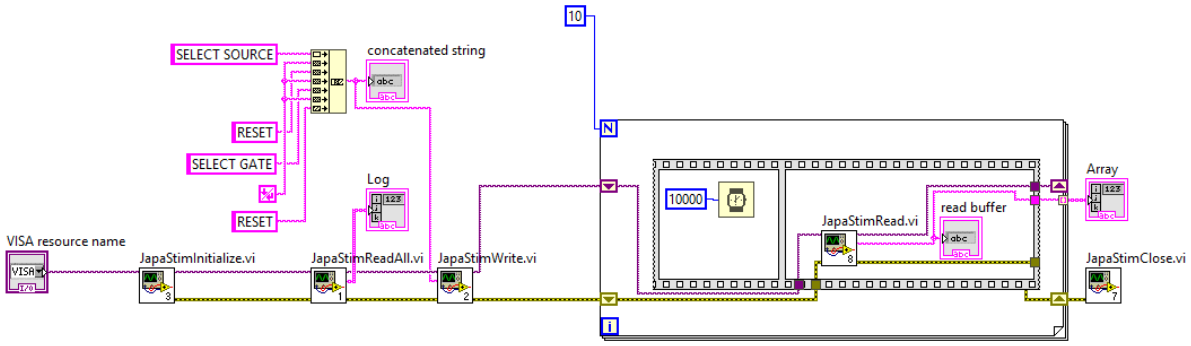

Figure 72: Main Japastim Program

A.2.1.2 Initialize

The initialization program opens up a visa connection, configures the baud rate for the serial port connection, and then buffers the output.

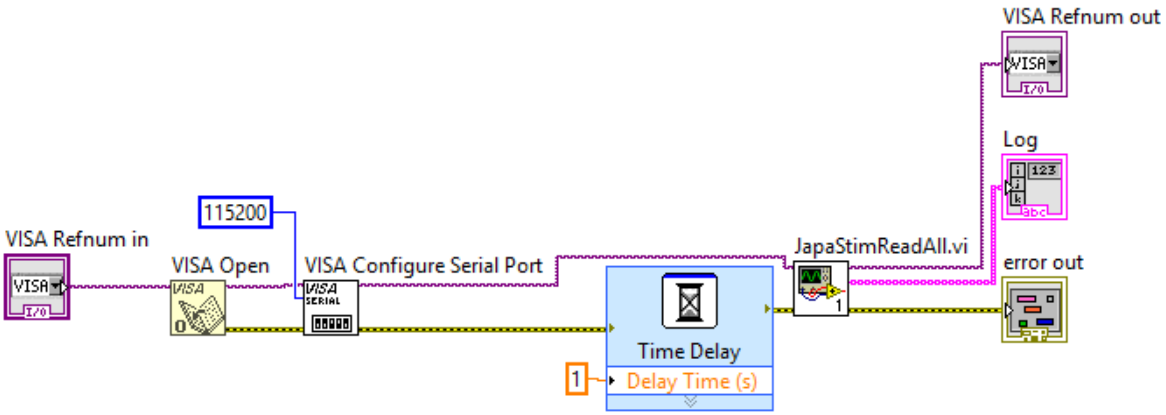

Figure 73: Japastim Initialize Program

A.2.1.3 Read All

The read all program queries the device for the number of available bytes, and reads until there are none remaining. Due to the delimited nature of the output it

needs to read an arbitrary number of times in order to verify complete reading of the Japastims output buffer

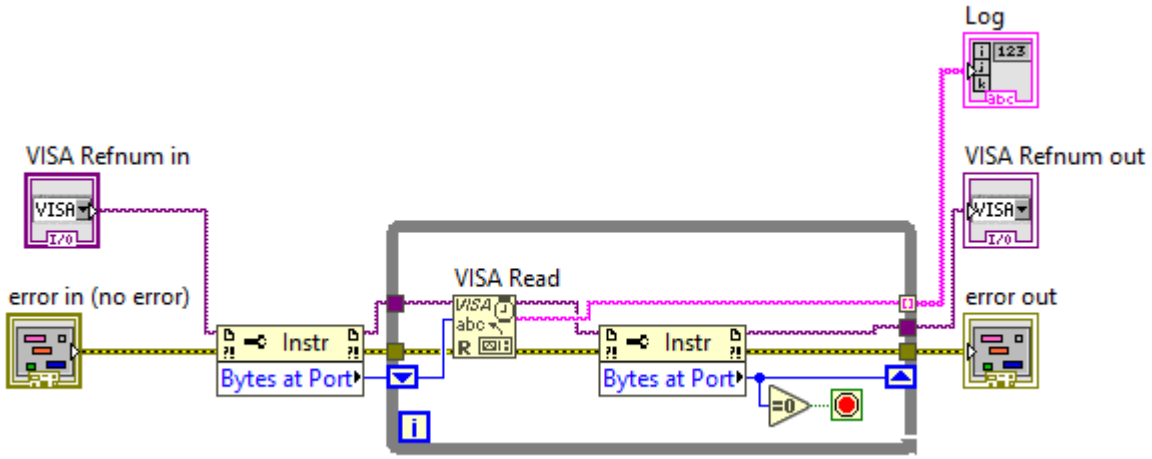

Figure 74: Japastim Read All program

A.2.1.4 Read

The Japastim read function will read a single string from the output buffer of the Japastim device until it encounters an endline character.

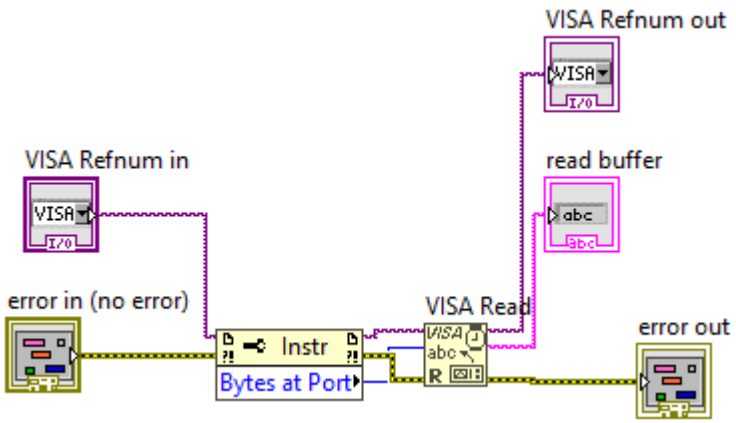

Figure 75: Japastim Read function

A.2.1.5 Write

The Japastim write function will write a single string to the Japastim. Through the use of endline characters, multiple commands can be sent with a single string. This is critical for optimization due to the inherent temporal variance and delay inherent to USB communication. The write function simply concatenates an end line character and sends the input string into the conventional VISA writing program.

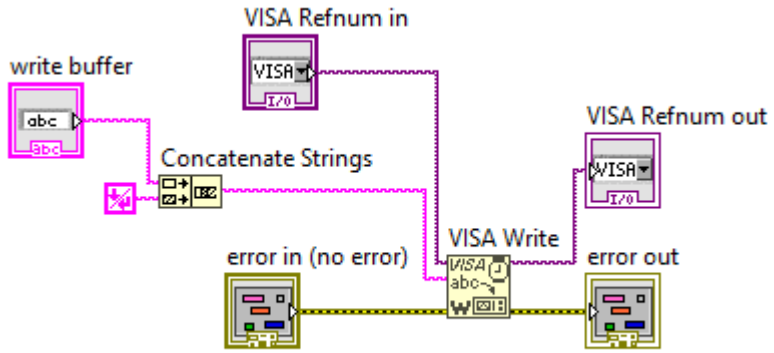

Figure 76: Japastim Write command

A.2.1.6 Close

The Japastim close function simply terminates the VISA connection using the built-in VISA protocols.

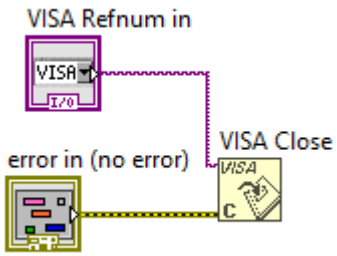

Figure 77: Japastim Close function

A.2.2 Summary

In this section we have detailed the functionality of our control system for the Japastim device. In the future we plan on integrating this with the main control program in order to more accurately control the timing and synchronization between the devices.

A.3 Appendix Summary

In this Appendix we have described the functionality of our control program for the built in hardware as well as the program controlling the Japastim device. They enable the automation of our equipment vastly expanding the feasibility of large scale manipulation and analysis.

Appendix B: Cell Culture

In this Appendix we will describe the methodology used for cell culture of the various types of cells used in our experiments. We will start with a discussion of the yeast culture and continue with a discussion of the neuron cells, Sf21 moth olfactory cells, and finally HEPG2 cells.

B.1 Yeast

Most of our initial experiments were done with yeast cells, which are extremely robust single celled fungi. The core of each of our yeast cultures was dried bakers yeast, the kind we used was スーパーカメリヤ dry yeast. Dried yeast is inherently inactive, and must first be activated before culturing can begin. To culture the yeast we placed it in sugar water on a hotplate(DMC-370) set to 30C and covered with a paper towel to keep it dark for 30 minutes. You can tell it is activated when the surface becomes frothy, caused by the emission of CO2 by the yeast.

Because dried yeast consists of a large portion of dead cells it can be unsuitable in its raw form. In order to eliminate dead cells and other assorted detritus, centrifugation is key. We set them in a centrifuge(Thermo Scientific ST 8FR) at 9G for 5 minutes in order to separate the dead cells and detritus from the living cells. For medium in the culture we used .1% sugar, and 1 mM EDTA. [131] The culture was kept warm and dark, and was occasionally re-centrifuged in order to maintain viability.

B.2 Neuron

The neuron culture was handled externally by Dr. Ikeuchi and his laboratory. In order to prime the TFT device before culturing the neurons, the device had to be suspended in Poly L Lysine(PLL) mixed with borate buffer at a 1mM concentration.

The neurons were harvested from embryos taken from 17 day pregnant mice. These were then placed in 1X Hanks Buffer Salt Solution(HBSS) and refrigerated. The brains were then extracted and the meninges surrounding the brain was

removed. The hippocampus was then isolated and placed in 1X HBSS. It was then rinsed several times with HBSS. The excess fluid was then removed and immersed in a mixture of 5mL HBSS, 5uL 10x Trypsin, and 50uL DNase. It is then incubated at room temperature for five minutes. It is then rinsed again with HBSS and stored in 5mL of feeding medium mixed with 50ul DNase. The cells are then extracted with a pipette and centrifuged at 800rpm for 5 minutes at 4C. The viable cells are then extracted and immersed in 5mL feeder medium made from 500ml neurobasal media, 10ml B27 supplement, 5ml 100x PS and 1.25 ml 200mM glutamine. The devices are then stored in an incubator set to 5% CO2 at 37C and 95% humidity for several weeks with the medium being refreshed every 2 days.

B.4 HepG2

The HepG2 culture wa handled by Ms. Eiler in our laboratory. The cells were cultured from frozen samples. To thaw the cells, the frozen sample was defrosted at 37C until there was no visible ice and then an additional 30 seconds. Then the vial was disinfected with 70% ethanol. The contents were then suspended in 10ml of HEG2 medium. This was then centrifuged at 200g for 10 minutes and then decanted. The cell pellet was then resuspended in 5ml of HEG2 medium and incubated for 24h at 5%CO2 37C. At this point the culture is viable and to maintain it the HEG2 medium was aspirated and replaced every three days, and the culture was split into new flasks when it became confluent.

B.3 Sf21

The culturing of Sf21 cells was handled by Dr. Terutsuki. The cells were cultured in Grace's insect medium from previously established long term cultures. The cell were modified so as to express the BMOR3 gene that makes them electrogenically respond to bombykal. They were cultured at 5%CO2 at 37C and the medium was regularly aspirated and refreshed, and cell splitting was performed to prevent confluence

B.5 Summary

In this appendix we have described the process by which the various cell lines were cultured and maintained.

Appendix C: Japastim

This section will explain the specifics of the Japastim device designed by the University of Bordeaux. It will first explain the specifications and capabilities of the device. Then there will be a discussion of the various commands available to it, and finally an annotated sample program..

C.1 Device Specs

The core of the device is an Arduino microprocessor. This is controlled through a conventional micro-USB serial connection. The device consists of two boards in a master/slave configuration called the Gate and Source boards and referred to as such in the commands. Each of these boards has 28 pin outputs in a conventional 2 row configuration so as to facilitate the use of ribbon cable. It is powered by a 27V DC connection, and for the transmission of negative voltages a -5V DC input must be connected as well. There is also an external BNC connection for the transmission of arbitrary signals to the pins. A picture of the device is shown below in Figure .

FIGURE:JAPASTIM

C.2 Commands

RESET

Resets the board to default settings

SELECT (SOURCE/GATE)

Selects the source or gate board so it knows which board to send commands to

VGEN #

Sets the internal variable VGEN to the DC voltage entered into the command

STIM (VGEN/GND/HIZ)

Sets the internal STIM variable to either the VGEN variables value, ground, or high impedance respectively.

OUT (PINS)=(STIM/ARB)

Sets the output pins indicated on the current board to the assigned value. Pins are indicated in a comma delimited list with groups of pins indicated by colons. For example OUT 1,2,4:9=STIM would set pins 1,2 and pins 4-9 to the value indicated by STIM.

C.3 Sample Program

Following this is a sample program, it resets both cards and then sends a 12V DC signal to pins 1,2, and 3 while setting all other pins to a high impedance configuration.

```
SELECT SOURCE

RESET

SELECT GATE

RESET

VGEN 12

STIM VGEN

OUT 1:3=STIM
```

STIM HIZ

OUT 4:28=STIM

C.4 Summary

In this appendix we have described the Japastim device as well as explained and demonstrated the commands used in its operation.

Bibliography

[1] H. Gest, “The discovery of microorganisms by Robert Hooke and Antoni van Leeuwenhoek, fellows of the Royal Society,” *Notes Rec. R. Soc.*, vol. 58, no. 2, pp. 187–201, 2004.

[2] H. PUCHTLER and F. SWEAT, “A REVIEW OF EARLY CONCEPTS OF AMYLOID IN CONTEXT WITH CONTEMPORARY CHEMICAL LITERATURE FROM 1839 TO 1859,” *J. Histochem. Cytochem.*, vol. 14, no. 2, pp. 123–134, Feb. 1966.

[3] D. Brewster, “LX. Observations on the absorption of specific rays, in reference to the undulatory theory of light,” *London, Edinburgh, Dublin Philos. Mag. J. Sci.*, vol. 2, no. 11, pp. 360–363, May 1833.

[4] E. L. Nichols and E. Merritt, “V. The Luminescence of Sidot Blende,” *Phys. Rev. (Series I)*, vol. 21, no. 4, pp. 247–259, Oct. 1905.

[5] J. R. Basford, “A historical perspective of the popular use of electric and magnetic therapy,” *Arch. Phys. Med. Rehabil.*, vol. 82, no. 9, pp. 1261–1269, 2001.

[6] A. G. Bailey, “The charging of insulator surfaces,” *J. Electrostat.*, vol. 51–52, no. 1–4, pp. 82–90, 2001.

[7] M. L. Schagrin, “Resistance to Ohm’s Law,” *Am. J. Phys.*, vol. 31, no. 7, pp. 536–547, 2005.

[8] H. J. Curtis, “Transverse Electric Impedance of the Squid Giant Axon,” *J. Gen. Physiol.*, vol. 21, no. 6, pp. 757–765, 1938.

[9] K. S. Cole, “ELECTRIC IMPEDANCE OF THE FROG EGG,” *J. Gen. Physiol.*, vol. 25, no. 5, pp. 765–775, May 1942.

[10] M. E. Spira and A. Hai, “Multi-electrode array technologies for neuroscience and cardiology,” *Nat. Nanotechnol.*, vol. 8, no. 2, pp. 83–94, 2013.

[11] K. Najafi and K. D. Wise, “An Implantable Multielectrode Array with On-Chip Signal Processing,” *IEEE J. Solid-State Circuits*, vol. 21, no. 6, pp. 1035–1044, 1986.

[12] G. Becq *et al.*, “About MEA impedance measurement and analysis To cite this version : HAL Id : hal-00318561 About MEA impedance measurement and analysis,” 2008.

[13] B. H. Cornish, I. H. Bunce, L. C. Ward, L. C. Jones, and B. J. Thomas, “Bioelectrical impedance for monitoring the efficacy of lymphoedema treatment programmes,” *Breast Cancer Res. Treat.*, vol. 38, no. 2, pp. 169–176, 1996.

[14] V. Vijay *et al.*, “High-density CMOS microelectrode array system for impedance spectroscopy and imaging of biological cells,” *Proc. IEEE Sensors*, pp. 5–7, 2017.

[15] Y. Chen *et al.*, “CMOS high density electrical impedance biosensor array for tumor cell detection,” *Sensors Actuators, B Chem.*, vol. 173, pp. 903–907, 2012.

[16] A. Yufera and A. Rueda, “A CMOS Bio-impedance measurement system,” *Proc. 2009 IEEE Symp. Des. Diagnostics Electron. Circuits Syst. DDECS 2009*, pp. 252–257, 2009.

[17] K. Nomura, H. Ohta, K. Ueda, T. Kamiya, M. Hirano, and H. Hosono, “Thin-film transistor fabricated in single-crystalline transparent oxide semiconductor,” *Science (80-.).*, vol. 300, no. 5623, pp. 1269–1272, 2003.

[18] M. Katayama, “TFT-LCD technology,” *Thin Solid Films*, vol. 341, pp. 140–147, 1999.

[19] F. A. Shaik, Y. Ikeuchi, G. Cathcart, S. Ihida, H. Toshiyoshi, and A. TIxier-Mita, “Extracellular neural stimulation and recording with a Thin-Film-Transistor (TFT) array device,” *TRANSDUCERS 2017 - 19th Int. Conf. Solid-State Sensors, Actuators Microsystems*, pp. 206–209, 2017.

[20] B.-D. Ségard *et al.*, “Review on thin-film transistor technology, its applications, and possible new applications to biological cells,” *Jpn. J. Appl. Phys.*, vol. 55, no. 4S, p. 04EA08, 2016.

[21] A. Tixier-Mita, B. D. Segard, Y. J. Kim, Y. Matsunaga, H. Fujita, and H. Toshiyoshi, “TFT display panel technology as a base for biological cells electrical manipulation - Application to dielectrophoresis,” *Proc. IEEE Int. Conf. Micro Electro Mech. Syst.*, vol. 2015-Febru, no. February, pp. 354–357, 2015.

[22] F. A. Shaik *et al.*, “Thin-film-transistor array: an exploratory attempt for high throughput cell manipulation using electrowetting principle,” *J. Micromechanics Microengineering*, vol. 27, no. 5, p. 054001, May 2017.

[23] A. Han and A. B. Frazier, “Ion channel characterization using single cell impedance spectroscopy,” vol. 1, pp. 1412–1414, 2006.

[24] K. Claudia *et al.*, “Label-free detection of Babesia bovis infected red blood cells using impedance spectroscopy on a microfabricated flow cytometer,” vol. 102, pp. 63–68, 2007.

[25] L. Jang and M. Wang, “Microfluidic device for cell capture and impedance measurement,” pp. 737–743, 2007.

[26] H. Park, D. Kim, and K. Yun, “Single-cell manipulation on microfluidic chip by dielectrophoretic actuation and impedance detection,” *Sensors Actuators B. Chem.*, vol. 150, no. 1, pp. 167–173, 2010.

[27] K. C. Cheung, M. Di Berardino, G. Schade-kampmann, and M. Hebeisen, “Microfluidic Impedance-Based Flow Cytometry,” 2010.

[28] L. Chen, D. Wu, and M. S. Lu, “An integrated micro-manipulation and biosensing platform built in glass-based LTPS TFT technology,” *J. Micromechanics Microengineering*, vol. 22, no. 9, 2012.

[29] J. S. Ploem, “The use of a vertical illuminator with interchangeable dichroic mirrors for fluorescence microscopy with incidental light.,” *Z. Wiss. Mikrosk.*, vol. 68, no. 3, pp. 129–42, Nov. 1967.

[30] W. H. Li and G. Zheng, “Photoactivatable fluorophores and techniques for biological imaging applications,” *Photochem. Photobiol. Sci.*, vol. 11, no. 3, pp. 460–471, 2012.

[31] R. M. Martin, H. Leonhardt, and M. C. Cardoso, “DNA labeling in living cells,” *Cytom. Part A*, vol. 67, no. 1, pp. 45–52, 2005.

[32] C. Lo Celso, F. Progatzky, and M. J. Dallman, “From seeing to believing: labelling strategies for in vivo cell-tracking experiments,” *Interface Focus*, vol. 3, pp. 1–14, 2013.

[33] G. Buzsáki, “Large-scale recording of neuronal ensembles.,” *Nat. Neurosci.*, vol. 7, no. 5, pp. 446–51, 2004.

[34] L. J. Breckenridge *et al.*, “Advantages of using microfabricated extracellular electrodes for in vitro neuronal recording,” *J. Neurosci. Res.*, vol. 42, no. 2, pp. 266–276, 1995.

[35] S. L. BeMent, K. D. Wise, D. J. Anderson, K. Najafi, and K. L. Drake, “Solid-State Electrodes for Multichannel Multiplexed Intracortical Neuronal Recording,” *IEEE Trans. Biomed. Eng.*, vol. BME-33, no. 2, pp. 230–241, 1986.

[36] D. Terutsuki, H. Mitsuno, Y. Okamoto, T. Sakurai, and A. Tixier-mita, “ODOR-SENSITIVE FIELD EFFECT TRANSISTOR (OSFET) BASED ON INSECT CELLS EXPRESSING INSECT ODORANT RECEPTORS Department of Advanced Interdisciplinary Studies , The University of Tokyo , Tokyo , JAPAN Department of Electrical Engineering and Information Syst,” pp. 394–397, 2017.

[37] A. Han, L. Yang, and A. B. Frazier, “Quantification of the heterogeneity in breast cancer cell lines using whole-cell impedance spectroscopy,” *Clin. Cancer Res.*, vol. 13, no. 1, pp. 139–143, 2007.

[38] K. Cheung, S. Gawad, and P. Renaud, “Impedance spectroscopy flow cytometry: On-chip label-free cell differentiation,” *Cytom. Part A*, vol. 65, no. 2, pp. 124–132, 2005.

[39] I. O. K’Owino and O. A. Sadik, “Impedance spectroscopy: A powerful tool for rapid biomolecular screening and cell culture monitoring,” *Electroanalysis*, vol. 17, no. 23, pp. 2101–2113, 2005.

[40] P. Kassanos, I. F. Triantis, and A. Demosthenous, “A CMOS magnitude/phase measurement chip for impedance spectroscopy,” *IEEE Sens. J.*, vol. 13, no. 6, pp. 2229–2236, 2013.

[41] A. Hassibi and T. H. Lee, “A programmable 0.18-μm CMOS electrochemical sensor microarray for biomolecular detection,” *IEEE Sens. J.*, vol. 6, no. 6, pp. 1380–1388, 2006.

[42] A. M. Scientific, “MED Probe for Basic/Plex System,” 2017.

[43] J. Pine, “A history of MEA development,” *Adv. Netw. Electrophysiol. Using Multi-Electrode Arrays*, pp. 3–23, 2006.

[44] T. C, S. P, L. G, B. Y, and O. L, “A miniature microelectrode array to monitor the bioelectric activity of cultured cells,” *Exp. Cell Res.*, vol. 74, no. 972, pp. 61–66, 1972.

[45] M. S. Ju, H. C. Chien, G. S. Chen, C. C. K. Lin, C. H. Chang, and C. W. Chang, “Design and fabrication of multi-microelectrode array for neural prosthesis,” *J. Med. Biol. Eng.*, vol. 22, no. 1, pp. 33–40, 2002.

[46] A. R. A. Rahman, C. M. Lo, and S. Bhansali, “A micro-electrode array biosensor for impedance spectroscopy of human umbilical vein endothelial cells,” *Sensors Actuators, B Chem.*, vol. 118, no. 1–2, pp. 115–120, 2006.

[47] J. R. Buitenweg, W. L. C. Rutten, W. P. A. Willems, and J. W. Van Nieuwkasteele, “Measurement of sealing resistance of cell-electrode interfaces in neuronal cultures using impedance spectroscopy,” *Med. Biol. Eng. Comput.*, vol. 36, no. 5, pp. 630–637, 1998.

[48] S. Martinoia and P. Massobrio, “ISFET-neuron junction: Circuit models and extracellular signal simulations,” *Biosens. Bioelectron.*, vol. 19, no. 11, pp. 1487–1496, 2004.

[49] V. Viswam *et al.*, “Multi-Functional Microelectrode Array System,” in *IEEE International Solid State Circuits Conference*, 2016, pp. 394–396.

[50] Y. Song, N. Lin, C. Liu, H. Jiang, G. Xing, and X. Cai, “Biosensors and Bioelectronics Short communication A novel dual mode microelectrode array for neuroelectrical and neurochemical recording in vitro,” *Biosens. Bioelectron.*, vol. 38, no. 1, pp. 416–420, 2012.

[51] V. Benfenati *et al.*, “A transparent organic transistor structure for bidirectional stimulation and recording of primary neurons,” *Nat. Mater.*, vol. 12, no. 5, pp. 1–9, 2013.

[52] J. J. Cair *et al.*, “The use of a vertical illuminator with interchangeable dichroic mirrors for fluorescence microscopy with incidental light.,” *Biosens. Bioelectron.*, vol. 21, no. 3, pp. 129–42, May 2005.

[53] Š. Skalová, V. Vyskočil, J. Barek, and T. Navrátil, “Model Biological Membranes and Possibilities of Application of Electrochemical Impedance Spectroscopy for their Characterization,” *Electroanalysis*, vol. 30, no. 2, pp. 207–219, 2018.

[54] H. Benjamin, S. Bhansali, S. B. Hoath, W. L. Pickens, and R. Smallwood, “A planar micro-sensor for bio-impedance measurements,” *Sensors Actuators, B Chem.*, vol. 111–112, no. SUPPL., pp. 430–435, 2005.

[55] R. Go´mez *et al.*, “Microfluidic biochip for impedance spectroscopy of biological species,” *Biomed. Microdevices*, vol. 3, no. 3, pp. 201–209, 2001.

[56] D. A. Borkholder, I. E. Opris, N. I. Maluf, and G. T. A. Kovacs, “Planar electrode array systems for neural recording and impedance measurements,” no. Figure 1, pp. 106–107, 2002.

[57] Gamry Instruments, “Basics of Electrochemical Impedance Spectroscopy,” 2019. [Online]. Available: https://www.gamry.com/application-notes/EIS/basics-of-electrochemical-impedance-spectroscopy/.

[58] B. Lertanantawong, A. P. O'Mullane, J. Zhang, W. Surareungchai, M. Somasundrum, and A. M. Bond, "Investigation of mediated oxidation of ascorbic acid by ferrocenemethanol using large-amplitude fourier transformed ac voltammetry under quasi-reversible electron-transfer conditions at an indium tin oxide electrode," *Anal. Chem.*, vol. 80, no. 17, pp. 6515–6525, 2008.

[59] J. Sapp, "The Prokaryote-Eukaryote Dichotomy: Meanings and Mythology," *Microbiol. Mol. Biol. Rev.*, vol. 69, no. 2, pp. 292–305, 2005.

[60] K. N. Theocharis AD, Skandalis SS, Gialeli C, "Extracellular Matrix Structure," *Adv. Drug Deliv. Rev.*, vol. 97, pp. 4–27, 2016.

[61] C. Frantz, K. M. Stewart, and V. M. Weaver, "The extracellular matrix at a glance," *J. Cell Sci.*, vol. 123, no. 24, pp. 4195–4200, 2010.

[62] and R. P. Milo, Ron, *Cell biology by the numbers*. 2015.

[63] M. Videos, *Microbiology of Antibody & Antigen Recognition*. 2018.

[64] J. R. North, "Immunosensors: Antibody-based biosensors," *Trends Biotechnol.*, vol. 3, no. 7, pp. 180–186, Jul. 1985.

[65] J. ZHOU *et al.*, "Odor Discrimination By Mitral Cells in Rat Olfactory Bulb Using Microwire Array Recording," *J. Innov. Opt. Health Sci.*, vol. 05, no. 01, p. 1250003, 2012.

[66] C. Ziegler, "Cell-based biosensors," pp. 552–559, 2000.

[67] A. Poghossian, S. Ingebrandt, A. Offenhäusser, and M. J. Schöning, "Field-effect devices for detecting cellular signals," *Semin. Cell Dev. Biol.*, vol. 20, no. 1, pp. 41–48, 2009.

[68] M. Wang *et al.*, "Application of impedance spectroscopy for monitoring colloid Au-enhanced antibody immobilization and antibody-antigen reactions," *Biosens. Bioelectron.*, vol. 19, no. 6, pp. 575–582, 2004.

[69] R. Pei, Z. Cheng, E. Wang, and X. Yang, "Amplification of antigen-antibody interactions based on biotin labeled protein-streptavidin network complex using impedance spectroscopy," *Biosens. Bioelectron.*, vol. 16, no. 6, pp. 355–361, 2001.

[70] F. Patolsky, B. Filanovsky, E. Katz, and I. Willner, "Photoswitchable Antigen−Antibody Interactions Studied by Impedance Spectroscopy," *J. Phys. Chem. B*, vol. 102, no. 50, pp. 10359–10367, 2002.

[71] L. Yang and Y. Li, “AFM and impedance spectroscopy characterization of the immobilization of antibodies on indium-tin oxide electrode through self-assembled monolayer of epoxysilane and their capture of Escherichia coli O157:H7,” *Biosens. Bioelectron.*, vol. 20, no. 7, pp. 1407–1416, 2005.

[72] O. A. Sadik *et al.*, “Differential impedance spectroscopy for monitoring protein immobilization and antibody-antigen reactions,” *Anal. Chem.*, vol. 74, no. 13, pp. 3142–3150, 2002.

[73] J. J. FitzGerald, S. P. Lacour, S. B. McMahon, and J. W. Fawcett, “Microchannels as axonal amplifiers,” *IEEE Trans. Biomed. Eng.*, vol. 55, no. 3, pp. 1136–1146, 2008.

[74] P. Li, U. Bakowsky, F. Yu, C. Loehbach, F. Muecklich, and C. M. Lehr, “Laser ablation patterning by interference induces directional cell growth,” *IEEE Trans. Nanobioscience*, vol. 2, no. 3, pp. 138–145, 2003.

[75] A. Y. Cheung, H. Wang, and H. ming Wu, “A floral transmitting tissue-specific glycoprotein attracts pollen tubes and stimulates their growth,” *Cell*, vol. 82, no. 3, pp. 383–393, 1995.

[76] P. K. Weimer, “TFT - new thin-film transistor,” *Proc. Inst. Radio Eng.*, vol. 50, no. 6, p. 1462, 1962.

[77] J. C. Erskine and A. Cserhati, “Cadmium selenide thin-film transistors,” *J. Vac. Sci. Technol.*, vol. 15, no. 6, pp. 1823–1835, 2002.

[78] J. Yao *et al.*, “IEEE TRANSACTIONS ON ELECTRON DEVICES 58 1121 2011 IGZO photosensitive characteristics.pdf,” vol. 58, no. 4, pp. 1121–1126, 2011.

[79] Fridman, “The Physics of Amorphous-Silicon Thin-Film Transistors,” *IEEE Trans. Electron Devices*, vol. 36, no. 12, pp. 2753–2763, 1989.

[80] B. Stannowski, *Silicon-based thin-film transistors with a high stability*. 2002.

[81] M. Stewart, R. S. Howell, L. Pires, and M. K. Hatalis, “Polysilicon TFT technology for active matrix OLED displays,” *IEEE Trans. Electron Devices*, vol. 48, no. 5, pp. 845–851, 2001.

[82] I. Pappas, D. Tassis, S. Siskos, and C. A. Dimitriadis, “Characteristics of double-gate polycrystalline silicon thin-film transistors for AMOLED pixel design,” *2010 IEEE Int. Conf. Electron. Circuits, Syst. ICECS 2010 - Proc.*, pp. 301–304, 2010.

[83] K. Fukuda *et al.*, “Reverse-Offset Printing Optimized for Scalable Organic Thin-Film Transistors with Submicrometer Channel Lengths,” *Adv. Electron. Mater.*, vol. 1, no. 8, p. 1500145, 2015.

[84] V. Fiore *et al.*, “complementary TFT technology on flexible substrate An Integrated 13 . 56 - MHz RFID Tag in a Printed Organic Complementary TFT Technology on Flexible Substrate,” vol. 62, no. 6, pp. 1668–1678, 2018.

[85] D. Kumaki and S. Tokito, “Organic TFT Circuits Fabricated with High Resolution Printing System,” *Int. Conf. Electron. Packag.*, pp. 441–442, 2017.

[86] A. F. Paterson *et al.*, “Recent Progress in High-Mobility Organic Transistors: A Reality Check,” *Adv. Mater.*, vol. 30, no. 36, pp. 1–33, 2018.

[87] V. Pecunia, K. Banger, and H. Sirringhaus, “High-Performance Solution-Processed Amorphous- Oxide-Semiconductor TFTs with Organic Polymeric Gate Dielectrics,” pp. 0–5, 2015.

[88] H. Hosono, J. Kim, Y. Toda, T. Kamiya, and S. Watanabe, “Transparent amorphous oxide semiconductors for organic electronics : Application to inverted OLEDs,” vol. 114, no. 2, pp. 233–238, 2017.

[89] T. Kamiya and H. Hosono, *Oxide TFTs*. 2016.

[90] H. Hosono, “Ionic amorphous oxide semiconductors : Material design , carrier transport , and device application,” vol. 352, pp. 851–858, 2006.

[91] Z. Fan *et al.*, “ZnO nanowire field-effect transistor and oxygen sensing property,” vol. 5923, no. 2004, 2012.

[92] M. W. J. Prins *et al.*, “Depletion-type thin-film transistors with a ferroelectric insulator Depletion-type thin-film transistors with a ferroelectric insulator,” vol. 458, no. 1997, pp. 16–19, 2004.

[93] “Novel oxide amorphous semiconductors : transparent conducting amorphous oxides Possible Candidate for HMCs,” vol. 203, pp. 334–344, 1996.

[94] J. S. Discrete, K. Nomura, H. Ohta, A. Takagi, and T. Kamiya, “Room-temperature fabrication of transparent flexible thin-film transistors using amorphous oxide semiconductors,” vol. 432, no. November, pp. 3383–3386, 2004.

[95] J. Socratous *et al.*, “Electronic Structure of Low-Temperature Solution-Processed Amorphous Metal Oxide Semiconductors for Thin-Film Transistor Applications,” pp. 1–13, 2015.

[96] “Sharp Begins Production of Worlds First LCD Panels Incorporating IGZO Oxide Semiconductors.” [Online]. Available: http://www.sharp-world.com/corporate/news/120413.html. [Accessed: 20-May-2019].

[97] Y. Hara *et al.*, “IGZO-TFT technology for large-screen 8K display,” *J. Soc. Inf. Disp.*, vol. 26, no. 3, pp. 169–177, 2018.

[98] N. Corp, “Lock-in Amplifier/Pre-Amplifier,” 2013. [Online]. Available: http://www.nfcorp.co.jp/english/pro/mi/loc/loc/index.html.

[99] Matsusada, “PK-80 シリーズ,” 2019. [Online]. Available: https://www.matsusada.co.jp/product/psel/dcps/pk80/.

[100] Keysight, “33220A ファンクション / 任意波形発生器、20 MHz.” [Online]. Available: https://www.keysight.com/en/pd-127539-pn-33220A/function-arbitrary-waveform-generator-20-mhz?cc=JP&lc=jpn.

[101] Amtek, “Faraday Cages,” 2017. [Online]. Available: https://www.techmfg.com/products/fieldcancellation/faradaycages.

[102] J. A. Steinkamp, B. E. Lehnert, and N. M. Lehnert, “Discrimination of damaged/dead cells by propidium iodide uptake in immunofluorescently labeled populations analyzed by phase-sensitive flow cytometry,” *J. Immunol. Methods*, vol. 226, no. 1–2, pp. 59–70, 1999.

[103] Olympus, *Reflected Fluorescence System*. .

[104] Olympus, “Research Inverted System Microscope IX71/IX81.”

[105] Photometrics, “Cascade II:512.”

[106] A. E. Helal, P. Sathre, and W. C. Feng, “MetaMorph: A Library Framework for Interoperable Kernels on Multi- A nd Many-Core Clusters,” *Int. Conf. High Perform. Comput. Networking, Storage Anal. SC*, pp. 119–129, 2017.

[107] C. Elliott, V. Vijayakumar, W. Zink, and R. Hansen, “National Instruments LabVIEW: A Programming Environment for Laboratory Automation and Measurement,” *J. Lab. Autom.*, vol. 12, no. 1, pp. 17–24, 2007.

[108] C. A. Schneider, W. S. Rasband, and K. W. Eliceiri, “NIH Image to ImageJ: 25 years of image analysis.,” *Nat. Methods*, vol. 9, no. 7, pp. 671–5, 2012.

[109] K. M. Motsegood and P. P. Elastomer, “Three-Dimensional Micro-Channel Fabrication in PDMS,” *J. Microelectromechanical Syst.*, vol. 9, no. 1, pp. 76–81, 2010.

[110] G. A. Cathcart, “ALGORITHMIC OPEN-SURFACE IDENTIFICATION AND LOCATION OF DROPLETS ON A TRANSPARENT TFT SUBSTRATE FOR DROPLET-BASED MICROFLUDICS,” in *Microtas*, 2018.

[111] D. Rancic Moogk, “Minimum Viable Product and the Importance of Experimentation in Technology Startups,” *Technol. Innov. Manag. Rev.*, vol. 2, no. 3, pp. 23–26, 2018.

[112] A. Soley *et al.*, “On-line monitoring of yeast cell growth by impedance spectroscopy,” *J. Biotechnol.*, vol. 118, no. 4, pp. 398–405, Sep. 2005.

[113] H. Fricke and H. J. Curtis, “Electric Impedance of Suspensions of Yeast Cells.,” *Nature*, vol. 134, no. 3377, pp. 102–103, 1934.

[114] X. Liu, Y. Cui, T. Zhao, D. Kawashima, H. Obara, and M. Takei, “Quantitative Detection of Living Yeast Fraction From Mixed Living and Dead Cell Solution by Micro Electrical Impedance Spectroscopy,” *IEEE Access*, vol. 7, no. 2016, pp. 33970–33977, 2019.

[115] E. E. Krommenhoek *et al.*, “Monitoring of yeast cell concentration using a micromachined impedance sensor,” vol. 115, pp. 384–389, 2006.

[116] G. A. Cathcart, A. Tixier-Mita, S. Ihida, F. Shaik, and H. Toshiyosh, “Simultaneous optical and electrical monitoring of cells on a transparent thin film transistor array,” in *2017 19th International Conference on Solid-State Sensors, Actuators and Microsystems (TRANSDUCERS)*, 2017, pp. 1672–1675.

[117] V. Mersch-Sundermann, S. Knasmüller, X. J. Wu, F. Darroudi, and F. Kassie, “Use of a human-derived liver cell line for the detection of cytoprotective, antigenotoxic and cogenotoxic agents,” *Toxicology*, vol. 198, no. 1–3, pp. 329–340, 2004.

[118] G. A. Cathcart, A. Tixier-mita, S. Ihida, F. Shaik, and H. Toshiyosh, “SIMULTANEOUS OPTICAL AND ELECTRICAL MONITORING OF CELLS ON A a) b),” pp. 1672–1675, 2017.

[119] G. C. Rains, J. K. Tomberlin, and D. Kulasiri, “Using insect sniffing devices for detection,” *Trends Biotechnol.*, vol. 26, no. 6, pp. 288–294, 2008.

[120] T. Nakamoto, M. Kakizaki, Y. Suzuki, H. Mitsuno, and R. Kanzaki, “Response analysis of odor sensor based upon insect olfactory receptors using image processing method,” *Proc. IEEE Sensors*, vol. 2014-Decem, no. December, pp. 1491–1494, 2014.

[121] J. Krieger, E. Große-Wilde, T. Gohl, and H. Breer, “Candidate pheromone receptors of the silkmoth Bombyx mori,” *Eur. J. Neurosci.*, vol. 21, no. 8, pp. 2167–2176, 2005.

[122] G. Kasang, K. E. Kaissling, O. Vostrowsky, and H. J. Bestmann, “Bombykal, a Second Pheromone Component of the Silkworm Moth Bombyx mori L,” *Angew. Chemie Int. Ed. English*, vol. 17, no. 1, pp. 60–60, 1978.

[123] E. Große-Wilde, A. Svatoš, and J. Krieger, “A Pheromone-binding protein mediates the bombykol-induced activation of a pheromone receptor in vitro,” *Chem. Senses*, vol. 31, no. 6, pp. 547–555, 2006.

[124] NexCelom, “Insect Cells:Introduction to analysis,” 2019. [Online]. Available: nexcelom.com.

[125] J. Berg, *Biochemistry 5th Edition*. 2002.

[126] B. Sengupta, “The effect of cell size and channel density on neuronal information encoding and energy effeciency.,” *J. cereb Flow Metab.*, 2013.

[127] Ohno, “Undergraduate Thesis,” 2016.

[128] D. Yu, X., Lu, R., Ma, Z. , Liu, Z. , Hao, Y., Li, Q., Xu, “An impedance array biosensor for detection of multiple antibody–antigen interactions,” *Analyst*, vol. 131, no. 6, pp. 745–750, 2006.

[129] L. Polgár, “The catalytic triad of serine peptidases,” vol. 62, pp. 2161–2172, 2005.

[130] R. Li and L. Liriano, “A bone sample cleaning method using trypsin for the isolation of DNA,” *Leg. Med.*, vol. 13, no. 6, pp. 304–308, 2011.

[131] M. Kwolek-Mirek and R. Zadrag-Tecza, “Comparison of methods used for assessing the viability and vitality of yeast cells,” *FEMS Yeast Res.*, vol. 14, no. 7, pp. 1068–1079, 2014.

Publications

Journal Papers

1. (Under Review) **Cathcart, G. A.** Tixier-Mita, A. Ihida, S. Eiler, A. Toshiyoshi, H. "Non-Mutative Cell Viability Measurement on an IGZO Transparent Thin Film Transistor Electrode Array" IEEJ Transactions

2. Shaik, F. A., **Cathcart, G. A.**., Ihida, S., Ikeuchi, Y., Tixier-Mita, A., & Toshiyoshi, H. (2018). Electrical Stimulation, Recording and Impedance-Based Real-Time Position Detection of Cultured Neurons Using Thin-Film-Transistor Array. *Journal of Microelectromechanical Systems*, *27*(3), 424-433.

3. Shaik, F. A., **Cathcart, G.,** Ihida, S., Lereau-Bernier, M., Leclerc, E., Sakai, Y., ... & Tixier-Mita, A. (2017). Thin-film-transistor array: An exploratory attempt for high throughput cell manipulation using electrowetting principle. *Journal of Micromechanics and Microengineering*, *27*(5), 054001.

4. A. Tixier-Mita, S. Ihida, D. Blanchard,M. Shinohara, A. Eiler, **G. Cathcart**, et. al "Paper 2D Dielectrophoresis Using an Active Matrix Array made by Thin-Film-Transistor Technology." IEEJ Transactions 2019

5. Tixier-Mita, A., Ihida, S., **Cathcart, G. A.,** Shaik, F. A., & Toshiyoshi, H. (2016). More Than Moore Applications with Thin-Film-Transistors Array Substrates from Liquid Cristal Display: New Devices for Biological Cells Analyses. *ECS Transactions*, *72*(3), 39-46.

6. Tixier-Mita, A., Ihida, S., Ségard, B. D., **Cathcart, G. A.**, Takahashi, T., Fujita, H., & Toshiyoshi, H. (2016). Review on thin-film transistor technology, its applications, and possible new applications to biological cells. *Japanese Journal of Applied Physics*, *55*(4S), 04EA08.

International Conference Papers

1. ***Cathcart, G. A.****, Tixier-Mita, A. Ihida, S., Shaik, F. A., Toshiyoshi, H "Algorithmic open surface identification and location of droplets on a transparent TFT substrate for droplet based microfluidics." in Proc. 22nd int. conf. On miniaturized systems for chemistry and life Science(uTAS), Kaohsiung Taiwan, Nov. 11-15 2018*

2. ***Cathcart, G. A.****, Shaik, F. A. Ihida, S. Toshiyoshi, H. Tixier-Mita, A. "Simultaneous optical and electrical monitoring of cells on a tranparent thin film transistor array" in Proc. 19th Int. Conf. On solid state sensors actuators and microsystems(Transducers) Kahosiung, Taiwan, June 18-22 2017*

3. ***Cathcart, G. A.****, Tixier-Mita, A. Ihida, S. Shaik, F. A., Toshiyoshi H. "Tranparent Thin Film Transistor Electrode Array for Real Time in-vitro electrical characterization of cell cultures"d, the 11th Anual IEEE international conference on nano/micro engineered and molecular systems(IEEE-NEMS) Sendai, Japan 17-20 April, 2016*

4. *Faruk Azam Shaik,* ***Grant Cathcart****, Satoshi Ihida, Myriam Lereau-Bernier, Yasuyuki Sakai, Hiroshi Toshiyoshi, and Agnes Tixier-Mita, "HepG2 CELLS PATTERNING BY EWOD ON THIN-FILM-TRANSISTOR ARRAY DEVICES- AN ANALYSIS TO PREVENT CELL DEATH," in Proc. 21st Int. Conf. on Miniaturized Systems for Chemistry and Life Science (µTAS 2017), Oct. 22-26, 2017, Savannah, GA, US.*

5. *Faruk A. Shaik,* ***Grant Cathcart****, Satoshi Ihida, Hiroshi Toshiyoshi, and Agnes Tixier-Mita, "Extracellular Neural Stimulation and Recording with a Thin-Film-Transistor Array Device," in Proc. 19th Int. Conf. on Solid-State Sensors, Actuators and Microsystems (Transducers 2017), June 18-22, 2017, Kaohsiung Exhibition Center, Kaohsiung, Taiwan. (oral)*

6. *F. A. Shaik,* ***G. Cathcart****, S. Ihida, J. Kawada, Y. Ikeuchi, A. Tixier-Mita, and H. Toshiyoshi, "An exploratory attempt for Electrowetting on Thin-Film-Transistor array," in Proc. Asia-Pacific Conference of Transducers and Micro-Nano Technology (APCOT 2016), June 26 - 29, 2016, Kanazawa, Japan, pp. 47-48.*

7. *Shaik Faruk Azam,* ***Grant Alexander Cathcart****, Satoshi Ihida, Hiroshi Toshiyoshi, and Agne`s Tixier-Mita, "A TFT electrode array for real time active interface to cells culture," The Institute of Electrical Engineers of Japan (IEEJ), Himeji, Japan, June 29 - 30, 2017.*

Acknowledgements

I would like to express my thankfulness to Professors Toshiyoshi and Tixier-Mita for their continued support, particularly for their patience when dealing with my eccentricities. I would also like to thank Mr. Ihida for his invaluable advice regarding the device as well as handling the design constraints that allowed me to turn my ideas into reality. I would like to thank Ms. Koizumi for handling the bureaucracy and red tape for me, and for tolerating my constant forgetting of deadlines, and tracking me down which wasn't always the easiest task. I would also like to thank Dr. Shaik for constantly supporting me and working with me on many experiments.

I would like to thank Dr. Ikeuchi, and Dr. Sakai, and Ms. Eiler for helping with the cell culture and providing biological expertise. I would also like to thank Mr. Zhu, and Ms. Ohno for working with me on applying my impedance spectroscopy techniques to antibody/antigen sensing. I would also like to thank Dr. Murakami for easing my accustomization to Japan and his continued support. Finally, I would like to express my gratitude to everyone in Toshiyoshi laboratory for their constant support and friendship.